

THE NUCLEAR STRUCTURE OF  $^{166}\text{Er}$

THE NUCLEAR STRUCTURE OF  $^{166}_{\text{Er}}$

By

JOSHUA DANIEL PANAR, M.Sc.

A Thesis

Submitted to the School of Graduate Studies  
in Partial Fulfilment of the Requirements

for the Degree  
Doctor of Philosophy

McMaster University

September 1977

DOCTOR OF PHILOSOPHY (1977)  
(Physics)

MCMASTER UNIVERSITY  
Hamilton, Ontario

TITLE: The Nuclear Structure of  $^{166}\text{Er}$

AUTHOR: Joshua Daniel Panar, B.Sc. (University of Alberta)

M.Sc. (University of Alberta)

SUPERVISOR: Professor D. G. Burke

NUMBER OF PAGES: xiv, 165

## ABSTRACT

Two-quasiparticle states in  $^{166}\text{Er}$  have been studied using the  $^{167}\text{Er}(d,t)^{166}\text{Er}$ ,  $^{167}\text{Er}(^3\text{He},\alpha)^{166}\text{Er}$ ,  $^{165}\text{Ho}(^3\text{He},d)^{166}\text{Er}$ , and  $^{165}\text{Ho}(\alpha,t)^{166}\text{Er}$  reactions. Beams of 15 MeV deuterons, 24 MeV  $^3\text{He}^{++}$ , and 27 MeV  $\alpha$  particles were produced by the McMaster University model FN tandem Van de Graaff accelerator. The reaction products were analyzed with an Enge split-pole magnetic spectrograph and detected with photographic emulsions. Angular distributions were obtained for the  $(d,t)$  and  $(^3\text{He},d)$  reactions at twelve and ten angles, respectively. The data were fitted with a peak finding program to yield peak energies and cross sections up to  $\sim 2700$  keV in excitation energy, although selected peaks were investigated at somewhat higher energies.

The interpretation of the data was performed within the framework of the Unified model, incorporating pairing effects. In the neutron transfer study, two-quasiparticle states formed by removing a particle from the predominantly  $7/2^+$  [633]  $^{167}\text{Er}$  ground state were investigated, while the proton transfer study dealt with two-quasiparticle states formed by adding a particle to the  $7/2^-$  [523] ground state of  $^{165}\text{Ho}$ . Several previous assignments have been supported while many new ones are suggested or proposed. In contrast, several other assignments proposed in an earlier proton transfer study have been refuted.

Earlier observations that several states were populated in both the neutron transfer and proton transfer reactions have been confirmed and extended. In addition, the observation in the (d,t) reaction of several states populated by  $\ell=0$  neutron transfers has been interpreted in terms of a complex mixing scheme involving the  $7/2^+ [633] \pm 1/2^+ [400]$  configurations.

## ACKNOWLEDGMENTS

Out of necessity an experimental research project in nuclear physics involves the cooperation of a large number of people and though I would like to individually thank all those who so greatly contributed to this work, it would be an overwhelming task.

In particular, however, I would like to express my sincere appreciation to Professors M. W. Johns and D. G. Burke for the opportunity to pursue this study at McMaster University. Special thanks are further due to Dr. Burke for his guidance and friendship throughout the course of this project. Both he and his family have made my stay at McMaster University most interesting and enjoyable..

I would also like to thank the members of my supervisory committee, Drs. J. C. Waddington and G. L. Keech for their patience and kind assistance.

The preparation of the  $^{167}\text{Er}$  targets by Ray Sheline and Bob Leonard of Florida State University was appreciated as was the aid of J. O'Donnell and Dr. Y. Peng with the  $^{165}\text{Ho}$  targets.

Many thanks go to my fellow overnight experimenters, Oddmund Straume, Henry Cheung, Ross Hirning and Om Jolly for their help with the data collection, their valuable discussions and comments during the analysis stage - and their more or less tolerant acceptance of a punny sense of humour.

Phil Ashbaugh, John McKay, Bob McNaught and the technical staff of the Tandem Laboratory were most helpful, both in minimizing the equipment downtime and in speedily repairing the inevitable. For her cheerfully supplying an endless stream of pencils and assistance, I would particularly like to thank Edna Williams.

The cooperation of the staff at the McMaster University Computing Centre was greatly appreciated. The knowledgeable aid of Dr. Paul Dunmore was particularly welcome.

Special thanks are also due to Annette Rosati and Helen Kennelly for the heroic and efficient job of typing the manuscript.

The continuing support and encouragement of my parents has been deeply appreciated. I am most grateful for their long standing interest in my work, and for their confidence.

I am also grateful to Melody and Meri for their support and understanding during the past months. A very special "thank you very much".

The work was supported by the National Research Council of Canada.

## TABLE OF CONTENTS

		<u>Page</u>
CHAPTER 1	INTRODUCTION	1
CHAPTER 2	EXPERIMENTAL DETAILS	9
2.1	Introduction	9
2.2	Targets	11
2.3	Neutron Transfer Reactions	12
(a)	The $^{167}\text{Er}(d,t)^{166}\text{Er}$ Reaction	12
(b)	The $^{167}\text{Er}(^3\text{He},\alpha)^{166}\text{Er}$ Reaction	24
2.4	Proton Transfer Reactions	25
(a)	The $^{165}\text{Ho}(^3\text{He},d)^{166}\text{Er}$ Reaction	25
(b)	The $^{165}\text{Ho}(\alpha,t)^{166}\text{Er}$ Reaction	26
2.5	Normalizations and Cross Section Calculations	33
CHAPTER 3	THEORETICAL CONSIDERATIONS	36
3.1	General	36
3.2	Nuclear Shapes and Vibrations	36
3.3	The Unified <sup>o</sup> Model	39
(a)	The Model	39
(b)	Wave Function Separability	40
(c)	Angular Momentum Notation	40
(d)	The Nilsson Model	42
(e)	The Vibrational Hamiltonian	47
(f)	The Rotational Hamiltonian	48
(g)	The Pairing Interaction	55

	<u>Page</u>
(h) Mixing Interactions	62
(1) The $\vec{l} \cdot \vec{s}$ Splitting Interaction	62
(2) The $\Delta N=2$ Mixing	64
(3) The Neutron-Proton Interaction	65
3.4 Cross Section Calculation	67
(a) Formalism	67
(b) DWBA Calculations	69
CHAPTER 4 INTERPRETATION	73
4.1 General	73
4.2 States Populated in the Neutron Transfer Reactions	80
(a) The Ground State Band	80
(b) The $K^\pi = 2^+$ $\gamma$ -Vibrational Band	85
(c) The $K^\pi = 2^-$ Octupole Vibrational Band	86
(d) The $7/2^+ [633] \pm 5/2^- [523]$ Bands	97
(e) The $7/2^+ [633] \pm 1/2^- [521]$ Bands	101
(f) The $7/2^+ [633] \pm 11/2^- [505]$ Bands	104
(g) The $l=0$ Neutron Transfers and the $7/2^+ [633] \pm 1/2^+ [400]$ , $7/2^+ [633] \pm 3/2^+ [402]$ , $7/2^+ [633] \pm 1/2^+ [660]$ , $7/2^+ [633] - 3/2^+ [651]$ , and $7/2^+ [633] - 5/2^+ [642]$ Bands	106
(h) Miscellaneous States	118

	<u>Page</u>
4.3 States Populated in the Proton Transfer Reactions	124
(a) The Ground State Band	124
(b) The $K^\pi = 2^+$ $\gamma$ -Vibrational Band	128
(c) The $7/2^- [523] \pm 1/2^+ [411]$ Bands	128
(d) The $7/2^- [523] + 7/2^+ [404]$ Band	136
(e) The $7/2^- [523] \pm 1/2^- [541]$ Bands	140
(f) The $7/2^- [523] \pm 5/2^+ [402]$ and the $7/2^- [523] \pm 3/2^+ [411]$ Bands	144
(g) The $7/2^- [523] + 9/2^- [514]$ Band	150
(h) Miscellaneous States	152
CHAPTER 5 CONCLUSIONS	158
REFERENCES	161

LIST OF FIGURES

	<u>Page</u>
2.1.1 Enge split-pole spectrograph pole face shapes	10
2.3.1 $^{167}\text{Er}(d,t)^{166}\text{Er}$ and $^{167}\text{Er}(^3\text{He},\alpha)^{166}\text{Er}$ spectra	17
2.4.1 $^{165}\text{Ho}(^3\text{He},d)^{166}\text{Er}$ and $^{165}\text{Ho}(\alpha,t)^{166}\text{Er}$ spectra	27
3.3.1 Coupling schemes	41
3.3.2 Nilsson diagram for neutron levels	45
3.3.3 Nilsson diagram for proton levels	46
3.3.4 Fullness parameter v.s. single particle energy with and without a finite pairing interaction	56
4.1.1 Expanded energy scale $^{167}\text{Er}(d,t)^{166}\text{Er}$ and $^{167}\text{Er}(^3\text{He},\alpha)^{166}\text{Er}$ spectra	78
4.1.2 Expanded energy scale $^{165}\text{Ho}(^3\text{He},d)^{166}\text{Er}$ and $^{165}\text{Ho}(\alpha,t)^{166}\text{Er}$ spectra	79
4.2.1 Ratios of the cross sections of the $(^3\text{He},\alpha)$ and $(d,t)$ reactions	81
4.2.2 The $(d,t)$ angular distributions to the ground state band	84
4.2.3 The $(d,t)$ angular distributions to the $7/2^+[633]+3/2^-[521]$ two neutron configurations	90
4.2.4 The $(d,t)$ angular distributions to the $7/2^+[633]+5/2^-[523]$ two neutron configuration	100

	<u>Page</u>
4.2.5 The (d,t) angular distributions to the $7/2^+[633] \pm 1/2^-[521]$ two neutron configurations	100
4.2.6 The (d,t) angular distributions to states populated with prominent $\ell=0$ neutron transfer components	107
4.2.7 Expanded energy scale of $^{167}\text{Er}(d,t)^{166}\text{Er}$ spectrum at $6\ 1/2^0$ indicating states popu- lated by $\ell=0$ neutron transfers	108
4.2.8a The (d,t) angular distributions to miscel- laneous states	120
4.2.8b The (d,t) angular distributions to miscel- laneous states	121
4.2.8c The (d,t) angular distributions to miscel- laneous states	122
4.2.8d The (d,t) angular distributions to miscel- laneous states	123
4.3.1 Ratios of the cross sections of the ( $^3\text{He},d$ ) and ( $\alpha,t$ ) reactions	126
4.3.2 The ( $^3\text{He},d$ ) angular distributions to the ground state band	127
4.3.3 The ( $^3\text{He},d$ ) angular distributions to the $7/2^-[523] \pm 1/2^+[411]$ two proton configurations	130
4.3.4 The ( $^3\text{He},d$ ) angular distribution to the $7/2^-[523] + 7/2^+[404]$ band head	138

	<u>Page</u>
4.3.5 The ( $^3\text{He},d$ ) angular distributions to the $7/2^- [523] \pm 1/2^- [541]$ two proton configurations	138
4.3.6 The ( $^3\text{He},d$ ) angular distributions to the $7/2^- [523] \pm 5/2^+ [402]$ two proton configurations	147
4.3.7a The ( $^3\text{He},d$ ) angular distributions to miscel- laneous states	153
4.3.7b The ( $^3\text{He},d$ ) angular distributions to miscel- laneous states	154
4.3.7c The ( $^3\text{He},d$ ) angular distributions to miscel- laneous states	155
4.3.7d The ( $^3\text{He},d$ ) angular distributions to miscel- laneous states	156

## LIST OF TABLES

		<u>Page</u>
2.3.1	Energies, experimental cross sections and assignments for states observed in the neutron transfer reactions	18
2.4.1	Energies, experimental cross sections and assignments for states observed in the proton transfer reactions	28
3.4.1	DWBA parameters used	71
4.1.1	Nilsson single particle energies and pairing factors for neutron orbitals	76
4.1.2	Nilsson single particle energies and pairing factors for proton orbitals	77
4.2.1	Experimental and theoretical cross sections for states of the ground state band populated in the neutron transfer reactions	83
4.2.2	Experimental and theoretical cross sections for states of the $7/2^+ [633] \pm 3/2^- [521]$ configurations	88
4.2.3	Experimental and theoretical cross sections for states of the $7/2^+ [633] + 5/2^- [523]$ configuration	98
4.2.4	Experimental and theoretical cross sections for states of the $7/2^+ [633] \pm 1/2^- [521]$ configurations	98

	<u>Page</u>
4.2.5 Experimental and theoretical cross sections for the $7/2^+$ [633]+ $11/2^-$ [505] bandhead	105
4.2.6 Mixing calculation input matrix, I=3	111
4.2.7 Mixing calculation input matrix, I=4	112
4.2.8 Mixing calculation output matrix, I=3	113
4.2.9 Mixing calculation output matrix, I=4	114
4.3.1 Experimental and theoretical cross sections for states of the ground state band popula- ted in the proton transfer reactions	125
4.3.2 Experimental and theoretical cross sections for states of the $7/2^-$ [523] $\pm 1/2^+$ [411] con- figurations	132
4.3.3 Experimental and theoretical cross sections for states of the $7/2^-$ [523] $+7/2^+$ [404] band- head	137
4.3.4 Experimental and theoretical cross sections for states of the $7/2^-$ [523] $\pm 1/2^-$ [541] con- figurations	142
4.3.5 Experimental and theoretical cross sections for states of the $7/2^-$ [523] $\pm 5/2^+$ [402] and $7/2^-$ [523] $-3/2^+$ [411] configurations	145
4.3.6 Experimental and theoretical cross sections for states of the $7/2^-$ [523] $+9/2^-$ [514] con- figuration	151

CHAPTER 1  
INTRODUCTION

This study of the rare earth deformed nucleus  $^{166}\text{Er}$  is properly categorized as being in the field of low energy nuclear physics. The field is generally considered to have two basic divisions: the study of the makeup of the nucleus (nuclear structure physics), and the study of the processes through which the nuclear structure is investigated (primarily decay mechanisms and reaction mechanisms).

Nuclear structure physics deals with the interactions between the particles which make up the nucleus, the couplings and configurations of these particles, and the evaluation of the parameters describing the nucleus (e.g. spins, parities and other quantum numbers). These parameters are obtained either by observing the results of natural decay processes involving the nucleus, or by observing the interactions of test particles with the nucleus.

These test particle interactions are generically known as nuclear reactions, and the detailed investigation of how nuclear reactions take place combined with their parameterization constitutes the study of reaction mechanisms. Analogously, the detailed mechanisms whereby the decay processes take place are also studied, and these are likewise parameterized. While the studies of the decay and reaction

mechanisms are somewhat interdependent with the investigations of the nuclear structure, the two disciplines can in practice be tolerably well separated, particularly if variations introduced into the study from the branch not being pursued are minimized. The study of  $^{166}\text{Er}$  by direct reactions, as discussed in this thesis, is an investigation of the nuclear structure of  $^{166}\text{Er}$ . The direct reaction mechanisms are presumed to be well-enough known so that one can extract nuclear structure information from the data with adequate reliability.

A standard method of investigating nuclear structure is to construct a reasonable model of the nucleus and to predict the results of commonly used reactions with this model. These are compared with the experimentally observed data and on the basis of this comparison, the validity of the model is assessed.

In the study of odd mass deformed rare earth nuclei, it has long been known that the Unified model generally explains the low lying observed spectra. This model combines single particle excitations in a deformed potential with collective excitation modes, resulting primarily in rotational bands built upon single particle or vibrational states. Many examples of this application of the model appear in the literature, and by now most of the readily accessible odd mass rare earth nuclei have been fairly well studied. A more complex level of nuclear structure is found in the even-even

nuclei, where two similar nucleons, each in a Nilsson orbital, couple together to form the simplest type of state. It is configurations of this type in  $^{166}\text{Er}$  that form the main subject in the present study. As with the odd nuclei, the even-even nuclei exhibit collective vibrational modes of excitation, and rotational structure is observed to be built upon both the two-quasiparticle and vibrational states.

In the present work, the two-quasiparticle states in  $^{166}\text{Er}$  are studied by single particle transfer reactions. These are "direct" reactions in that the transfer of the single particle between the incident projectile and the target nucleus is considered to take place at the nuclear surface, directly involving only the Nilsson orbital into which or from which the translocation takes place. Thus, apart from gross nuclear rotational effects, the remainder of the target nucleus is considered to be essentially unaffected, and compound nuclear effects (whereby the excitation energy is shared by many or all the nuclear particles in a nearly infinite number of excitation modes) are avoided.

The  $^{167}\text{Er}(d,t)^{166}\text{Er}$  and  $^{167}\text{Er}(^3\text{He},\alpha)^{166}\text{Er}$  neutron pickup reactions were used in the present work to study states in  $^{166}\text{Er}$  formed by removing a neutron from the target ground state of  $^{167}\text{Er}$ , while the  $^{165}\text{Ho}(^3\text{He},d)^{166}\text{Er}$  and  $^{165}\text{Ho}(\alpha,t)^{166}\text{Er}$  proton stripping reactions populated states in  $^{166}\text{Er}$  by adding a proton to the ground state configuration of  $^{165}\text{Ho}$ . In all of the reactions the residual nucleus

could, in general, be left in an excited state. As the incident particles in the beam were essentially monoenergetic, the excitation energies for the various states could be determined by measuring the energies of the corresponding reaction products. The orbital angular momentum transferred to a state could be determined by observing the angular distribution (with respect to the incoming beam direction) of outgoing particles from reactions populating the state (particularly for the (d,t) and ( $^3\text{He},d$ ) reactions). Often, the same information was available from ratios of the cross sections for the two reactions populating the state  $(d\sigma/d\Omega(^3\text{He},\alpha)_{\theta_1} / d\sigma/d\Omega(d,t)_{\theta_2})$  or  $(d\sigma/d\Omega(^3\text{He},d)_{\theta_3} / d\sigma/d\Omega(\alpha,t)_{\theta_4})$ ; the angles,  $\theta$ , refer to the direction of the outgoing particles with respect to the incoming beam).

For states suspected (on the basis of their energy spacings) of forming a rotational band, the configurations could often be determined by noting the relative intensities with which the levels were populated. The relative intensities for the members are predicted to vary from band to band, and these characteristic intensity "fingerprints" are therefore of considerable importance for band identification.

In the experiments of this study, the incoming beams of particles were provided by a tandem Van de Graaff accelerator, and an Enge split-pole magnetic spectrograph was used to determine the energies, intensities and directions of the outgoing particles with respect to the incoming beam.

In the past, a number of studies of  $^{166}\text{Er}$  levels were made. Three natural decay processes populate the low lying states in  $^{166}\text{Er}$ , the  $^{166}\text{Ho}$  ground state  $\beta$ -decay, the  $^{166}\text{Ho}$  metastable state (1200 years)  $\beta$ -decay and the  $^{166}\text{Tm}$  electron capture decay. All these processes have been well studied (e.g. Reich and Cline, 1970; Zylicz et al., 1966); the population of states in  $^{166}\text{Er}$  has been observed up to an excitation energy of  $\sim 1830$  keV in the Ho decays, and up to  $\sim 2300$  keV in the Tm decay. Above  $\sim 1500$  keV most of the assignments from those works have been tentative, and prior to this work several particle transfer reaction studies have been performed in attempts to resolve the ambiguities and investigate the spectra at higher energies. These studies have met with varying degrees of success.

The  $^{165}\text{Ho}(^3\text{He},d)^{166}\text{Er}$  angular distribution study by Kubo (1968) suffered primarily from poor resolution due to the very thick holmium targets employed ( $\sim 100\mu\text{g}/\text{cm}^2$ ). As that study was undertaken primarily to investigate the structure of the  $K^\pi = 2^-$  octupole vibrational band up to  $\sim 1850$  keV, levels above that energy were not analyzed in detail.

In a  $^{167}\text{Er}(d,t)^{166}\text{Er}$  reaction study Burke et al. (1969) made assignments of levels only up to  $\sim 1850$  keV because of the complexity of the higher lying spectrum. The reaction was studied at three angles, so angular distributions sufficiently detailed to permit identification of

the neutron transfer  $l$ -values were not obtained. In particular, the forward peaking displayed in the present study by the many neutron transfers having major  $l=0$  components was not observable. A further problem with that work arose as the accuracy of the energy calibration of the Niels Bohr Institute's Elbek magnetic spectrograph was in question at the time the experiments were performed.

In a  $^{165}\text{Ho}(^3\text{He},d)^{166}\text{Er}$  and  $^{165}\text{Ho}(\alpha,t)^{166}\text{Er}$  study, published in 1974, Katori et al. (1974) presented assignments for about a dozen levels and tentative assignments for about a dozen more. Several major errors in that study have been uncovered in the present work, and these findings invalidate all except two of their assignments (these two were previously discussed in the work of Kubo and in the decay studies). The errors arose from two main sources. First, the experimental resolution was of the order of  $\sim 50$  keV FWHM, far too great for this type of study, and in many cases, the multiplet nature of the peaks was not discovered.

The second problem concerned the determination of transferred  $l$ -values. Normally in  $(^3\text{He},d)$  reactions, the  $Q$ -values (typically zero to  $\pm$  a few MeV in this mass region) result in the transferred particle carrying very little energy and hence very little angular momentum to the target nucleus. Thus  $(^3\text{He},d)$  reactions favour low values of angular momentum transfer. (In the neutron pickup reactions, this is similarly true for the  $(d,t)$  reactions.) On the

other hand, the large negative Q-values of the ( $\alpha, t$ ) reactions (typically -10 to -16 MeV in this mass region) result in the transferred proton carrying a large amount of energy and thus potentially a large angular momentum to the target nucleus. (In the neutron pickup case the analogous reaction is ( ${}^3\text{He}, \alpha$ ).)

It would appear that Katori et al. reversed this relationship by attributing large peaks in the ( ${}^3\text{He}, d$ ) reaction to states populated by high  $l$ -value proton transfers, and by attributing large peaks in the ( $\alpha, t$ ) reaction to states populated by low  $l$ -value transfers. It is not clear from their paper just why this was done, but many obviously incorrect assignments followed from it.

The observation of some of these difficulties prompted the proton transfer studies of the present investigation. By using long collection times with stable beams and relatively thin targets, a good set of  ${}^{165}\text{Ho}({}^3\text{He}, d){}^{166}\text{Er}$  angular distributions was obtained. The  ${}^{165}\text{Ho}(\alpha, t){}^{166}\text{Er}$  reactions provided further information on the transferred  $l$ -values. These were of particular use for the confirmations of several assignments where the states were populated by high  $l$ -value proton transfers. The data in these studies were investigated up to  $\sim 2700$  keV with occasional assignments up to  $\sim 3500$  keV.

At the time that the proton transfer work was under way, separated isotope targets of  ${}^{167}\text{Er}$  were obtained. The

$^{167}\text{Er}(d,t)^{166}\text{Er}$  reaction study was repeated to obtain complete angular distributions, and the  $^{167}\text{Er}(^3\text{He},\alpha)^{166}\text{Er}$  reaction was studied to aid in the identification of states populated by high  $\ell$ -value neutron transfers. Analysis in the present work is much more extensive than in the previous study, with assignments now being made up to  $\sim 2700$  keV in excitation energy. The accurate energy determinations of the present studies confirmed and extended the earlier observation that several states were populated in both the neutron transfer and proton transfer reactions.

CHAPTER 2  
EXPERIMENTAL DETAILS

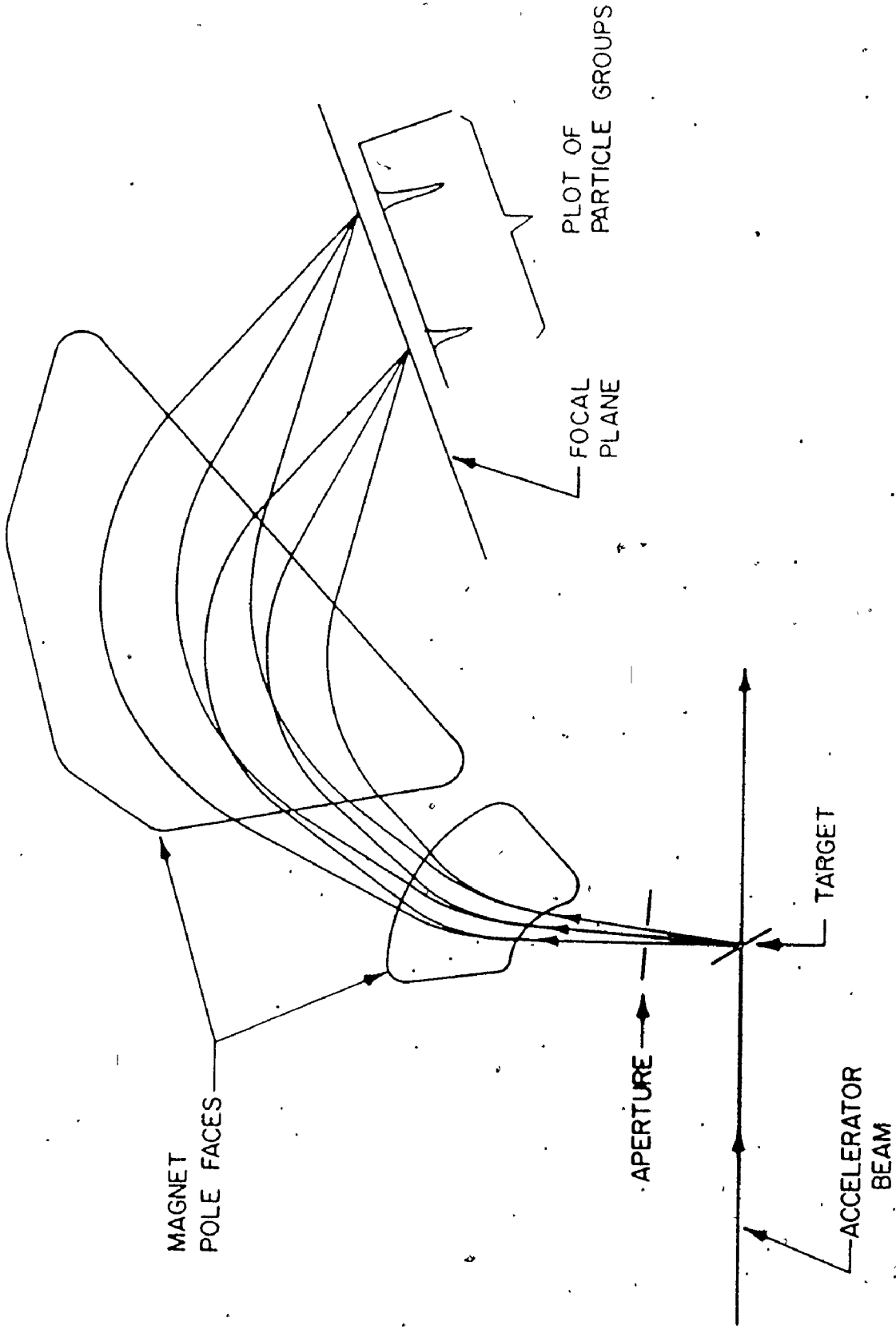
2.1 Introduction

The experimental programme consisted of populating and studying states in the even-even rare earth nuclide  $^{166}\text{Er}$ , using four different reactions. Two of these,  $(d,t)$  and  $(^3\text{He},\alpha)$ , "picked up" a neutron out of a target of  $^{167}\text{Er}$ ; the other two,  $(^3\text{He},d)$  and  $(\alpha,t)$ , "stripped" a proton from the incident projectile into a target of  $^{165}\text{Ho}$ .

The beams of incident ions were provided by the McMaster University FN Tandem Accelerator, and the outgoing particles were momentum analyzed at selected angles to the incoming beam using an Enge split-pole magnetic spectrograph (Spencer and Enge, 1967). Fig. 2.1.1 shows the shapes of the magnetic pole faces and typical trajectories of charged particles in this type of spectrograph. The light reaction products were detected at the spectrograph focal plane with photographic emulsions. After they were developed, the photographic plates were scanned in 0.25 mm strips by microscope to obtain the number of tracks as a function of distance along the focal plane. In the neutron transfer reactions the range scanned included excitation energies up to  $\sim 3200$  keV, although due to the increase in the density of states with excitation energy the data were analyzed to

Fig. 2.1.1

Typical particle trajectories through the  
Enge split-pole magnetic spectrograph.



only  $\sim 2700$  keV. The proton transfer reaction data were scanned up to  $\sim 3600$  keV for the ( $^3\text{He},d$ ) and ( $\alpha,t$ ) reactions. While certain peaks were analyzed up to these energies, detailed analysis went to only  $\sim 2700$  keV.

In the analysis, these data were fitted with a peak finding program. The resulting peak areas were normalized to provide differential cross sections for the states in  $^{166}\text{Er}$  in a manner described in Sect. 2.5.

## 2.2 Targets

As natural erbium has several stable isotopes, and the direct reaction cross sections on the even mass nuclides are typically twice as large as those from  $^{167}\text{Er}$ , separated isotope targets had to be prepared. Targets of  $^{167}\text{Er}$   $\sim 45 \mu\text{g}/\text{cm}^2$  thick were deposited directly on  $40 \mu\text{g}/\text{cm}^2$  carbon foils by R. Leonard, using the Florida State University isotope separator. This procedure resulted in enrichments estimated to be  $> 99\%$ . The target thickness was determined from elastic scattering measurements during the experiments.

The targets for the proton transfer reactions were made at McMaster University by evaporating metallic  $^{165}\text{Ho}$ , which is the only stable isotope of holmium, onto  $20 \mu\text{g}/\text{cm}^2$  carbon foils on glass slides. The foils were then floated off the slides onto a surface of distilled water and picked up on target frames. As these targets became exceedingly

brittle within a few days, and holmium is readily available, new targets were prepared immediately prior to each run. The thickness of  $^{165}\text{Ho}$  used in the present experiments was 35-40  $\mu\text{g}/\text{cm}^2$ .

### 2.3 Neutron Transfer Reactions

#### (a) The $^{167}\text{Er} (d,t) ^{166}\text{Er}$ Reaction

The  $^{167}\text{Er} (d,t) ^{166}\text{Er}$  reaction was studied at twelve angles ( $6\frac{1}{2}$ , 10, 15, 20, 25, 30, 35, 40, 45, 50, 60 and  $75^\circ$ ) using  $\sim 1.8 \mu\text{A}$  beams of 15 MeV deuterons. (The forward angle was limited to about  $6^\circ$  by the position of the shielding separating the Faraday cup from the spectrograph entrance window.)

As the density of states was known to be quite high above the pairing gap, it was particularly important to optimize the resolution. Various effects contribute to the peak width and, where possible, attempts were made to minimize these. The contributions can generally be separated into those arising in the target (target thickness effects) and those coming from the properties of the beam and spectrograph.

One target thickness effect resulted from the fact that the reactions could take place at different depths in the target. This fact, combined with different values of  $dE/dx$  for the incoming and outgoing particles, broadened the peaks. Another consequence of the target thickness was

the energy straggling of the beam and reaction products in the target. By keeping the targets thin, compatible with obtaining reasonable count rates, the contribution from each effect was limited to about 3 keV.

Increases in the peak width due to variations in the beam energy arose in several ways. These beam energy variations (due mainly to terminal voltage instabilities) were usually  $\leq 2$  keV (Cairns, 1974), while straggling of the beam, mainly in the stripper foil, contributed  $\leq 400$  eV. Further peak broadening came from the finite beam spot size on the target. This spot size is translated into a peak width contribution on the focal plane because of the finite magnification of the spectrograph. The instrument's magnification is  $M_H = 0.35$ , and as the focal plane is at an angle of  $\sim 45^\circ$  to the particle trajectories, the magnification factor is  $\sim 0.5$ . Thus, a typical beam spot size of  $\sim 1$  mm would contribute  $\sim 6$  keV to the peak width for tritons of  $\sim 12$  MeV. This effect was minimized in the (d,t) experiment by placing a 0.5 mm wide vertical slit at the target position immediately prior to the measurements (Jolly, 1975). The beam was focussed through this opening and care was taken to avoid any further adjustments of the beam handling parameters once the slit was replaced by the target. In this way the beam spot width contribution was reduced to  $\sim 3$  keV.

In practice, because of the dispersive properties of the beam handling system, there is a partial correlation

between the energy of the incident particle in the beam and the point within the beam spot at which this particle hits the target. Thus, one can use a combination of the spectrograph's dispersion and its horizontal magnification to achieve "dispersion compensation" which partially corrects for the beam energy spread across the beamspot (Tippett, 1972).

Contributions to the peak width from aberrations in the spectrograph are minimal with the solid angles employed in these experiments ( $\leq 2$  msr). This is deduced from a comparison of the ( $^3\text{He},d$ ) and ( $\alpha,t$ ) reaction data, where, for similar beam spot sizes, the peak width in mm is not constant (as would be expected if the spectrograph aberrations predominated). Instead, the observed peak widths were approximately constant in energy, suggesting that effects due to target thickness or beam energy instabilities were dominant.

With all the above factors contributing to the total peak width, the overall resolution obtained was a respectable  $\sim 7.5$  keV FWHM for almost all of the ( $d,t$ ) spectra.

The tritons were detected with Kodak NTB emulsions 50 microns thick. Aluminum absorbers (0.10 mm thick) were placed on the plates to stop knock-on carbon atoms which originated in the target backing. For collection times of 1-2 hours (6000-10000  $\mu\text{C}$  through the target) and a spectrograph acceptance solid angle of 1.8 msr, a maximum of about

1000 counts per 0.25 mm strip was obtained. All the spectra in this study were fitted with the computer code SPECT. As a first step this program fitted a sample peak in a spectrum to a gaussian shape with an exponential tail. This generated shape was then used to locate the other peaks in the spectrum and to yield the number of counts in each peak. Checks on these generated intensities were performed by comparing them with peak areas summed by hand. For well fitted peaks the agreement was usually within 5% and for isolated peaks it was within 1%.

The precision of the measured excitation energies is limited by uncertainties in the measured peak positions and in the spectrograph calibration. Most of the peaks of interest in the (d,t) spectrum had shapes, widths and intensities that were good enough to reduce the statistical error on the peak positions to  $\leq 0.5$  keV. On the other hand, the uncertainties in the spectrograph calibration contribute possible errors of 1-2 keV in the excitation energies obtained from the (d,t) spectra. The energy calibration was determined by placing a radioactive source of  $^{212}\text{Pb}$  at the target position. The positions along the focal plane at which the 8.78 MeV  $\alpha$ -particles (Rytz, 1960) appeared were measured as a function of the magnetic field for the spectrograph. A least squares fitting routine was used to generate a fourth order polynomial relating  $\rho$ , the radius of curvature in the magnetic field, to the position on the

focal plane. The uncertainty in excitation energy which arises from this method has been estimated by comparing measured values with those obtained much more precisely from gamma decay studies in several cases where this has been possible. For example, excitation energies from previous studies of  $^{166}\text{Er}$  are listed in Table 2.3.1 for comparison with averaged values from the (d,t) and ( $^3\text{He},\alpha$ ) reactions of the present work. The energies shown for levels below 2.0 MeV agree with previously known values usually to within 1 keV.

A typical fitted spectrum is shown in Fig. 2.3.1. Where assignments are known, the peaks are labelled with the spin and the two-quasiparticle Nilsson orbital configuration. The region from 1300 to 3200 keV is shown with an expanded scale in Sect. 4, and in this region assignments are presented on that drawing (Fig. 4.1.1) The angular distributions from the (d,t) reaction are presented in Figs. 4.2.2 to 4.2.7.

Experimental differential cross sections at  $\theta=45^\circ$  and  $\theta=50^\circ$  for the (d,t) and ( $^3\text{He},\alpha$ ) reactions, respectively, are also shown in Table 2.3.1. For each level with a smooth (d,t) angular distribution that was compared with a theoretical distribution, the cross section presented in the table is the value at  $\theta=45^\circ$  for the theoretical fit to all the data points. In Sect. 4 these "averaged" cross sections at  $\theta=45^\circ$  are used as measures of the observed

Fig. 2.3.1

The spectra obtained from the  $^{167}\text{Er}(d,t)^{166}\text{Er}$  reaction at  $\theta=45^\circ$  and the  $^{167}\text{Er}(^3\text{He},\alpha)^{166}\text{Er}$  reaction at  $\theta=50^\circ$ . The fits to the data were produced with the fitting program SPECT. Several peaks are labelled with their spins and configuration assignments. Further assignments are presented in Figure 4.1.1. The broad peak at  $\sim 250$  keV in the (d,t) spectrum is due to a  $^{13}\text{C}$  impurity in the target backing.

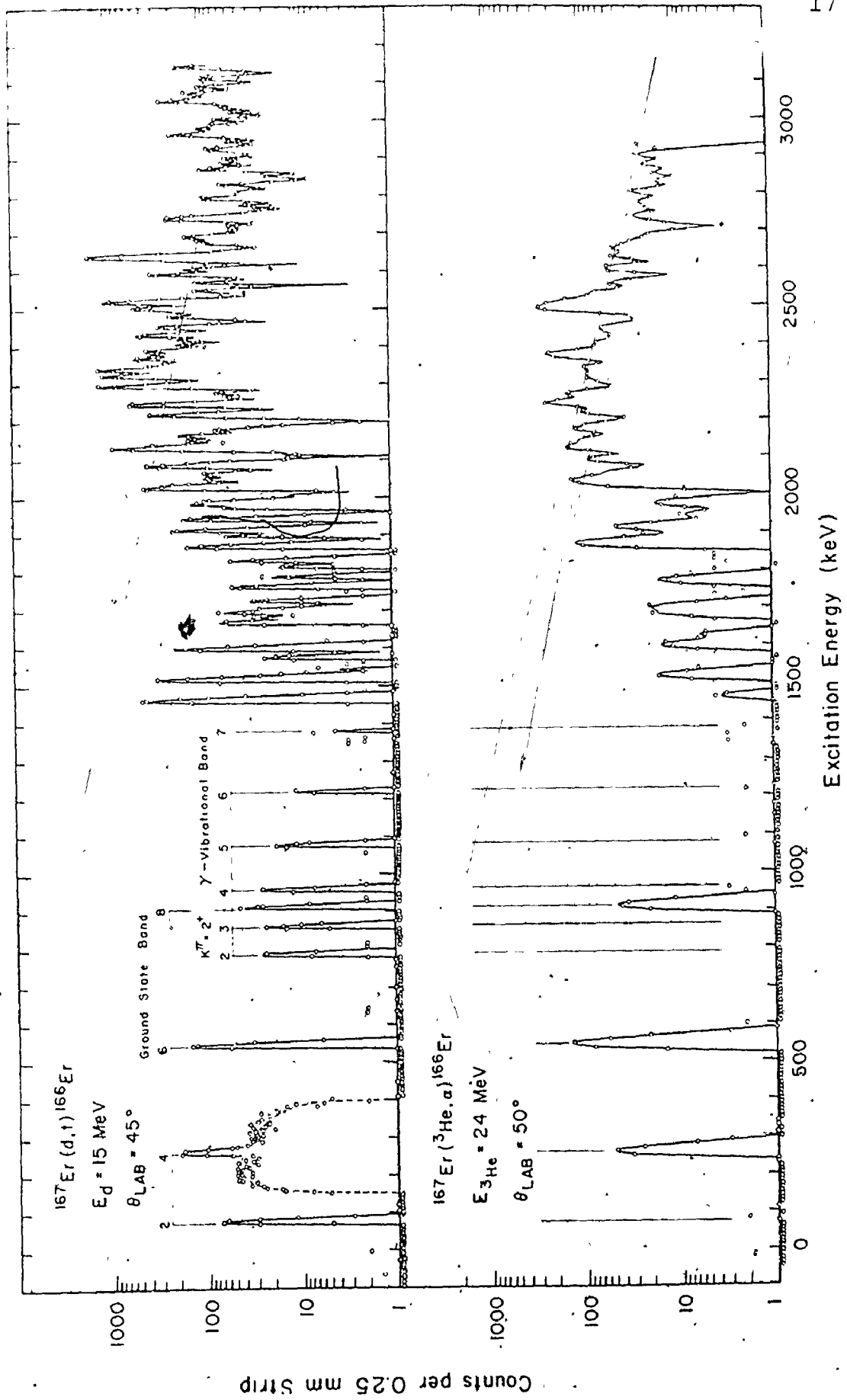


Table 2.3.1

## States Observed in the Neutron Transfer Reactions

(prev.)	Energy (keV)		$d\sigma/d\Omega$ ( $\mu\text{b}/\text{sr}$ )		I K <sup><math>\pi</math></sup>	Interpretation
	(d, t)	( <sup>3</sup> He, $\alpha$ )	(d, t) $\theta=45^\circ$	( <sup>3</sup> He, $\alpha$ ) $\theta=50^\circ$		
0.0					0 0 <sup>+</sup>	7/2 <sup>+</sup> [633]-7/2 <sup>+</sup> [633]
80.6	79	$\sim 80$	17.3	<1.0	2 0 <sup>+</sup>	7/2 <sup>+</sup> [633]-7/2 <sup>+</sup> [633]
265.0	265	265	$\sim 39$	6.5	4 0 <sup>+</sup>	7/2 <sup>+</sup> [633]-7/2 <sup>+</sup> [633]
545.4	545	547	34	17.2	6 0 <sup>+</sup>	7/2 <sup>+</sup> [633]-7/2 <sup>+</sup> [633]
785.9	786		5.6		2 2 <sup>+</sup>	$\gamma$ -Vibrational Band
859.4	859		5.6		3 2 <sup>+</sup>	$\gamma$ -Vibrational Band
911.2	911	910	8.2	6.0	8 0 <sup>+</sup>	7/2 <sup>+</sup> [633]-7/2 <sup>+</sup> [633]
956.2	957		5.8		4 2 <sup>+</sup>	$\gamma$ -Vibrational Band
1075.3	1075		4.1		5 2 <sup>+</sup>	$\gamma$ -Vibrational Band
1215.9	1215		2.3		6 2 <sup>+</sup>	$\gamma$ -Vibrational Band
1376.0	1375		<1.0		7 2 <sup>+</sup>	$\gamma$ -Vibrational Band
1458.0	1458	1460	103	<1.0	2 2 <sup>-</sup>	7/2 <sup>+</sup> [633]-3/2 <sup>-</sup> [521]
1514.0	1514	1516	72	2.1	3 2 <sup>-</sup>	7/2 <sup>+</sup> [633]-3/2 <sup>-</sup> [521]
1572.1	1572		5.0		4 2 <sup>-</sup>	7/2 <sup>+</sup> [633]-3/2 <sup>-</sup> [521]

(continued next page)

Table 2.3.1 (continued)

Energy (keV) (prev.)	(d, t) ( <sup>3</sup> He, α)	dσ/dΩ (μb/sr)		I	K <sup>π</sup>	Interpretation a)
		(d, t) θ=45°	( <sup>3</sup> He, α) θ=50°			
1596.2	1596	46	1.9	4	2 <sup>-</sup>	7/2 <sup>+</sup> [633] - 3/2 <sup>-</sup> [521]
1665.8	1666	14.8	/	5	2 <sup>-</sup>	7/2 <sup>+</sup> [633] - 3/2 <sup>-</sup> [521]
1679	1682	4.7	1.9			
1692.3	1692	12.4	/	5	2 <sup>-</sup>	7/2 <sup>+</sup> [633] - 3/2 <sup>-</sup> [521]
1703	1697	4.2	2.0			
1722		7.0				
1760	1765	10.9	2.1			
1786.9	1787	3.5		6	(2) <sup>-</sup>	(7/2 <sup>+</sup> [633] - 3/2 <sup>-</sup> [521])
1813		3.4				
1829		9.9		6	2 <sup>-</sup>	7/2 <sup>+</sup> [633] - 3/2 <sup>-</sup> [521]
1868	1865	33	15.5			
1896		11.3				
1910	1911	47	5.3	6	6 <sup>-</sup>	7/2 <sup>+</sup> [633] + 5/2 <sup>-</sup> [523]
1939	1941	38	<1.0	(2)	1 <sup>+</sup>	7/2 <sup>+</sup> [633] - 5/2 <sup>+</sup> [642]

(continued next page)

Table 2.3.1 (continued)

(prev.)	Energy (keV)		$d\sigma/d\Omega$ ( $\mu\text{b}/\text{sr}$ )		I	$K^\pi$	Interpretation
	(d,t)	( $^3\text{He},\alpha$ )	(d,t) $\theta=45^\circ$	( $^3\text{He},\alpha$ ) $\theta=50^\circ$			
	1969	1971	11.8	2.2			
1979.0	1979		26				$\ell=0$
	1987		15.9				
2001.8	2003		2.2				
	2022	2021	96	8.0	4	$4^-$	$7/2^+ [633] + 1/2^- [521]$
	2031	2034	29	12.7	(5)	$1^-$	$7/2^+ [633] - 5/2^+ [642]$
	2050	$\sim 2050$	22	8.8	7	$6^-$	$7/2^+ [633] + 5/2^- [523]$
	2061	2061	28	4.7			
	2080	b)	88	b)	(3)	$3^-$	$7/2^+ [633] - 1/2^- [521]$
	2090	2093	10.3	11.2	(6)	$1^+$	$7/2^+ [633] - 5/2^+ [642]$
	2122	2123	28	18.1	(5)	$4^-$	$7/2^+ [633] + 1/2^- [521]$
	2128		190				
	2149	2146	33	11.2	{(4)	$3^-$	$7/2^+ [631] - 1/2^- [521]$
	2161		38		{(7)	$1^+$	$7/2^+ [633] - 5/2^+ [642]$
							$\ell=0$

(continued next page)

Table 2.3.1 (continued)

(prev.)	Energy (keV)		$d\sigma/d\Omega$ ( $\mu\text{b}/\text{sr}$ )		I	K $\pi$	Interpretation
	(d, t)	( $^3\text{He}, \alpha$ )	(d, t) $\theta=45^\circ$	( $^3\text{He}, \alpha$ ) $\theta=50^\circ$			
	2175	2172	14.3	13.2			a)
	2182	2184	3.4	5.4			
	2216	2215	86	12.5	(3	3 $^-$	7/2 $^+$ [633]-1/2 $^-$ [521])
	2244	2242	143	30	5	5 $^-$	7/2 $^+$ [633]+3/2 $^-$ [521]
	2265	2268	12.4	16.7			
	2274		13.8				
2290.6	2293	2297	289	7.1			$\ell=0$
	2318	2315	277	9.8			$\ell=0$
	2336	2336	243	11.1			
	2353		75				
	2365	2369	115	10.2	6	5 $^-$	7/2 $^+$ [633]+3/2 $^-$ [521]
	2377		81	23			
	2386		73				$\ell=0$
	2405	2399	49	7.6			
	2416	2419	37	4.9			
	2427		98				

(continued next page)

Table 2.3.1 (continued)

(prev.)	Energy (keV)		$d\sigma/d\Omega$ ( $\mu\text{b}/\text{sr}$ )		I	$K^\pi$	Interpretation
	(d, t)	( $^3\text{He}, \alpha$ )	(d, t) $\theta=45^\circ$	( $^3\text{He}, \alpha$ ) $\theta=50^\circ$			
	2438	2438	$\sim 28$				$\ell=0$
	2447	2452	83	6.8			
	2476	2481	58	2.9			
	2494	2496	57	34	(9	$9^-$	$7/2^+ [633] + 11/2^- [505]$
	2499		94				$\ell=0$
	2514	2510	237	18.7			$\ell=0$
	2522		$\sim 28$				
		2534		7.8			
	2545		41				
	2567	2560	26	5.2			
	2578		8.8				
	2588	2583	76	7.8			$\ell=0$
	2603		30				
	2622		21				
	2633	2629	388	5.3			$\ell=0$
	2648	2650	11.4	2.7			

(continued next page)

Table 2.3.1 (continued)

(prev.)	Energy (keV)		$d\sigma/d\Omega$ ( $\mu\text{b}/\text{sr}$ )		I	K $\pi$	Interpretation
	(d, t)	( $^3\text{He}, \alpha$ )	(d, t) $\theta=45^\circ$	( $^3\text{He}, \alpha$ ) $\theta=50^\circ$			
	2670		2.7				a)
	2677		19.1				
	2687	2688	$\sim 20$				
	2734		48				$l=0$

- a) Predominant two-quasiparticle configuration or transferred  $l$ -value(s)
- b) Peak Obscured.

strength for each state in comparisons with predicted values. This is a convenient way to effectively use data from almost all angles in comparison with theory, instead of data at one angle only.

In Table 2.3.1, where an assignment has been made for a level, the level is labelled in the final columns with either the spin, projection and parity, and its predominant two-quasiparticle Nilsson configuration or with the predominant  $\ell$ -value(s) of the transferred particle. The  $\gamma$ -vibrational band is labelled under that title and tentative assignments are enclosed in parentheses. Comparisons of the cross sections with predicted values will be presented in Chapter 4 for many of the states.

(b) The  $^{167}\text{Er} (^3\text{He}, \alpha) ^{166}\text{Er}$  Reaction.

The  $^{167}\text{Er} (^3\text{He}, \alpha) ^{166}\text{Er}$  reaction was investigated at angles of 25, 50 and 60° with 1.0 to 1.5  $\mu\text{A}$  beams of 24 MeV  $^3\text{He}^{++}$ . The  $\alpha$  particles from this reaction were detected with Ilford K-1 emulsions, 50 microns thick, covered with aluminum absorbers 0.25 mm thick to stop tritons produced in competing reactions. The  $^{167}\text{Er}$  target used in the (d,t) reactions was also used in this study, but longer collection times were required (4-5 hours or  $\sim 20,000 \mu\text{C}$  through the target). With a spectrograph acceptance solid angle of 1.8 msr a maximum of  $\sim 150$  counts per 0.25 mm strip was obtained.

The spectrum at  $50^\circ$  is shown in Fig. 2.3.1 (and Fig. 4.1.2). Due to the decreased dispersion of the ( $^3\text{He}, \alpha$ ) reaction, compared with the other reactions, and because not all the peaks were well resolved the excitation energy uncertainties could be as great as  $\pm 5$  keV, though generally, they were somewhat less than this. The best resolution obtained for the ( $^3\text{He}, \alpha$ ) reaction was  $\sim 21$  keV FWHM, the main contributions to the peak width coming from target thickness effects and spectrograph aberrations.

#### 2.4 Proton Transfer Reactions

##### (a) The $^{165}\text{Ho} (^3\text{He}, d) ^{166}\text{Er}$ Reactions

The  $^{165}\text{Ho} (^3\text{He}, d) ^{166}\text{Er}$  reaction was studied with 1.0 - 2.0  $\mu\text{A}$  beams of 24 MeV  $^3\text{He}^{++}$  at ten angles; 6, 10, 15, 20, 25, 30, 40, 45, 60 and  $75^\circ$ .

The deuterons were detected with Kodak NTB type emulsions, 50 microns thick. At the same time, Ilford K-1 emulsions were used to detect  $\alpha$  particles from the  $^{165}\text{Ho} (^3\text{He}, \alpha) ^{164}\text{Ho}$  reaction, but these data were not analyzed as a part of the present study. To stop tritons from competing reactions, aluminum absorbers 0.56 mm in thickness were placed on the NTB plates, while the absorbers on the K-1 plates were 0.25 mm aluminum.

With the target thicknesses that were used (cf. Sect. 2.2) and a spectrograph acceptance solid angle of 1.8 msr, the data were collected for about 4 hours per ex-

posure ( $\sim 20,000 \mu\text{C}$  through the target). This resulted in approximately 500 counts per 0.25 mm strip for the strongest peaks in the spectrum.

A typical spectrum is shown in Fig. 2.4.1. The observed resolution for the ( $^3\text{He},d$ ) reaction was  $\sim 13.5$  keV FWHM. The assignments, where known, are labelled in the same manner as on the neutron transfer figures. The region from 1300 to 3200 keV is shown with assignments on an expanded scale, in Fig. 4.1.2. The ( $^3\text{He},d$ ) angular distributions are presented in Figs. 4.3.2 to 4.3.7.

Table 2.4.1 lists averaged excitation energies for the ( $^3\text{He},d$ ) and ( $\alpha,t$ ) reactions, as well as excitation energies from previous studies of  $^{166}\text{Er}$  for comparison. In addition, the experimental cross sections at  $\theta = 45^\circ$  and  $\theta = 60^\circ$  for the ( $^3\text{He},d$ ) and ( $\alpha,t$ ) reactions, respectively, are presented in the same table. The values from the ( $^3\text{He},d$ ) study were obtained by applying the "averaging" procedure used for the ( $d,t$ ) cross sections of Table 2.3.1. The labelling convention is also that of Table 2.3.1.

(b) The  $^{165}\text{Ho}(\alpha,t)^{166}\text{Er}$  Reaction

The  $^{165}\text{Ho}(\alpha,t)^{166}\text{Er}$  reaction was studied with 1.3 - 1.5  $\mu\text{A}$  beams of 27 MeV  $\alpha$  particles at angles of 50 and  $60^\circ$ . The tritons were detected on Kodak NTB emulsions, 50 microns thick, and aluminum absorbers 0.10 mm thick were used to prevent knock-on carbon atoms from the target backings and singly charged  $\alpha$  particles from reaching the

Fig. 2.4.1

The spectra obtained from the  $^{165}\text{Ho}(^3\text{He},d)^{166}\text{Er}$  reaction at  $\theta=45^\circ$  and the  $^{165}\text{Ho}(\alpha,t)^{166}\text{Er}$  reaction at  $\theta=50^\circ$ . The fits to the data were produced with the fitting program SPECT. Several peaks are labelled with their spin and configuration assignments. The parentheses around the label indicate a tentative assignment and the broken line indicates a tentatively assigned spin. The dashed curve indicates a broad peak due to a  $^{13}\text{C}$  impurity in the target backing.

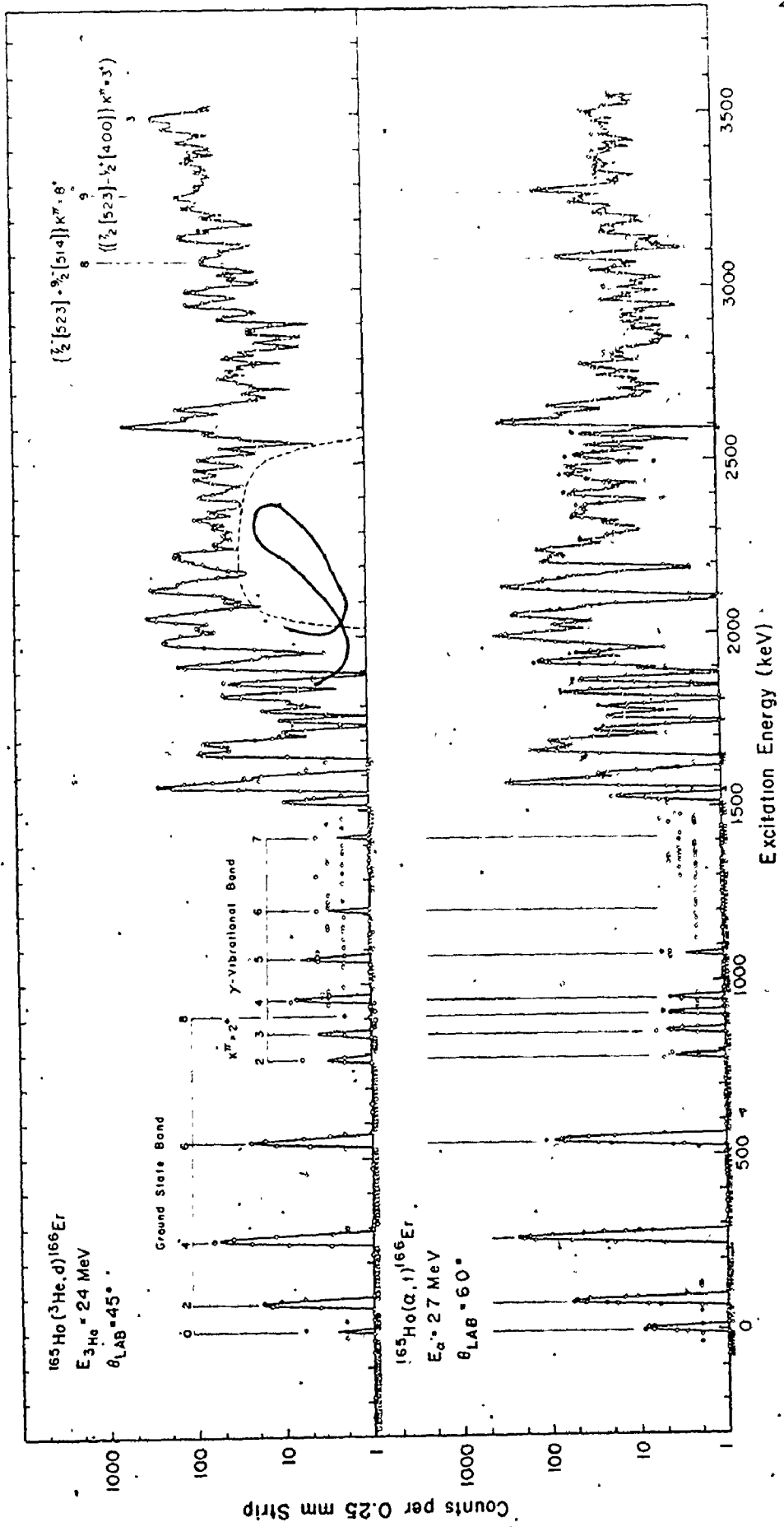


Table 2.4.1

States Observed in the Proton Transfer Reactions

(prev.)	Energy (keV)		$d\sigma/d\Omega$ ( $\mu\text{b}/\text{sr}$ )		I	K $\pi$	Interpretation
	( $^3\text{He}, d$ )	( $\alpha, t$ )	( $^3\text{He}, d$ ) $\theta=45^\circ$	( $\alpha, t$ ) $\theta=60^\circ$			
0	0	-1	<1.0	<1.0	0	0 <sup>+</sup>	7/2 <sup>-</sup> [523]-7/2 <sup>-</sup> [523]
80.6	79	80	1.6	6.1	2	0 <sup>+</sup>	7/2 <sup>-</sup> [523]-7/2 <sup>-</sup> [523]
265.0	264	264	5.2	24	4	0 <sup>+</sup>	7/2 <sup>-</sup> [523]-7/2 <sup>-</sup> [523]
545.4	543	546	2.6	10.7	6	0 <sup>+</sup>	7/2 <sup>-</sup> [523]-7/2 <sup>-</sup> [523]
785.9	786	785	<1.0	<1.0	2	2 <sup>+</sup>	$\gamma$ -Vibrational Band
859.4		859		<1.0	3	2 <sup>+</sup>	$\gamma$ -Vibrational Band <sup>a</sup>
911.2	~910	910	<1.0	<1.0	8	0 <sup>+</sup>	7/2 <sup>-</sup> [523]-7/2 <sup>-</sup> [523]
956.2	956	953	<1.0	<1.0	4	2 <sup>+</sup>	$\gamma$ -Vibrational Band
1075.3	1075	1077	<1.0	<1.0	5	2 <sup>+</sup>	$\gamma$ -Vibrational Band
1215.9	1215		<1.0	<1.0	6	2 <sup>+</sup>	$\gamma$ -Vibrational Band
1458.0		1452		<1.0			
1528.2		1529		1.6			
1572.1	1572	27	17.7	29	4	4 <sup>-</sup>	7/2 <sup>-</sup> [523]+1/2 <sup>+</sup> [411]
1596.2	1594	1.9	1.7	3.0	4	4 <sup>-</sup>	7/2 <sup>-</sup> [523]+1/2 <sup>+</sup> [411]
1665.8	1665	9.8	7.2	13.5	5	4 <sup>-</sup>	7/2 <sup>-</sup> [523]+1/2 <sup>+</sup> [411]
1680	1680	3.0	~2.6	~1.0			

(continued next page)

Table 2.4.1 (continued)

(prev.)	Energy (keV)		$d\sigma/d\Omega$ ( $\mu\text{b}/\text{sr}$ )		I	$K^\pi$	Interpretation a)	
	( $^3\text{He}, d$ )	( $\alpha, t$ )	( $^3\text{He}, d$ ) $\theta=45^\circ$	( $\alpha, t$ ) $\theta=60^\circ$				
1692.3	1692	1692	8.2	$\sim 5.0$	$\sim 12.8$	5	$4^-$	$7/2^- [523] + 1/2^+ [411]$
1719	1721	1718	1.2	1.4	2.6			
	1754	1760	$< 1.0$	$< 1.0$	2.2			
1786.9	1784	1786	1.9	1.7	2.5	6	$4^-$	$7/2^- [523] + 1/2^+ [411]$
	1813		$< 1.0$					
1827.5	1828	1828	6.4	4.9	5.7	6	$(4)^-$	$(7/2^- [523] + 1/2^+ [411])$
	1865	1863	4.4	3.5	4.5			
1917.7	1916	1915	18.0	11.9	13.8	3	$3^-$	$7/2^- [523] - 1/2^- [411]$
1938.2	1937	1939	1.4	2.0	4.5			
1979.0	1976	1976	13.2	9.2	11.2	4	$4^+$	$7/2^- [523] + 1/2^- [541]$
	1988	1989	19.4	16.9	35	7	$7^-$	$7/2^- [523] + 7/2^+ [404]$
2001.8	2002	2001	14.9	10.3	12.7	4	$3^-$	$7/2^- [523] - 1/2^+ [411]$
(2021)	2023	2021	11.7	7.3	10.4			

(continued next page)

Table 2.4.1 (continued)

Energy (keV)		$d\sigma/d\Omega$ ( $\mu\text{b}/\text{sr}$ )			Interpretation	
(prev.)	( $^3\text{He}, d$ )	( $^3\text{He}, d$ )	( $^3\text{He}, d$ )	( $\alpha, t$ )	I	$K^\pi$ a)
		$\theta=45^\circ$	$\theta=60^\circ$	$\theta=60^\circ$		
2043	2047	14.9	15.8	19.0	5	$4^+$ $7/2^- [523] + 1/2^- [541]$
2055	2058	33	19.1	17.2	(1)	$1^- [523] - 5/2^+ [402]$
					(2)	$2^- [523] - 3/2^+ [411]$
2073	2074	2.0	2.9	3.5	(5)	$3^- [523] - 1/2^+ [411]$
2113	2118	2.2	1.9	2.2	(6)	$4^+ [523] + 1/2^- [541]$
2132	2132	36	26	38	(3)	$3^+ [523] - 1/2^- [541]$
2151	2153	$\sim 13.0$	11.3	$\sim 8$	(3)	$2^- [523] - 7/2^+ [411]$
2166	2167	$\sim 3.5$	1.8	2.0	(2)	$1^- [523] - 5/2^+ [402]$
2204	2203	5.0	$\sim 6$	11.6	(3)	$1^- [523] - 5/2^+ [402]$
2217	2217	8.7	6.2	8.0	(4)	$2^- [523] - 3/2^+ [411]$
2223	2229	11.7	9.8	$\sim 5$	(4)	$3^+ [523] - 1/2^- [541]$
2240	2238	11.2	$\sim 8.5$	12.9	(4)	$3^+ [523] - 1/2^- [541]$

(continued next page)

Table 2.4.1 (continued)

Energy (keV)	$d\sigma/d\Omega$ ( $\mu\text{b}/\text{sr}$ )		I · K <sup>n</sup>	Interpretation
	( <sup>3</sup> He, d) $\theta=45^\circ$	( <sup>3</sup> He, d) $\theta=60^\circ$		
2266	4.3	3.2		3.6
2279				1.6
2290.6	3.1	1.0		
2311	4.2	2.6		2.0
2334	8.4	6.6		5.1
2347				3.4
2357	4.1	3.2		3.4
2368				
(2388)	~4	4.5		~2
2399	~6	6.3		~6
2417	~3			1.8
2436	3.4	~2.3		2.5
2451	9.3	7.6		6.1
2476	7.0	7.1		6.2

(continued next page)

Table 2.4.1 (continued)

(prev.)	Energy (keV)		$d\sigma/d\Omega$ ( $\mu\text{b}/\text{sr}$ )		I	K $\pi$	Interpretation
	( $^3\text{He}, d$ )	( $\alpha, t$ )	( $^3\text{He}, d$ ) $\theta=45^\circ$	( $^3\text{He}, d$ ) $\theta=60^\circ$			
	2503	2506	5.9	7.2			5.7
	2536	2537	3.0	5.7			3.4
	2569	2567	<2				3.0
	2583		7.7	7.0			b)
	2608	2608	74	56	6	6 $^-$	7/2 $^-$ [523]+5/2 $^+$ [402]
	2631	2633	11.9	9.5			9.8
	2655	2654	14.2	10.3			8.3
	2674	2668	5.2	3.6			2.1
	2912	2911	4.5	3.8			1.3
	2953	2955	10.9	10.0			2.1
	2994	2991	10.8	8.7			1.9
	3075	3078	6.7	$\sim 4$	8	8 $^+$	7/2 $^-$ [523]+9/2 $^-$ [514]
	3086	3088	5.0	7.5			2.8

(continued next page)

Table 2.4.1 (continued)

(prev.)	Energy (keV)		$d\sigma/d\Omega$ ( $\mu\text{b}/\text{sr}$ )		I	K $\pi$	Interpretation
	( $^3\text{He}, d$ )	( $\alpha, t$ )	( $^3\text{He}, d$ ) $\theta=45^\circ$	( $^3\text{He}, d$ ) $\theta=60^\circ$			
	3147	3146	12.4	1.9			a)
	3161	3159	10.5	1.2			
	3240	3237	11.7	4.7			
	3273	3273	11.2	6.1	9	8 $^+$	7/2 $^-$ [523]-9/2 $^-$ [514]
	3476		15.1				
	3501		25.0	22	3	3 $^-$	7/2 $^-$ [523]-1/2 $^+$ [400]

a) Predominant two-quasiparticle configuration

b) Plate join

plates.

Collection times of  $\sim 6$  hours per exposure (50,000  $\mu\text{C}$  through the target) resulted in  $\sim 350$  counts per 0.25 mm strip for the strongest peaks in the spectrum. The spectrum at  $60^\circ$  is presented in Fig. 2.4.1 (and Fig. 4.1.2). The resolution for the  $(\alpha, t)$  reaction was  $\sim 14.5$  keV FWHM.

## 2.5 Normalizations and Cross Section Calculations

During the experiments, a monitor detector was mounted in the scattering chamber to collect particles elastically scattered off the target at  $30^\circ$  to the beam direction. When the number of such scattered particles,  $N_{\text{mon}}$ , was combined with the known monitor and spectrograph solid angles ( $d\Omega_{\text{mon}}$  and  $d\Omega_{\text{sp}}$ , respectively) and the elastic scattering cross section from the DWBA calculation (cf. Sect. 3.4.b), the peak intensities in the reaction spectrum,  $N_{\text{sp}}$ , could be converted into differential cross sections.

$$\frac{d\sigma}{d\Omega} = \left(\frac{d\sigma}{d\Omega}\right)_{\text{elastic}}^{30^\circ} \times \frac{N_{\text{sp}}}{N_{\text{mon}}} \times \frac{d\Omega_{\text{mon}}}{d\Omega_{\text{sp}}} \times \frac{1}{\text{T.P.}} = Y_{\text{NORM}} \times N_{\text{sp}} \quad 2.5.1.$$

The factor T.P. is the target purity expressed as a decimal fraction.

The monitor detectors were Si(Li) particle detectors and Si surface barrier devices with sufficient resolution to separate particles scattered off the target material from those scattered by the carbon backings or light impurities in the target. Typically, the detectors that were used had

resolutions of 40 keV FWHM on the 5.48 MeV  $\alpha$  line from an  $^{241}\text{Am}$  source. The  $30^\circ$  position for the counter was employed as the count rates (which increase rapidly at forward angles) were not too high, while the elastic cross section is still  $\sim 100\%$  of the Rutherford scattering value and could thus be obtained reliably from DWBA calculations.

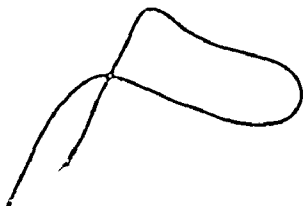
A second method of normalization involved making a short exposure immediately before or after a regular exposure. With the spectrograph set at  $30^\circ$  to the incident beam direction, the particles elastically scattered from the target material were collected on a photographic emulsion. These tracks were later counted to yield  $N_{sp}$  (short). The regular and short runs were normalized by comparing the spectrograph solid angles and integrated currents through the targets ( $d\Omega_{sp}$  and  $d\Omega_{sp}$  (short), I.C. and I.C. (short) respectively), and the differential cross section was calculated using the expression

$$\begin{aligned} \frac{d\sigma}{d\sigma} &= \left(\frac{d\sigma}{d\sigma}\right)_{\text{elastic}}^{30^\circ} \times \frac{N_{sp}}{N_{sp}(\text{short})} \times \frac{d\Omega_{sp}(\text{short})}{d\Omega_{sp}} \times \frac{\text{I.C.}(\text{short})}{\text{I.C.}} \times \frac{1}{T.P.} \\ &= Y_{\text{NORM}} \times N_{sp} \end{aligned} \quad 2.5.2$$

The  $Y_{\text{NORM}}$  values obtained by the two methods usually agreed to within 10%.

The error in the  $Y_{\text{NORM}}$  calculation is estimated to be  $\sim 15\%$ , while the error in the counting and fitting of the

data was  $\sim 5 - 10\%$ . When combined with the statistical error, these gave a total error in the cross section of typically 16 - 20% for the largest "clean" peaks in the spectra, a value consistent with observations from repeated measurements.



## CHAPTER 3

### THEORETICAL CONSIDERATIONS

#### 3.1 General

The nucleus  $^{166}\text{Er}$  exhibits the rotational band structure characteristic of a deformed nucleus, and so in this work it is studied in the context of the Unified model. This chapter will briefly discuss some of the theoretical aspects of nuclear shapes and vibrational excitations. The Unified model with pairing and various mixing effects will be considered, and finally, an outline of the reaction formalism will be presented.

Many comprehensive treatments of the theory, as applied to nuclei in the deformed rare earth region already exist (Bunker and Reich, 1971; Jones, 1969). Thus, much of the material covered in this section is based, to a large extent, on these previous studies.

#### 3.2 Nuclear Shapes and Vibrations

The shape of a deformed nucleus can be defined in terms of the spherical harmonics, the nuclear radius being (Bohr, 1952) \*

$$R(\theta, \phi) = R_0 \left( 1 + \sum_{\lambda\mu} a_{\lambda\mu} Y_{\lambda\mu}(\theta, \phi) \right). \quad 3.2.1$$

Here,  $R_0 \approx 1.2A^{1/3}$  fm, the  $a_{\lambda\mu}$  are coefficients defining the nuclear shape and the  $Y_{\lambda\mu}(\theta, \phi)$  are normalized spherical

harmonics of order  $\lambda$  and projection  $\mu$ . As  $\lambda = 1$  is equivalent to a translation of the system, the lowest term considered in the expansion is commonly  $\lambda = 2$  (quadrupole deformation). The parameters of the quadrupole deformation are usually expressed in terms of two new parameters,  $\beta$  and  $\gamma$ , such that

$$\begin{aligned} a_{21} &= a_{2-1} = 0 \\ a_{20} &= \beta \cos \gamma \\ a_{22} &= a_{2-2} = \frac{1}{\sqrt{2}} \beta \sin \gamma \end{aligned} \quad 3.2.2$$

and

$$R = R_0 \left[ 1 + \sqrt{\frac{5}{16\pi}} \beta (\cos \gamma (3 \cos^2 \theta - 1) + \sqrt{3} \sin \gamma \sin^2 \theta \cos 2\phi) \right] \quad 3.2.3$$

Thus,  $\beta$  is a measure of the departure from sphericity ( $0 \leq \beta \leq \infty$ ) and  $\gamma$  is a measure of the departure from axial symmetry ( $0^\circ \leq \gamma \leq 60^\circ$ ). Another commonly used deformation parameter,  $\delta$ , is related to  $\beta$ , according to

$$\delta = 3 \sqrt{\frac{5}{16\pi}} \beta \approx 0.95\beta.$$

As the multipole terms of odd order do not contribute to the equilibrium ground state and the  $\lambda = 4$  (hexadecapole) terms are small (cf. Sect. 3.3d), the deformed nuclear shape is commonly characterized by  $\beta$ . If the "radius" along the symmetry axis is longer than that along the minor axes ( $\beta > 0$ ), the nucleus is "prolate"

(football shaped); if the "radius" in a plane normal to the symmetry axis is longer than that along this axis ( $\beta < 0$ ), the nucleus is "oblate" (hamburger shaped). Of course,  $\beta = 0$  defines a spherical nucleus.

Oscillations in the nuclear shape can occur. Theoretically, these collective motions of the nuclear matter can be viewed as complex "surface waves" moving around the nuclear body, giving rise to the appearance of vibrational motion. The angular momentum associated with these coherent particle motions allows the classification of the oscillations (in quanta called phonons) by their multipole order  $\lambda$  and projection  $\kappa$  ( $\equiv \mu$ ). The quadrupole ( $\lambda = 2$ ) vibrations can exist as oscillations of either the parameter  $\beta$  ( $\kappa = 0$ ) or  $\gamma$  ( $\kappa = 2$ ). In this mass region the quadrupole phonons typically have energies of 0.5 to 1.0 MeV.

While a static octupole ( $\lambda = 3$ ) deformation does not have good parity and hence cannot exist, octupole vibrations are permitted. The  $\kappa = 0$  octupole vibration has a pear shape with the bulge alternating between the ends of the nucleus. The other projections have more complicated shapes; for  $\kappa = 2$  it is  $\sim e^{im\phi} \cos\theta \sin^2\theta$  which would appear as an annular collar oscillating on the nuclear surface in a direction parallel to the principal axis.

### 3.3 The Unified Model

#### (a) The Model

The well known spherical shell model (Mayer and Jensen, 1955) successfully describes such nuclear effects as the shell closures (magic numbers) and the spins of low lying single particle levels in odd nuclei. On the other hand, the liquid drop model (Rainwater, 1950) accounted for observed deformations by minimizing the total nuclear energy as a function of the nuclear shape. However, neither model adequately described the observed spectra of deformed nuclei (such as those in the rare earth region), and so the unified model was developed. This model combines the shell and deformed liquid drop models by using a deformed potential to determine the single particle energies. It also incorporates collective effects such as vibrational and rotational motions. Thus, the Unified model gives rise to three terms in the nuclear Hamiltonian:  $H_{\text{DSP}}$ ,  $H_{\text{VIB}}$  and  $H_{\text{ROT}}$ :

The nuclear Hamiltonian, used to theoretically describe the experimentally observed nucleus, further includes effects due to pairing and mixings other than the rotational Coriolis term, so that

$$H_{\text{NUC}} = H_{\text{DSP}} + H_{\text{VIB}} + H_{\text{ROT}} + H_{\text{PAIRING}} + H_{\text{MIXING}}. \quad 3.3.1$$

Before discussing these terms in detail, digressions concerning the separability of the nuclear wave functions and the angular momentum notation are made.

### (b) Wave Function Separability

When the Unified model for the odd nucleus was proposed, the separation of the wavefunction into an inert deformed core and a single particle outside this core was adopted as an approximation to simplify the problem. In this approximation, the core rotations and vibrations were not considered to interact with the single particle motion, but this was soon modified to accept the now familiar Coriolis (rotation-particle) coupling. Other theoretical alternatives are available (e.g. Immele and Struble (1977)), but due to its simplicity, this separability approximation is still in general use. Specifically, in  $^{166}\text{Er}$ , the vibrational modes can be considered to result from coherent particle motions. This may result in large two quasi-particle components appearing in the vibrational wavefunctions (cf. Sect. 4.2.c).

### (c) Angular Momentum Notation

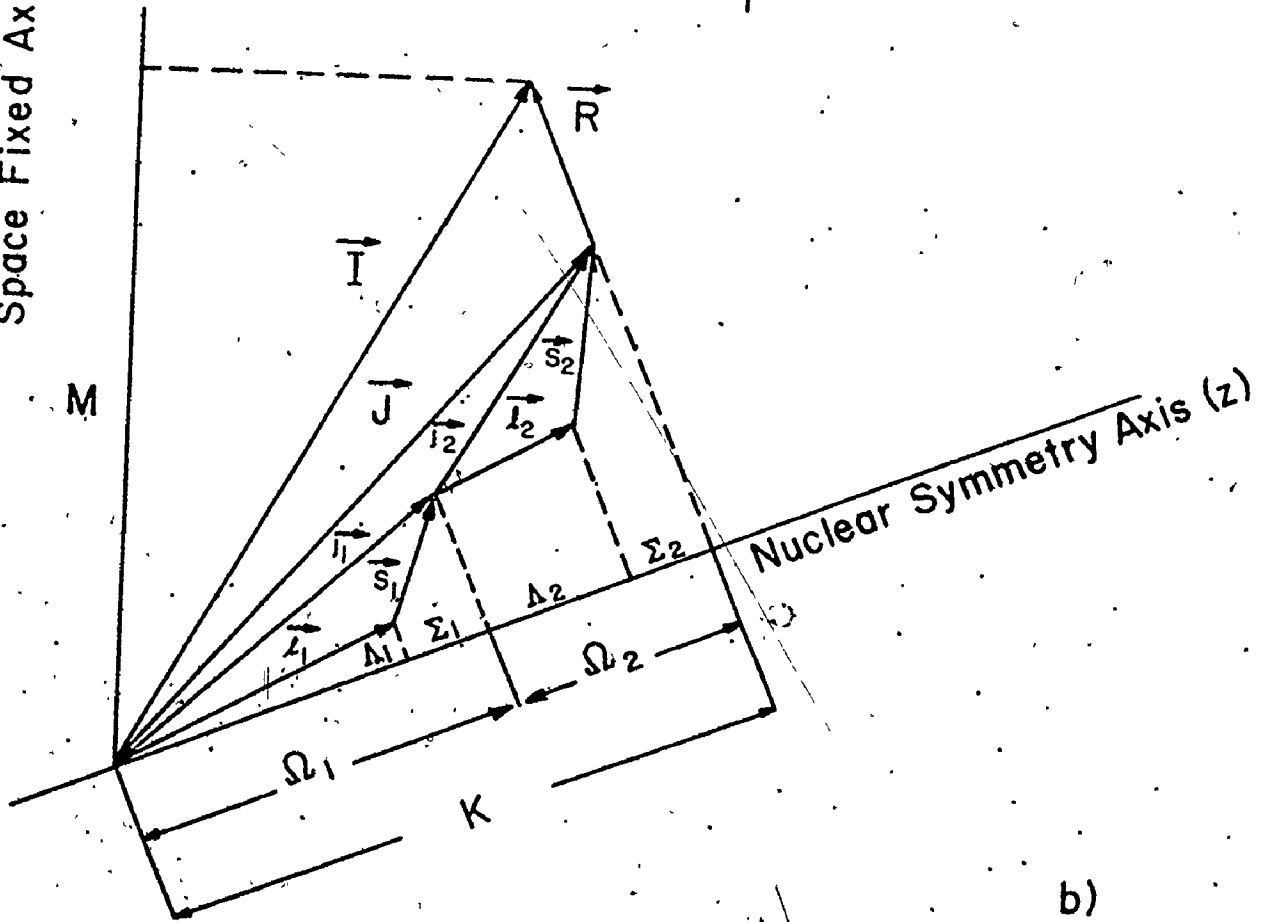
In discussing the angular momentum notation, separability of the wavefunction is assumed. Thus, for this ideal case the Coriolis interaction does not exist, and  $K$  is considered to be a good quantum number.

With reference to Fig. 3.3.1a, an axially symmetric deformed nucleus has an angular momentum vector  $\vec{R}$  associated with a rotation of the nucleus about an axis perpendicular to the symmetry axis  $z$ . If there is only one odd particle moving in an orbit rotating with the core, it has angular

Fig. 3.3.1

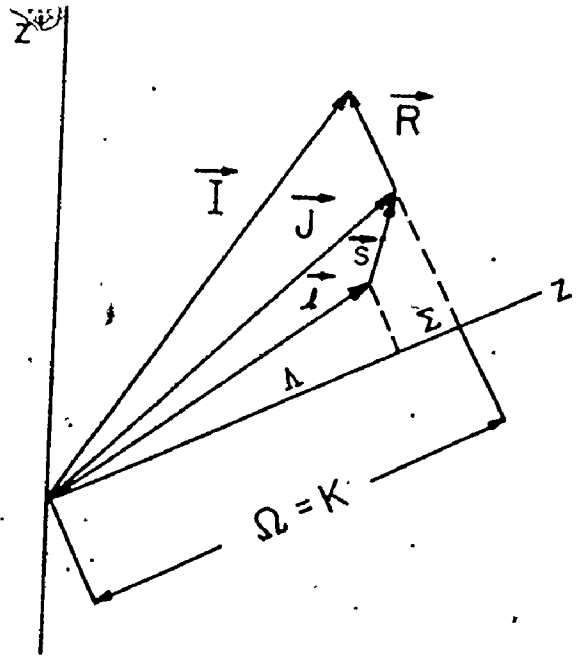
Angular momenta coupling schemes for a) odd A nuclei, and  
b) two-quasiparticle states in even-even or odd-odd nuclei.

Space Fixed Axis ( $z'$ )



b)

a)



momentum  $\vec{j} (= \vec{l} + \vec{s})$  which is not a conserved quantity. However, the total spin  $\vec{I} (= \vec{j} + \vec{R})$  is a constant of the motion as are its projections  $M$  and  $K$  on the space fixed and nuclear symmetry axes respectively. As  $K$  is a good quantum number, so too is  $\Omega$ , the projection of  $\vec{j}$  along the symmetry axis. The projections of  $\vec{l}$  and  $\vec{s}$  on the symmetry axis are  $\Lambda$  and  $\Sigma$  respectively, such that  $\Omega = \Lambda + \Sigma$ ,  $\Sigma = \pm \frac{1}{2}$ . The coupling of two particles outside the core is shown in Fig. 3.3.1b. Again,  $I$ ,  $M$  and  $K = |\Omega_1| + |\Omega_2|$  (parallel coupling as shown) or  $K = ||\Omega_1| - |\Omega_2||$  (anti-parallel coupling) are constants of the motion. (This is true for  $K$ , barring any mixing due to the Coriolis interaction (cf. Sec. 3.3.f).)

#### (d) The Nilsson Model

The properties of a nucleon in a deformed potential well were studied by Nilsson (Nilsson, 1955) with the Hamiltonian (cf. eq.3.3.1)

$$H_{\text{DSP}} = \frac{p^2}{2m} + V(r) + C\vec{l} \cdot \vec{s} + D\vec{l} \cdot \vec{l} \quad 3.3.2$$

where  $V(r)$  is a deformed harmonic oscillator potential

$$V(r) = \frac{1}{2} m \omega_0^2 r^2 (1 - 2\beta Y_2^0(\theta, \phi)). \quad 3.3.3$$

$C$ ,  $D$  and  $\omega_0$  were chosen so as to reproduce the spherical shell model energies ( $\beta = 0$ ). They are usually replaced by the parameters  $\kappa$  and  $\mu$  given by

$$\kappa = -C/2\hbar\omega_0$$

and

3.3.4

$$\mu = 2D/C$$

For the rare earth region commonly used values for these parameters are (Lamm, 1969; Nilsson et al. 1969)

$$\kappa = 0.0637 \quad \mu = 0.600 \quad (\text{for protons})$$

$$\kappa = 0.0637 \quad \mu = 0.420 \quad (\text{for neutrons}).$$

The Nilsson Hamiltonian ( $H_{\text{DSP}}$ ) can be rewritten with a spherically symmetric term  $H_0^0$ , and a deformed term,  $H_\delta$ , such that

$$H_{\text{DSP}} = H_0^0 + H_\delta + C\vec{l} \cdot \vec{s} + D\vec{l} \cdot \vec{l}, \quad 3.3.5$$

where

$$H_0^0 = \frac{1}{2}\hbar\omega_0 [-v^2 + \rho^2]$$

$$\text{and} \quad \rho^2 = \frac{m\omega_0}{\hbar} r^2. \quad 3.3.6$$

The  $H_\delta$  term can be expanded (Nilsson et al., 1969) in terms of the spherical harmonics or Legendre polynomials

$$H_\delta = \frac{1}{2}\hbar\omega_0 \rho^2 \left(1 - \frac{2}{3} \epsilon_2 P_2(\cos\theta)\right). \quad 3.3.7$$

Nilsson et al. (1969) also introduced the hexadecapole deformation as a  $P_4(\cos\theta)$  term,

$$H_{\delta} = \frac{1}{2} \hbar \omega_0 \rho^2 \left(1 - \frac{2}{3} \epsilon_2 P_2(\cos\theta) + 2\epsilon_4 P_4(\cos\theta)\right). \quad 3.3.8$$

The Nilsson Hamiltonian with the hexadecapole term included in  $H_{\delta}$  is used in the code NILS to generate the single particle energies  $\epsilon_{\nu}$  (cf. Sec. 3.3.g). In this work on  $^{166}\text{Er}$  the values of  $\epsilon_2 (=0.29)$  and  $\epsilon_4 (= -0.0125)$  were obtained from a study of the systematic variation of these parameters over the rare earth mass region.

The Hamiltonian (eq. 3.3.5) was solved using the basis  $|N\ell j\Omega\rangle$  (Chi, 1967) in which all the terms, except  $H_{\delta}$ , are diagonal such that -

$$\begin{aligned} \frac{1}{2}[-\nabla^2 + \rho^2] |N\ell j\Omega\rangle &= (N+3/2) |N\ell j\Omega\rangle & N=0, 1, 2, \dots \\ \ell^2 |N\ell j\Omega\rangle &= \ell(\ell+1) |N\ell j\Omega\rangle & \ell=N, (N-1), \dots, 1 \text{ or } 0 \\ j^2 |N\ell j\Omega\rangle &= j(j+1) |N\ell j\Omega\rangle & j=\ell \pm \frac{1}{2} \\ j_z |N\ell j\Omega\rangle &= \Omega |N\ell j\Omega\rangle & \Omega=-j, -(j-1), \dots, (j-1), j. \end{aligned} \quad 3.3.9$$

Thus, all terms with  $N' \neq N$  vanish except for those involving  $H_{\delta}$ , which connects states with  $\Delta N = 0, \pm 2$  (cf. Sect. 3.3.h.2)

The energy levels resulting from such a calculation are shown as a function of the deformation  $\epsilon_2$  in Fig. 3.3.2 for neutron states and in Fig. 3.3.3 for proton states where they are labelled with the asymptotic quantum numbers  $\Omega^{\pi} [Nn_2 \Lambda]$ . Each level can contain a pair of nucleons, one nucleon having projection  $\Omega$ , the other  $-\Omega$ . For ease of notation the parity is often not included in the orbital

Fig. 3.3.2

Nilsson diagram for neutron orbitals. ( $\kappa = 0.0637$  and  
 $\mu = 0.42$ ).

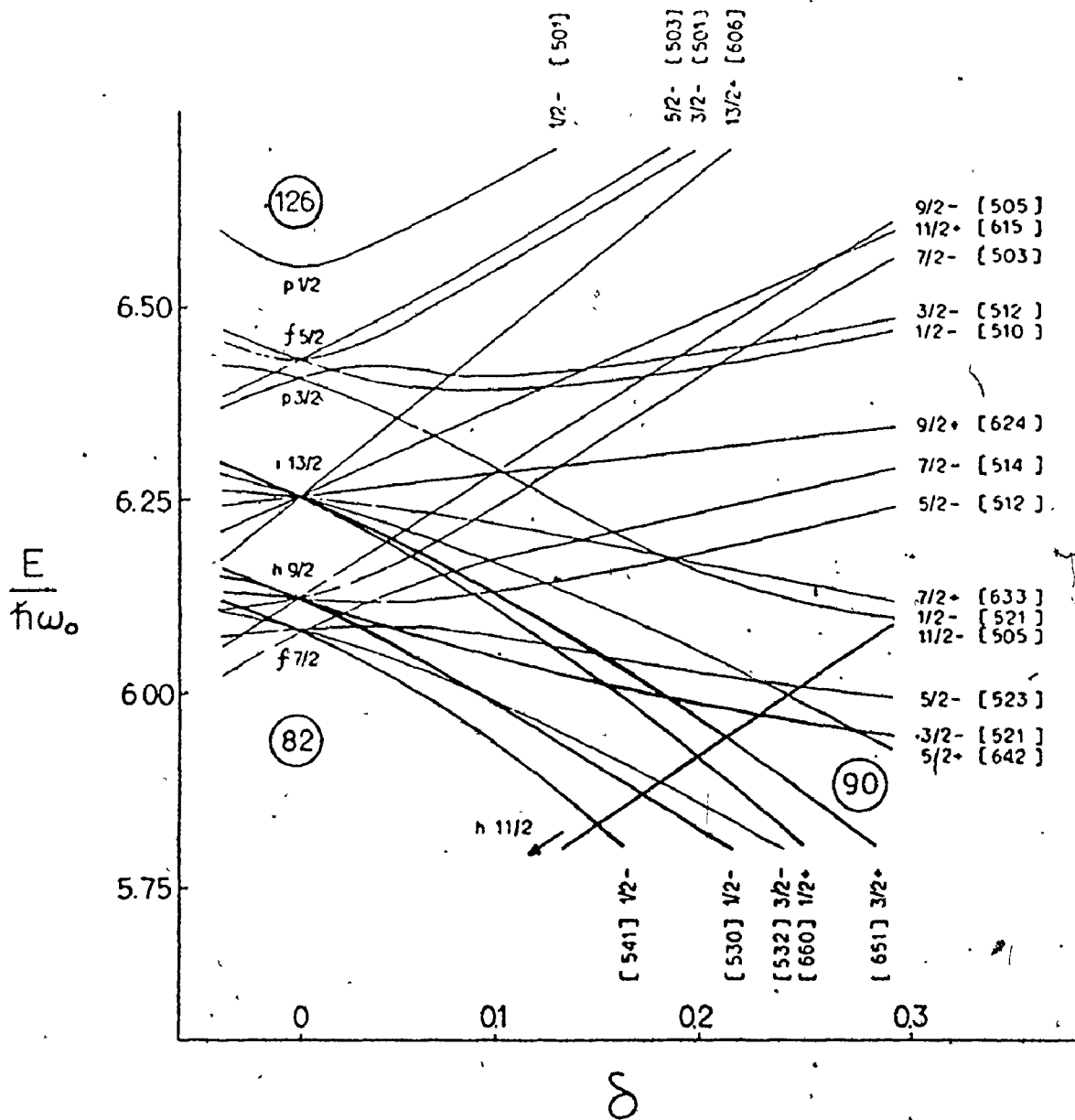
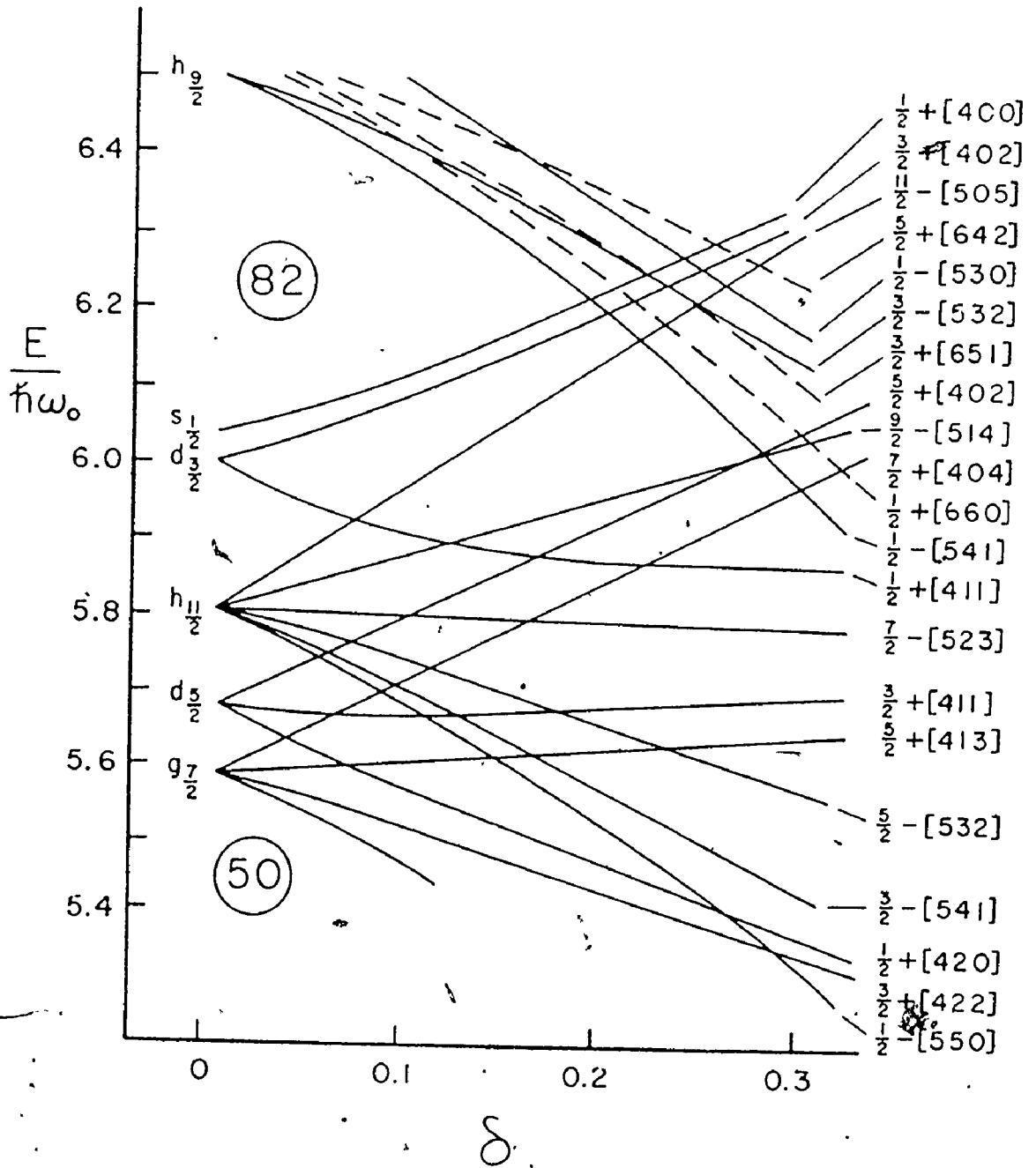


Fig. 3.3.3

Nilsson diagram for proton orbitals. ( $\kappa = 0.0037$  and  
 $\mu = 0.60$ ).



label and is  $(-1)^N$ .

The deformed single particle wavefunctions,  $\chi_{N\Omega}$ , corresponding to the labels  $\Omega\{Nn_z\Lambda\}$  are commonly expressed as a sum of spherical basis functions  $|N\ell j\Omega\rangle$ ,

$$\chi_{N\Omega} = \sum_{j\ell} C_{j\ell}(N,\Omega) |N\ell j\Omega\rangle \quad \Omega \leq j \leq N+\frac{1}{2}. \quad 3.3.10$$

The spherical expansion coefficients  $C_{j\ell}$  indicate the amplitude of each spherical state contained in the Nilsson orbital. For all calculations involving these wavefunctions the phase convention of Chi (1967) was followed for the  $C_{j\ell}$  coefficients.

#### (e) The Vibrational Hamiltonian

The vibrations which commonly occur in the rare earth nuclei have been discussed in Sec. 3.2, but in general, the vibrational states have not been considered theoretically as a microscopic treatment is beyond the scope of this work. (cf. e.g. Zheleznova et al., 1965; Immele and Struble, 1977). In addition, the single particle transfer reactions, such as those used in this study, do not usually populate purely collective excitations. However, in the case where one two-quasiparticle component makes up a large part of the vibrational wavefunction (e.g. the  $K^\pi = 2^-$  octupole vibration), population of these states by direct reactions can occur, and a more detailed investigation is attempted.

## (f) The Rotational Hamiltonian

The rotational energy of a deformed nucleus is given by

$$H_{\text{ROT}} = \frac{\hbar^2}{2\mathcal{I}} \vec{R}^2 \quad 3.3.11$$

where  $\mathcal{I}$  is the moment of inertia and the quantity  $\frac{\hbar^2}{2\mathcal{I}}$  is known as the rotational parameter,  $A$ . With reference to Fig. 3.3.1 and to the angular momentum quantities discussed above

$$\vec{R} = \vec{I} - \vec{j} \quad 3.3.12$$

and  $\vec{j} = \vec{j}_1 + \vec{j}_2$  for the two particles outside the core.  $\vec{R}$  can be further expanded such that

$$\begin{aligned} \vec{R}^2 &= R_x^2 + R_y^2 \\ &= (I_x - j_x)^2 + (I_y - j_y)^2 \\ &= (\vec{I}^2 - I_z^2) + (\vec{j}^2 - j_z^2) - 2(I_x j_x + I_y j_y) \end{aligned} \quad 3.3.14$$

By writing the second term in component form

$$\vec{j}^2 - j_z^2 = j_1^2 + j_2^2 - j_{1z}^2 - j_{2z}^2 + 2(j_{1x}j_{2x} + j_{1y}j_{2y}), \quad 3.3.15$$

and using the following labelling

$$H_R = A[I^2 - I_z^2 - j_{1z}^2 - j_{2z}^2 + j_1^2 + j_2^2]$$

$$H_{\text{PP}} = 2A[j_{1x}j_{2x} + j_{1y}j_{2y}]$$

$$\text{and } H_{\text{RPC}} = -2A\{I_x J_x + I_y J_y\} \quad 3.3.16$$

the rotational Hamiltonian can be written

$$H_{\text{ROT}} = H_R + H_{\text{PP}} + H_{\text{RPC}}. \quad 3.3.17$$

The antisymmetrized wave function for the even-even nuclear states is given in the separable form by (Hirning, 1975),

$$\begin{aligned} |IMK=\Omega_1+\Omega_2\rangle = & \left( \frac{2I+1}{(1+\delta_{12}) 32\pi^2} \right)^{\frac{1}{2}} \sum_{j_1 j_2} C_{j_1}^{\Omega_1} C_{j_2}^{\Omega_2} \{ [ \chi_{j_1}^{\Omega_1}(1) \chi_{j_2}^{\Omega_2}(2) \\ & - \chi_{j_2}^{\Omega_2}(1) \chi_{j_1}^{\Omega_1}(2) ] D_{MK}^I + (-)^{I-j_1-j_2} [ \chi_{j_1}^{-\Omega_1}(1) \chi_{j_2}^{-\Omega_2}(2) \\ & - \chi_{j_2}^{-\Omega_2}(1) \chi_{j_1}^{-\Omega_1}(2) ] D_{M-K}^I \} \quad 3.3.18 \end{aligned}$$

where the  $\chi$ 's are the intrinsic Nilsson wavefunctions (cf. Sect. 3.3.d)  $D$ 's are the usual rotation functions and the  $C_j^\Omega$  are the  $C_{j\ell}$ 's defined above.

When the matrix elements of this wavefunction are taken with  $H_{\text{ROT}}$  the diagonal matrix elements of  $H_R$  and  $H_{\text{PP}}$  give non-zero contributions,

$$\begin{aligned}
E_{\text{DIAGONAL}} &= \langle \text{IMK} = \Omega_1 + \Omega_2 | H_R + H_{\text{PP}} | \text{IMK} = \Omega_1 + \Omega_2 \rangle \\
&= E_0 + \frac{\hbar^2}{2\alpha} \{ [I(I+1) - K(K+1)] + (-)^{I+1} a_1 a_2 \delta_{K0} \delta_{\Omega_1, \frac{1}{2}} \\
&\quad + (-)^I \sum_{j_1 j_2} C_{j_1}^{\Omega_1} C_{j_1}^{\Omega_2} C_{j_2}^{\Omega_1} C_{j_2}^{\Omega_2} \delta_{K0} \delta_{N_1 N_2} \delta_{(1)(2)} \sqrt{j_1(j_1+1) + j_2(j_2+1)} \}.
\end{aligned}$$

Off-diagonal matrix elements are also generated for the rotational Hamiltonian. For  $H_R$  these are given by

$$\begin{aligned}
E_{\text{OD}} &= \langle \text{IMK} = \Omega_1' + \Omega_2' | H_R | \text{IMK} = \Omega_1 + \Omega_2 \rangle \\
&= \frac{\hbar^2}{2\alpha} \{ \sum_j [C_j^{\Omega_1'} C_j^{\Omega_1} \delta_{\Omega_1' \Omega_1} \delta_{2,2} + C_j^{\Omega_2'} C_j^{\Omega_2} \delta_{\Omega_2' \Omega_2} \delta_{1,1}] j(j+1) \\
&\quad - \sum_j [C_j^{\Omega_1'} C_j^{\Omega_2} \delta_{\Omega_1' \Omega_2} \delta_{2,1} + C_j^{\Omega_2'} C_j^{\Omega_1} \delta_{\Omega_2' \Omega_1} \delta_{1,2}] j(j+1) \\
&\quad - \sum_{j_1 j_2} \delta_{K,0} (-1)^{I-j_1-j_2} C_{j_2}^{\Omega_1'} C_{j_1}^{\Omega_2'} C_{j_1}^{\Omega_1} C_{j_2}^{\Omega_2} [j_1(j_1+1) + j_2(j_2+1)] \\
&\quad \times \delta_{\Omega_2', -\Omega_2} \delta_{\Omega_1', -\Omega_1}.
\end{aligned} \tag{3.3.20}$$

The term  $\delta_{2,2}$  implies the Nilsson state corresponding to  $\Omega_2'$  must be the same as that corresponding to  $\Omega_2$ .

The particle-particle interaction couples states

with the same  $K$ , but having  $\Omega$ 's differing by 1, e.g. if

$$\Omega_1 = \Omega_1' - 1 \text{ then } \Omega_2 = \Omega_2' + 1:$$

$$E_{PP} = \langle IMK = \Omega_1' + \Omega_2' | H_{PP} | IMK = \Omega_1 + \Omega_2 \rangle$$

$$= \frac{\hbar^2}{2\alpha} \sum_{\substack{j_1 j_2 \\ j_1' j_2'}} C_{j_1'}^{\Omega_1'} C_{j_2'}^{\Omega_2'} C_{j_1}^{\Omega_1} C_{j_2}^{\Omega_2} \sqrt{(j_1 + \Omega_1 + 1)(j_1 - \Omega_1)(j_2 - \Omega_2 + 1)(j_2 + \Omega_2)}$$

$$\times [ \delta_{j_1' j_1} \delta_{j_2' j_2} \delta_{\Omega_1' \Omega_1 + 1} \delta_{\Omega_2' \Omega_2 - 1} (-)^{I - j_1 - j_2} \delta_{K0} \delta_{j_2' j_1} \delta_{j_1' j_2} \delta_{\Omega_2' - \Omega_1 - 1} \delta_{\Omega_1' - \Omega_2 + 1} ]$$

$$+ \sqrt{(j_2 + \Omega_2 + 1)(j_2 - \Omega_2)(j_1 - \Omega_1 + 1)(j_1 + \Omega_1)} [ \delta_{j_1' j_1} \delta_{j_2' j_2} \delta_{\Omega_1' \Omega_1 - 1} \delta_{\Omega_2' \Omega_2 + 1}$$

$$+ (-)^{I - j_1 - j_2} \delta_{K0} ( \delta_{j_1' j_1} \delta_{j_2' j_2} \delta_{\Omega_1', -\Omega_1 + 1} \delta_{\Omega_2', -\Omega_2 - 1} \delta_{j_2' j_1} \delta_{j_1' j_2} \delta_{\Omega_2', -\Omega_2 + 1} \delta_{\Omega_1', -\Omega_2 - 1} ) ] \quad 3.3.21$$

$$\delta_{\Omega_2', -\Omega_2 + 1} \delta_{\Omega_1', -\Omega_2 - 1} ] ] .$$

The breakdown of the separability assumption involving the rotational and particle motions is accounted for by the Coriolis or rotation-particle coupling,  $H_{RPC}$ .  $H_{RPC}$  has the effect of mixing states with  $\Delta K = \pm 1$ , implying that for the Coriolis mixed states  $K$  is no longer a good quantum number.

$$\begin{aligned}
& \langle \text{IMK}' = \Omega_1' + \Omega_2' \mid H_{\text{RPC}} \mid \text{IMK} = \Omega_1 + \Omega_2 \rangle = \\
& - \frac{\hbar^2}{2\lambda} (1 + \delta_{K0} \delta_{12})^{-\frac{1}{2}} (1 + \delta_{K'0} \delta_{1'2}) \\
& \times \{ [\sum_j C_j^{\Omega_1'} C_j^{\Omega_1} \sqrt{(j - \Omega_1 + 1)(j + \Omega_1)} \delta_{\Omega_1' \Omega_1 - 1} \delta_{2'2} \\
& + \sum_j C_j^{\Omega_2'} C_j^{\Omega_2} \sqrt{(j - \Omega_2 + 1)(j + \Omega_2)} \delta_{\Omega_2' \Omega_2 - 1} \delta_{1'1} \\
& - \sum_j C_j^{\Omega_1'} C_j^{\Omega_2} \sqrt{(j - \Omega_2 + 1)(j + \Omega_2)} \delta_{\Omega_1' \Omega_2 - 1} \delta_{2'1} \\
& - \sum_j C_j^{\Omega_2'} C_j^{\Omega_1} \sqrt{(j - \Omega_1 + 1)(j + \Omega_1)} \delta_{\Omega_2' \Omega_1 - 1} \delta_{1'2}] \\
& \times \delta_{K'K-1} \delta_{N'N} \sqrt{(I - K + 1)(I + K)} \\
& + [\sum_j C_j^{\Omega_1'} C_j^{\Omega_1} \sqrt{(j + \Omega_1 + 1)(j - \Omega_1)} \delta_{\Omega_1' \Omega_1 + 1} \delta_{2'2} \\
& + \sum_j C_j^{\Omega_2'} C_j^{\Omega_2} \sqrt{(j + \Omega_2 + 1)(j - \Omega_2)} \delta_{\Omega_2' \Omega_2 + 1} \delta_{1'1} \\
& - \sum_j C_j^{\Omega_1'} C_j^{\Omega_2} \sqrt{(j + \Omega_2 + 1)(j - \Omega_2)} \delta_{\Omega_1' \Omega_2 + 1} \delta_{2'1} \\
& - \sum_j C_j^{\Omega_2'} C_j^{\Omega_1} \sqrt{(j + \Omega_1 + 1)(j - \Omega_1)} \delta_{\Omega_2' \Omega_1 + 1} \delta_{1'2}]
\end{aligned}$$

$$\times \delta_{K', K+1} \delta_{N', N} \sqrt{(I + K + 1)(I - K)}$$

$$+ (-)^{I+1+N_1+N_2} \sum_j (-)^{N_1+j-\frac{1}{2}} C_j^{\Omega_1'} C_j^{\Omega_1} \sqrt{(j-\Omega_1+1)(j+\Omega_1)} \delta_{\Omega_1', -\Omega_1+1} \delta_{2', 2}$$

$$- \sum_j (-)^{N_2+j-\frac{1}{2}} C_j^{\Omega_1'} C_j^{\Omega_2} \sqrt{(j-\Omega_2+1)(j+\Omega_2)} \delta_{\Omega_1', -\Omega_2+1} \delta_{2', 1}$$

$$- \sum_j (-)^{N_1+j-\frac{1}{2}} C_j^{\Omega_2'} C_j^{\Omega_1} \sqrt{(j-\Omega_1+1)(j+\Omega_1)} \delta_{\Omega_2', -\Omega_1-1} \delta_{1', 2}]$$

$$\times \delta_{K', -K+1} \delta_{N', N} \sqrt{(I - K + 1)(I + K)}$$

The Coriolis interaction will be particularly important when three conditions are met. First, the  $C_j^\Omega$ 's should have reasonably large values in both states for the same values of  $j$ . This is ensured when both interacting states involve orbitals originating from the same shell model configuration in the spherical limit. Second, when these  $C_j^\Omega$  with large values are found for large values of  $j$ , the matrix elements will be enhanced. The enhancement is somewhat more pronounced if the projections of the  $j$ 's  $\Omega_1$  and  $\Omega_2$ , are rather small in value. The third factor producing an increased Coriolis interaction is a large value for  $I$ , combined with smaller values for  $K$ . For example, very strong Coriolis mixing would be expected between the high spin ( $I$ ) members of the  $7/2^+[633]-5/2^+[642]$   $K = 1$  band and the  $7/2^+[633]-3/2^+[651]$   $K = 2$  band. As both the  $5/2^+[642]$  and  $3/2^+[651]$  orbitals originate with the  $i_{13/2}$  shell model state in the zero-deformation limit, the  $C_j^\Omega$  from both configurations will be large for  $j = 13/2$  (and the  $\Omega$  values are only  $5/2$  and  $3/2$ ). Thus, all the conditions for a strong Coriolis interaction are satisfied.

All the above matrix elements are modified by multiplicative factors due to the pairing interaction. These are presented at the end of the following subsection.

## (g) The Pairing Interaction

A well known feature of even-even nuclei is the existence of an energy gap between the ground state and the intrinsic (non-collective) excited states. This is attributed to the pairing interaction, as these excited states are formed by the coupling of two unpaired particles, as opposed to the ground state where the much lower energy (typically 1-2 MeV) is due to the pairing of particles in the same orbital. The pairing force is responsible not only for this energy gap, but also for the diffuseness of the Fermi surface (Fig. 3.3.4). In the absence of the pairing interaction the single particle Nilsson levels would be filled (with two nucleons each) in order of increasing energy. The level at which all nucleons would have been accounted for represents a sharp Fermi level ( $\epsilon_F$ ). No population of levels above the Fermi level would occur, and below it all levels would be completely filled (bottom, Fig. 3.3.4).

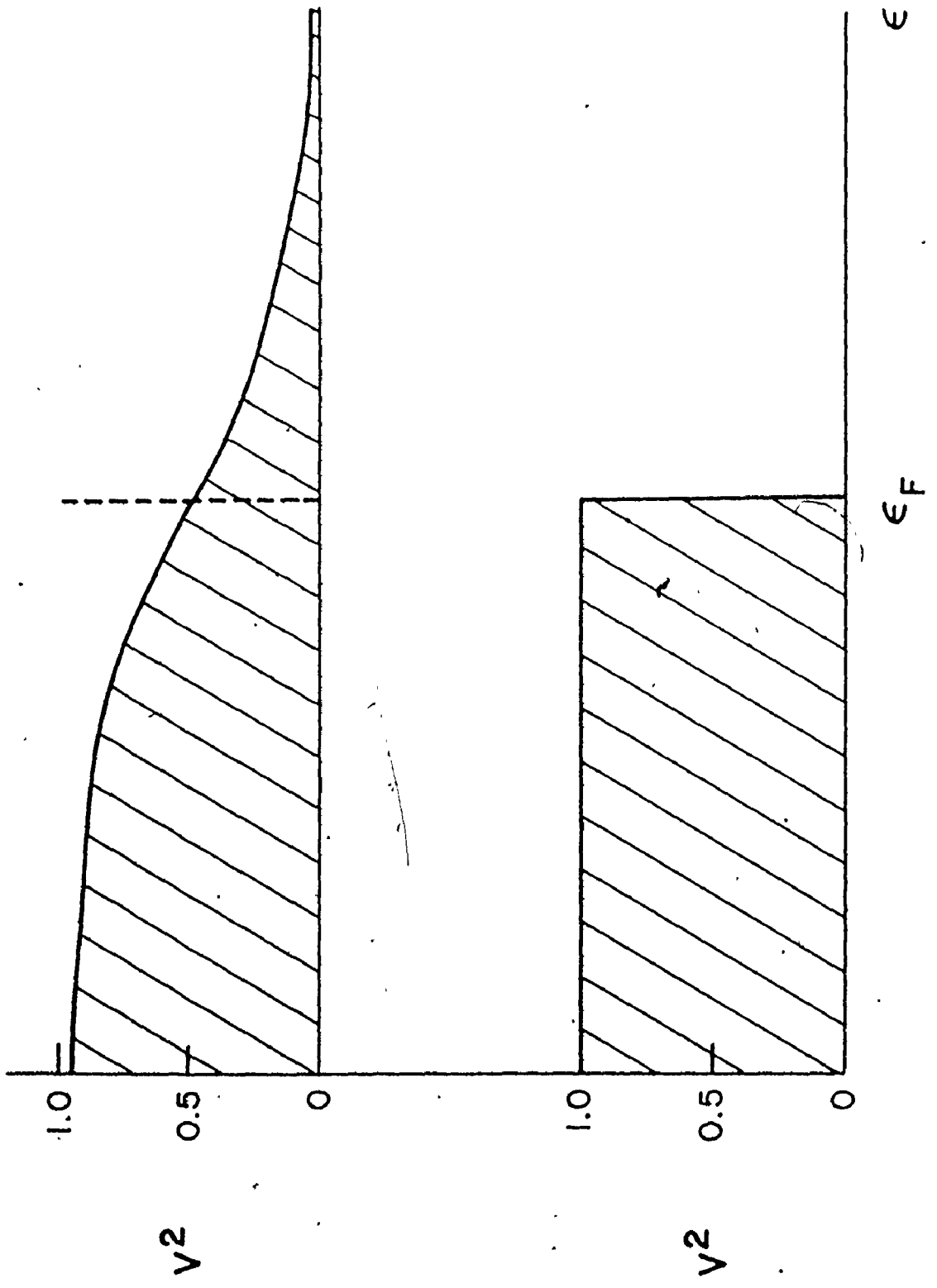
The BCS formalism is used to describe the effects of the pairing interaction (Bohr et al., 1958; Nathan and Nilsson, 1965). In the second quantization notation the pairing Hamiltonian is written as (Bardeen et al., 1957)

$$H_{\text{PAIRING}} = \sum_{\nu} \epsilon_{\nu} (a_{\nu}^{\dagger} a_{\nu}^{\dagger} a_{\nu} a_{\nu}) + \frac{G}{2} \sum_{\nu, \mu} a_{\nu}^{\dagger} a_{\nu}^{\dagger} a_{\mu} a_{\mu} \quad 3.3.23$$

where  $a_{\nu}^{\dagger}$  is a creation operator for the particle in the

Fig. 3.3.4

The fullness parameter vs. the single particle energy for a finite pairing interaction (upper) and for no pairing interaction (lower).  $\epsilon_F$  is the Fermi level.



deformed single particle state  $v$ ,

$a_v$  is the corresponding annihilation operator,

$\bar{v}$  is the time reversed state of  $v$ ,

and  $\epsilon_v$  is the energy of the single particle state  $v$ . (cf. Sec. 3.3.d).

In this formalism the ground state of the even-even nucleus is written as

$$\psi_g = \prod_v (U_v + V_v a_v^+ a_{\bar{v}}^+) |0\rangle \quad 3.3.24$$

where the product is over all single particle energy levels  $v$ , and  $|0\rangle$  is the vacuum state.  $U_v^2$  is the probability that the level  $v$  is empty;  $V_v^2$  is the probability that the level  $v$  contains a pair of nucleons. Obviously

$$U_v^2 + V_v^2 = 1. \quad 3.3.25$$

This ground state is represented in the upper-part of Fig. 3.3.4. It implies that there is a probability for pairs of particles to exist in levels above the Fermi surface, and for partially filled levels to exist below it.

The wave function for an odd  $A$  nucleus with the odd particle in level  $f$  is given by (Soloviev, 1961)

$$\psi_{\text{odd}} = a_f^+ \prod_{v \neq f} (U_v(f) + V_v(f) a_v^+ a_{\bar{v}}^+) |0\rangle \quad 3.3.26$$

where the  $U_v(f)$  and  $V_v(f)$  are calculated with the "blocking" of level  $f$  taken into account. "Blocking" implies that if

the odd particle is in a given single particle level  $f$ , a pair of particles can no longer enter that level without violating the Pauli principle. Thus, the pairs are "blocked" from level  $f$ , and in the BCS calculation this is effected by dropping the level  $f$  and the odd particle. It should be emphasized that the concept of  $U^2$  or  $V^2$  does not apply to a level with one real particle in it.

The concept of a quasiparticle can be introduced at this point. In eq. 3.3.26, the single particle in level  $f$  is due to the particle creation operator  $a_f^+$  acting on the vacuum state  $|0\rangle$ . Alternatively, by defining the quasiparticle creation operator (Bogoliubov, 1958; Valatin, 1958)

$$\alpha_f^+ = Ua_f^+ - Va_{\bar{f}} \quad 3.3.27$$

and having it act on the even-even BCS ground state (Nathan and Nilsson, 1965), the spin down particle ( $\bar{f}$ ) is destroyed to the extent that it existed in level  $f$ , and "the rest" of the spin up particle ( $f$ ) is created. This results in the same situation as before, a spin up real particle existing in the level  $f$ . As this particle was created out of the BCS ground state where it already existed with probability  $V_f^2$ , it is in some sense incorrect to state that a whole particle has been created in the level  $f$ . Rather, it is said that a quasiparticle has been created in level  $f$  from the BCS ground state where it already

"partially" existed.

For the case of no blocking

$$U_v^2 = \frac{1}{2} \left( 1 + \frac{\epsilon_v - \lambda}{\sqrt{(\epsilon_v - \lambda)^2 + \Delta^2}} \right)$$

and

3.3.28

$$V_v^2 = \frac{1}{2} \left( 1 - \frac{\epsilon_v - \lambda}{\sqrt{(\epsilon_v - \lambda)^2 + \Delta^2}} \right)$$

The pairing gap parameter,  $\Delta$ , can be empirically determined from the separation energies (Nilsson, 1961).

$$\Delta(Z, N) = \frac{1}{2} [2S_n(Z, N) - S_n(Z+1, N) - S_n(Z-1, N)] \quad 3.3.29$$

The values of the nucleon separation energies,  $S_n$ , in this mass region have been compiled by Meredith and Barber (1972). In this region  $\Delta$  is typically 0.7 to 1.2 MeV. The Fermi energy,  $\lambda$ , can be estimated with reference to the energy level diagrams (Figs. 3.3.2, 3.3.3) by knowing, a priori, the ground state configuration and the deformation of the nucleus under consideration.

However, it is also possible to solve for  $\Delta$  and  $\lambda$  on an iterative basis if the average number of neutrons or protons,  $\mathcal{N}$ , their single particle energies  $\epsilon_v$ , and the pairing interaction strength  $G$  are known, using

$$2/G = \sum_v \frac{1}{\sqrt{(\epsilon_v - \lambda)^2 + \Delta^2}} \quad 3.3.30$$

$$\text{and } \mathcal{N} = \sum_{\nu} \left\{ 1 - \frac{\epsilon_{\nu} - \lambda}{\sqrt{(\epsilon_{\nu} - \lambda)^2 + \Delta^2}} \right\}. \quad 3.3.30$$

Typical values of  $G$  are 0.170 and 0.156 for proton and neutron states respectively (Vallieres, 1976).

A computer code to perform these calculations was acquired (Vallieres, 1976), and the various  $U$ 's and  $V$ 's required for the theoretical cross section (cf. Sect. 3.4) and the Coriolis mixing (cf. Sect. 3.3.f) were obtained. In the cross section calculation when  $U_{\nu}$  and  $V_{\nu}$  are evaluated for orbitals in the odd target nucleus, the target ground state orbital must be blocked. This is readily accomplished with the program by dropping the single particle energy for this orbital from the sums and by reducing  $\mathcal{N}$  to  $N-1$  or  $Z-1$ . For the Coriolis mixing, the  $U_{\nu}$  and  $V_{\nu}$  ( $\nu \equiv k$  or  $k'$ ) for eq. 3.3.22 originate in the definition of the quasiparticle creation operator (eq. 3.3.27) and as such, they are the unblocked values of the BCS ground state of the final even-even nucleus.

The single quasiparticle energy for the odd nucleus ground state, which is composed of one particle in an orbital with single particle energy  $\epsilon_0$  outside a deformed core is given by

$$E_0 = \sqrt{(\epsilon_0 - \lambda)^2 + \Delta^2}. \quad 3.3.31$$

For excited states, the excitation energy is given by

$$E_v = \sqrt{(\epsilon_v - \lambda)^2 + \Delta^2} - E_0. \quad 3.3.32$$

In the even-even nucleus one is interested in two-quasiparticle states. To first order, their energies are approximated by adding the excitation energies of the two appropriate single quasiparticle states from the neighbouring odd nuclei, and then adding the pairing gap ( $\cong 2\Delta$ ) to that sum for each state except the  $K=0$  ground state. This procedure has been adopted as more highly model dependent estimates of the two quasiparticle states (e.g. Gallagher and Soloviev, 1962), produce values for these energies which do not appear to be any more precise than those produced by the much simpler first order approximation.

The pairing effects contribute correction factors to the off diagonal mixing matrix elements discussed in Sect. 3.3.f. For the rotational matrix elements (eq. 3.3.20) each term is to be multiplied by an expression of the form

$$(U_1' U_1 - V_1' V_1) \quad 3.3.33$$

where particle 2 is assumed to be the common Nilsson orbital ( $2 \cong 2'$ ).

For the particle-particle matrix elements (eq. 3.3.21) each term is to be multiplied by an expression of the form

$$(U_1' U_2' U_1 U_2 - V_1' V_2' V_1 V_2). \quad 3.3.34$$

The Coriolis matrix element will have each term multiplied by an expression of the form

$$(U_1' U_1 + V_1' V_1) \quad 3.3.35$$

where particle 2 is assumed to be the common Nilsson orbital.

#### (h) Mixing Interactions

Three different forms of mixing are described in this subsection, the first being common to all nuclei with two-quasiparticle states, and the others particularly, though not exclusively, noted in  $^{166}\text{Er}$ .

##### 1) The $\vec{L} \cdot \vec{S}$ Splitting Interaction

This interaction has the effect of splitting the degeneracy of the two-quasiparticle states for nuclear spins coupled in parallel and antiparallel manners (cf. Sect. 3.3.c). The effect is typically 30 to 300 keV (occasionally up to 500 keV) and it dramatically alters the energy spectrum.

In the case of coupling the spins of a proton and a neutron (doubly odd nucleus), a deuteron type of interaction ( $\Sigma = \Sigma_1 + \Sigma_2 = 1$ ) is favoured (Gallagher and Moszkowski, 1958). Thus the  $\Sigma = 1$  state lies lower than the  $\Sigma = 0$  state, which is a statement commonly referred to as the Gallagher-Moszkowski rule. A similar rule was proposed for even-even

nuclei (Gallagher, 1962) where the interaction is between identical particles. In this case, the  $\Sigma = 0$  bandhead lies lower than that for  $\Sigma = 1$ .

Calculations of the splitting energies were performed with the code SPLIT (Cheung, 1974), based on a spin dependent central potential in a zero range approximation (Pyatov, 1963),

$$H_{\text{int}} = -4\pi g \delta(|\vec{r}_1 - \vec{r}_2|) [1 - \alpha + \alpha \vec{\sigma}_1 \cdot \vec{\sigma}_2], \quad 3.3.36$$

where  $g$  is a dimensionless strength parameter, ( $g = 146.3$ ) and  $\alpha$  ( $= 0.11$ ) determines the contribution of the spin forces to the general pairing forces ( $0 \leq \alpha \leq k$ ).  $H_{\text{int}}$  is diagonalized with Nilsson model wavefunctions from the NILS calculation. (These wavefunctions were modified to follow the Chi phase convention.) This procedure results in splitting energies given by

$$\Delta E^{0-0} = -2\alpha \{A[1+(-1)^{I+N_1+N_2}] \delta_{K,0} + B\} \text{ for odd-odd nuclei}$$

and

3.3.37

$$\Delta E^{e-e} = (1-4\alpha) \{A[1+(-1)^{I+N_1+N_2}] \delta_{K,0} + B\} \text{ for even-even nuclei.}$$

Here,  $A$  and  $B$  are rather complex expressions involving the radial parts of the Nilsson wave functions. From eq. 3.3.37 it is evident that only the spin forces contribute to the odd-odd splitting, whereas in even-even nuclei the splitting is mainly due to Wigner (Elton, 1966) forces with the spin forces decreasing the effect.

In cases where the parallel coupling lies lower, the splitting energy must be increased by the factor  $2\left(\frac{n^2}{2s}\right) K_2$ , where  $K_2$  is the smaller value of the spin projection for the two orbitals being coupled. When the anti-parallel coupling lies lower, the splitting energy must be decreased by the same factor.

The lower lying coupling is commonly denoted by a "<" subscript on the K symbol, e.g. the lower lying (parallel) coupling of the  $7/2^- [523]$  and  $1/2^+ [411]$  proton orbitals would form a  $K_{<}^\pi = 4^-$  band in  $^{166}\text{Er}$ . Analogously, the higher lying coupling is labelled with a ">" subscript, e.g.  $K_{>}^\pi = 3^-$  in this case.

## 2) The $\Delta N = 2$ Mixing

Normally the  $\Delta N = 2$  interaction due to  $H_0$  in eq. 3.3.5 is neglected as states from different major shells are far apart and any mixing effects are small. However, in the rare earth region the  $1/2^+ [400]$  and  $3/2^+ [402]$  neutron orbitals can be at about the same single particle energies as the  $1/2^+ [660]$  and  $3/2^+ [651]$  orbitals, respectively (Elbek and Tjøm, 1969). Thus, the mixing effects could conceivably be quite substantial. Evidence supporting this is presented in the studies of Nd, Sm, Gd and Dy nuclei, and in Sect. 4.3.g of the present work (Burke et al., 1973; Nelson et al., 1973; Elbek and Tjøm, 1967; Grotdal et al., 1970).

In a theoretical treatment of the effect Andersen

(1968) found that a Woods-Saxon potential gave interaction strengths which were closer by an order of magnitude to the experimental values for  $^{159}\text{Gd}$  (Elbek and Tjøm, 1967) than were the strengths from the harmonic oscillator potential used in the original Nilsson model. However, the  $\Delta N = 2$  matrix elements were not calculated as a part of the present study, but rather, they were taken from studies of neighbouring nuclei. The effects of these matrix elements were evaluated simultaneously with the Coriolis mixing effects by constructing and diagonalizing a matrix involving the elements of both interactions. The Coriolis terms used in this calculation were evaluated with eqs. 3.3.22 and 3.3.35. It should be noted that the phase convention of Chi (1967) was consistently used for both the Coriolis and  $\Delta N = 2$  matrix elements.

### (3) The Neutron-Proton Interaction

The observation of level energies in the neutron transfer study which were coincident to within  $\sim \pm 2$  keV with level energies observed in the proton transfer study (cf. Sect. 4.2.c) implied that some form of n-p interaction was present in  $^{166}\text{Er}$ . The determination of the exact form of the interaction potential was beyond the scope of this study, but some general features of this type of interaction have been noted for a finite-range Gaussian central potential of the form (Massmann et al. (1974)).

$$V_{np} = e^{-(r^2/r_0^2)} (V_{TE}^P V_{TE} + V_{TO}^P V_{TO} + V_{SE}^P V_{SE} + V_{SO}^P V_{SO}). \quad 3.3.38$$

The P's are projection operators for spin triplet (T) or singlet (S) and even (E) or odd (O) relative orbital angular momentum. The Hamiltonian for the interaction is given by (following Massmann's notation).

$$V_{RESIDUAL}^{n-p} = \sum_{npn'p'} \langle np | V_{np} | n'p' \rangle a_n^+ a_p^+ a_{n'} a_{p'}. \quad 3.3.39$$

The n and n' (p and p') represent all the quantum numbers necessary to specify the Nilsson orbitals occupied by the two neutrons (protons). This gives for the off diagonal matrix element

$$m = \langle \psi_{n_1 n_2} | V_{RESIDUAL}^{n-p} | \psi_{p_1 p_2} \rangle. \quad 3.3.40$$

For parallel angular momentum projections  $\Omega_{n_1} + \Omega_{n_2}$  and  $\Omega_{p_1} + \Omega_{p_2}$ ,

$$|m| = \left| (U_{n_1} V_{n_2} U_{p_1} V_{p_2} + V_{n_1} U_{n_2} V_{p_1} U_{p_2}) \langle n_1 \bar{p}_2 | V_{np} | \bar{n}_2 p_1 \rangle \right. \\ \left. - (U_{n_1} V_{n_2} V_{p_1} U_{p_2} + V_{n_1} U_{n_2} U_{p_1} V_{p_2}) \langle n_1 \bar{p}_1 | V_{np} | \bar{n}_2 p_2 \rangle \right| \quad 3.3.41$$

Similar forms for antiparallel and "mixed" cases may be derived, but the important point is that they all contain terms involving  $U_{nucleon_1}$ ,  $V_{nucleon_2}$ . This implies the strongest n-p interaction is for states where the two protons

come from opposite sides of, but close to, the Fermi surface. The same holds true for the two neutrons. However, fairly strong interactions will still be evident where the two Nilsson orbitals for one type of particle are found on the same side of, but near to, the Fermi surface.

### 3.4 Cross Section Calculation

#### (a) Formalism

The differential cross section for the transfer of a single nucleon either to or from an odd target nucleus with a mixed ground state, thereby populating a mixed level in the resulting even-even nucleus, is

$$\frac{d\sigma}{d\Omega}(\theta) = N \sum_{j,l} |\beta_{jl}|^2 \sigma_{jl}^{DWBA}(\theta) \quad 3.4.1$$

where

$$\begin{aligned} \beta_{jl} = & \sum_{n\xi} a_{\xi}^i a_{n_1 n_2}^f \left[ \frac{1}{1+\delta_{n_1 n_2}} \right]^{\frac{1}{2}} \\ & \times \{ P_{n_1}^{n_1} C_{jl}^{n_1} \langle jK_{n_1} I_i K_{n_2} | I_f K_{n_1} + K_{n_2} \rangle \delta_{n_2, \xi} \\ & \times (\delta_{K_{n_2}, K_{\xi}} + (-1)^{I_i - \frac{1}{2}} \pi_{n_2} \delta_{K_{n_2}, -K_{\xi}}) \\ & - P_{n_2}^{n_2} C_{jl}^{n_2} \langle jK_{n_2} I_i K_{n_1} | I_f K_{n_1} + K_{n_2} \rangle \delta_{n_1, \xi} \delta_{K_{n_1}, K_{\xi}} \}. \quad 3.4.2 \end{aligned}$$

The  $\sigma_{jl}^{DWBA}(\theta)$  is the DWBA cross section at the angle  $\theta$ , and N

is the DWBA normalization (cf. Sect. 3.4.b). The  $a_{\xi}^i$  are the amplitudes of the Nilsson orbitals in the initial wavefunction. The  $a_{n_1 n_2}^f$  are the amplitudes in the final wavefunction of the state formed by coupling the Nilsson orbitals,  $n_1$  and  $n_2$ , to a state with  $K = K_{n_1} + K_{n_2}$ . The  $C_{j\ell}$  are the spherical expansion coefficients of the Nilsson model (cf. Sect. 3.3.d), and the  $\pi_n$  refers to the parity of the orbital  $n$  ( $\pi = (-1)^N$ ).

The  $P_n$  are the pairing factors for the orbital  $n$ , appropriate for the reaction and final state under consideration:

for a stripping reaction into the ground state,  
 $P_n =$  unblocked  $V$  of the ground state in the final nucleus;

for a stripping reaction into an excited state,  
 $P_n =$  blocked  $U$  of the Nilsson orbital  $n$  in the target nucleus;

for a pickup reaction into the ground state,  
 $P_n =$  unblocked  $U$  of the ground state in the final nucleus;

and for a pickup reaction into an excited state,  
 $P_n =$  blocked  $V$  of the Nilsson orbital in the target nucleus.

Note that the term "blocked" implies blocking of the target orbital in the calculation of  $U$  and  $V$  (cf.

The cross section calculations, both with and without Coriolis mixing were performed with the program EVEPLT (Hirning and Panar, 1976), for the neutron and proton states in  $^{166}\text{Er}$ . The DWBA cross section in eq. 3.4.1 is discussed in the following subsection.

(b) DWBA Calculations

The kinematics and angular dependence of the cross sections are contained in the single particle cross sections obtained from the Distorted Wave Born Approximation (DWBA) with the computer codes DWUCKII and DWUCK4 (Kunz, 1969, 1975). These calculations assume that the reaction is a direct reaction, i.e. a single particle is transferred either to or from a nucleus in such a manner that all the other nucleons in that nucleus remain undisturbed. The assumption is also made that the projectile moves in the average potential generated by the target nucleons. The potential is considered to be an optical model potential with the parameters chosen so as to reproduce data from elastic scattering off the target nucleus.

In addition to the optical potential, the incoming and outgoing particles are subjected to a Coulomb field of the form

$$V_c = \frac{ze^2}{2R} \left[ 3 - \left(\frac{r}{R}\right)^2 \right] \quad r \leq R$$

$$= \frac{ze^2}{r} \quad r > R,$$

where  $R = r_{oc} A^{1/3}$  and  $r_{oc}$  is the Coulomb radius.

The optical potential is of the form

$$V_{opt} = V_o f(r, r_o, a) + i \{ W_o f(r, r_o', a') + 4W_D \frac{d}{dr} f(r, r_o', a') \} \quad 3.4.4$$

where

$$f(r, r_o, a) = [1 + \exp(-\frac{r - r_o A^{1/3}}{a})]^{-1} \quad 3.4.5$$

is a Woods-Saxon well shape. The radius of the nuclear shape is  $r_o A^{1/3}$  and the diffuseness of this surface is  $a$ .  $V_o$  and  $W_o$  are the real and imaginary volume potential well depths, and  $W_D$  is the surface imaginary term. The latter term produces absorption at the nuclear surface, reflecting the fact that the direct reactions are presumed to occur at this surface.

The bound particle is further subjected to a spin-orbit potential

$$V_{bound} = V_{opt} + V_{SO}$$

where

$$V_{SO} = -V_o \frac{\lambda}{4.52} \frac{1}{r} \frac{d}{dr} f(r, r_o, a) \vec{l} \cdot \vec{s} \quad 3.4.6$$

The spin-orbit strength parameter is usually set as

$\lambda = 8$ .

The optical model parameters used are listed in Table 3.4.1. The (d,t) parameters were taken from a (d,t)

Table 3.4.1

## DWBA Parameters Used

Reaction	Par- ticle	V (MeV)	r <sub>OC</sub> (fm)	r (fm)	a' (fm)	W (MeV)	W <sub>D</sub> (MeV)	r' <sub>0</sub> (fm)	a' (fm)	V S.O. factor	V L.S. (MeV)	r <sub>L.S.</sub> (fm)	r <sub>L.S.</sub> <sup>a</sup> (fm)	Nonlocal parameter
<u>(d,t)</u>	d	-105	1.25	1.10	0.825	0	50.05	1.28	0.863	0	-22.52	0.98	1.0	.54
	t	-153	1.25	1.24	0.700	-16.42	0	1.42	0.890	0	0	0	0	.25
	Bound n	*	1.25	1.25	0.650	0	0	0	0	0	0	0	0	0
											0			
<u>(<sup>3</sup>He,α)</u>	<sup>3</sup> He	-175	1.40	1.14	0.723	-17.5	0	1.60	0.810	0	0	0	0	0
	α	-207	1.30	1.41	0.519	-25.8	0	1.41	0.519	0	0	0	0	0
	Bound n	*	1.25	1.25	0.650	0	0	0	0	8	0	0	0	0
<u>(He,d)</u>	<sup>3</sup> He	-175	1.40	1.14	0.723	-17.5	0	1.60	0.810	0	0	0	0	0
	d	-111	1.25	1.05	0.859	0	70.8	1.24	0.794	0	0	0	0	0
	Bound p	*	1.25	1.25	0.650	0	0	0	0	8	0	0	0	0
<u>(t)</u>	α	-200	1.25	1.40	0.600	-20.0	0	1.40	0.600	0	0	0	0	0
	t	-200	1.25	1.40	0.600	-50.0	0	1.40	0.600	0	0	0	0	0
	Bound p	*	1.25	1.25	0.650	0	0	0	0	8	0	0	0	0
														71

Adjusted to reproduce separation energy of bound particle.

study of  $^{150}\text{Sm}$  by Oelert et al., (1975). The  $(^3\text{He},\alpha)$  parameters are from similar studies on targets of even Yb isotopes (Burke et al., 1971). Both the  $(^3\text{He},d)$  and  $(\alpha,t)$  DWBA parameter sets were from a study of odd Re isotopes (Lu and Alford, 1971). The same sets of proton stripping parameters were successfully applied (Wagner et al., 1975; Panar et al., 1977) to a series of nuclei in the  $^{166}\text{Er}$  mass region ( $^{157-165}\text{Ho}$  odd A nuclei) with a scaled down lower cutoff of 9.43 fm, and this was therefore adopted in the present study.

The normalization constant,  $N$ , in eq. 3.4.1, was set to 3.33 for the  $(d,t)$  reactions (Kunz, 1974) and 6.0 for the  $(^3\text{He},d)$  reactions (e.g. Straume et al., 1976). The  $(^3\text{He},\alpha)$  and  $(\alpha,t)$  normalizing constants were determined by comparing the experimental  $(^3\text{He},\alpha)/(d,t)$  and  $(^3\text{He},d)/(\alpha,t)$  cross section ratios to predicted values for states where the  $\ell$ -value of the transferred particle is expected to be predominantly one value (O'Neil, 1971). In the present study the adopted values were  $N = 28$  for the  $(^3\text{He},\alpha)$  reaction (cf. Sect. 4.2.a) and  $N = 78$  for the  $(\alpha,t)$  reaction (cf. Sect. 4.4.a). Both these values are reasonable and correspond well to values found in a similar manner in previous studies (e.g. Burke et al., 1971; Wagner et al., 1975).

CHAPTER 4  
INTERPRETATION

4.1 General

In the  $(d,t)$  and  $({}^3\text{He},\alpha)$  reactions, states in  ${}^{166}\text{Er}$  are populated by picking up a neutron out of the  ${}^{167}\text{Er}$  target. Members of the ground state rotational band are formed when the picked up particle is the odd neutron in the target ground state. If any other neutron is picked out of a pair in the target, the unpaired neutron left behind will couple with the odd target neutron to create excited two-quasiparticle states of  ${}^{166}\text{Er}$ .

The  $({}^3\text{He},d)$  and  $(\alpha,t)$  reactions populate states in  ${}^{166}\text{Er}$ , by stripping a proton into the  ${}^{165}\text{Ho}$  target. Ground state rotational band members are formed when the stripped proton goes into the orbital of the odd particle in the target ground state resulting in a  $K = 0$  pair. If the stripped proton goes into any other orbital, it couples with the unpaired particle in the target ground state to create excited two-quasiparticle states of  ${}^{166}\text{Er}$ .

Cross sections depend both upon the structure of the target ground state and upon the orbital involved in the nucleon transfer (cf. Sect. 3.4). For the neutron pickup reactions, the  $I = 7/2$  (Smith and Unsworth, 1965) ground state of  ${}^{167}\text{Er}$  has a 0.996 amplitude for the  $7/2^+ [633]$

orbital (Kanestrøm and Løvholden, 1971) (or 0.979 according to Stott, et al., 1975), the largest of the minor components being the  $5/2^+$ [642] orbital. The other orbitals from which a neutron can be removed to populate low-lying two-quasiparticle states will be found, in general, lying just below the Fermi level. As the Fermi level is located near the  $7/2^+$ [633] orbital in  $^{167}\text{Er}$ , the pertinent Nilsson states will be the  $5/2^-$ [523],  $3/2^-$ [521],  $11/2^-$ [505],  $5/2^+$ [642],  $3/2^+$ [651],  $1/2^+$ [660],  $3/2^+$ [402] and  $1/2^+$ [400] orbitals. Not only are these "hole" states populated, but in addition, the smearing of the Fermi surface due to the pairing interaction permits the pickup of a neutron from orbitals just above the Fermi level. These include the  $1/2^-$ [521] and  $5/2^-$ [512] orbitals.

In the proton stripping reaction the target nucleus is the  $I^\pi = 7/2^-$  (e.g. Lindgren, 1965; Lederer et al., 1968) ground state of  $^{165}\text{Ho}$ . This is an essentially pure  $7/2^-$ [523] orbital, in contrast to the mixed configuration of the  $^{167}\text{Er}$  reaction target. The effectively pure ground state of  $^{165}\text{Ho}$  is a reflection of the relatively high excitation energies ( $\geq 1500$  keV) of any levels which could strongly Coriolis mix into it, whereas in  $^{167}\text{Er}$ , levels which have substantial Coriolis mixing with the ground state are found as low as 800 keV in excitation energy.

The orbitals involved in the proton stripping reactions are located just above the Fermi level. As this

is found near the  $7/2^- [523]$  orbital in  $^{165}\text{Ho}$ , the relevant Nilsson states will be the  $1/2^+ [411]$ ,  $7/2^+ [404]$ ,  $5/2^+ [402]$ ,  $9/2^- [514]$  and  $1/2^- [541]$  orbitals. The smearing of the Fermi surface should also allow proton stripping into orbitals below the Fermi level, for example, into the  $3/2^+ [411]$  orbital.

Tables 4.1.1 and 4.1.2 list the Nilsson single particle-energies and pairing factors,  $P^2$ , for the neutron and proton orbitals respectively. The single particle energies were obtained with the code NILS as described in Section 3.3.d, and the pairing factors were calculated with the program PAIRBCS as described in Section 3.3.g.

The assignments of the levels observed in this study are discussed in the following subsections. The states populated in the neutron transfer reactions are treated first, followed by those populated in the proton transfer reactions. Most subsections have associated with them a table listing, for the states under discussion, the averaged energies from the direct reaction studies, the experimentally determined cross sections, theoretically determined cross sections from the code EVEPLT (without and with Coriolis mixing included, cf. Sect. 3.4.a), and the assignments for the states. Tentative assignments are indicated by parentheses.

Figs. 4.1.1 and 4.1.2 show portions of the spectra of Figs. 2.3.1 and 2.4.1 on an expanded scale, with the state assignments indicated. Dashed lines and numbers in

Table 4.1.1

## Neutron State Single Particle Orbitals

Orbital	S.P. Energy (MeV)	"p"	$p^2$
$1/2^-$ [530]	49.149	V	0.991
$1/2^+$ [660]	49.155	V	0.991
$1/2^+$ [400]	49.462	V	0.989
$3/2^-$ [532]	49.538	V	0.988
$3/2^+$ [402]	49.654	V	0.987
$3/2^+$ [651]	49.872	V	0.985
$11/2^-$ [505]	51.048	V	0.951
$5/2^+$ [642]	51.069	V	0.950
$3/2^-$ [521]	51.146	V	0.944
$5/2^-$ [523]	51.758	V	0.837
$7/2^+$ [633]	52.595	U	0.720
$1/2^-$ [521]	52.717	V	0.218
$5/2^-$ [512]	53.378	V	0.064

Table 4.1.2

## Proton State Single Particle Orbitals

Orbital	S.P. Energy (MeV)	"p"	$p^2$
$3/2^+$ [411]	40.328	U	0.236
$7/2^-$ [523]	41.049	V	0.519
$1/2^+$ [411]	41.590	U	0.825
$7/2^+$ [404]	42.090	U	0.911
$1/2^-$ [541]	42.218	U	0.923
$5/2^+$ [402]	42.616	U	0.949
$9/2^-$ [514]	42.690	U	0.953
$1/2^+$ [400]	42.729	U	0.955

Fig. 4.1.1 <sup>0</sup>

Expanded portions of Fig. 2.3.1 showing the two neutron configurations. Tentative assignments are indicated by parantheses around the configuration labels. Tentatively assigned spins are indicated by broken lines.

The dagger (+) indicates that the state is primarily composed of the  $7/2^- [523] + 1/2^+ [411]$   $K^\pi = 4^-$  two proton configuration.

The single asterisk (\*) indicates that the label refers to the major component of this state, although population in the (d,t) reaction is predominantly through a  $7/2^+ [633] \pm 1/2^+ [400]$  admixture. A complex mixing scheme, discussed in the text, can introduce several minor components into this state.

The double asterisk (\*\*) indicates that these two states are predominantly composed of the two components indicated. The complex mixing scheme, noted above, can introduce various minor components into these states.

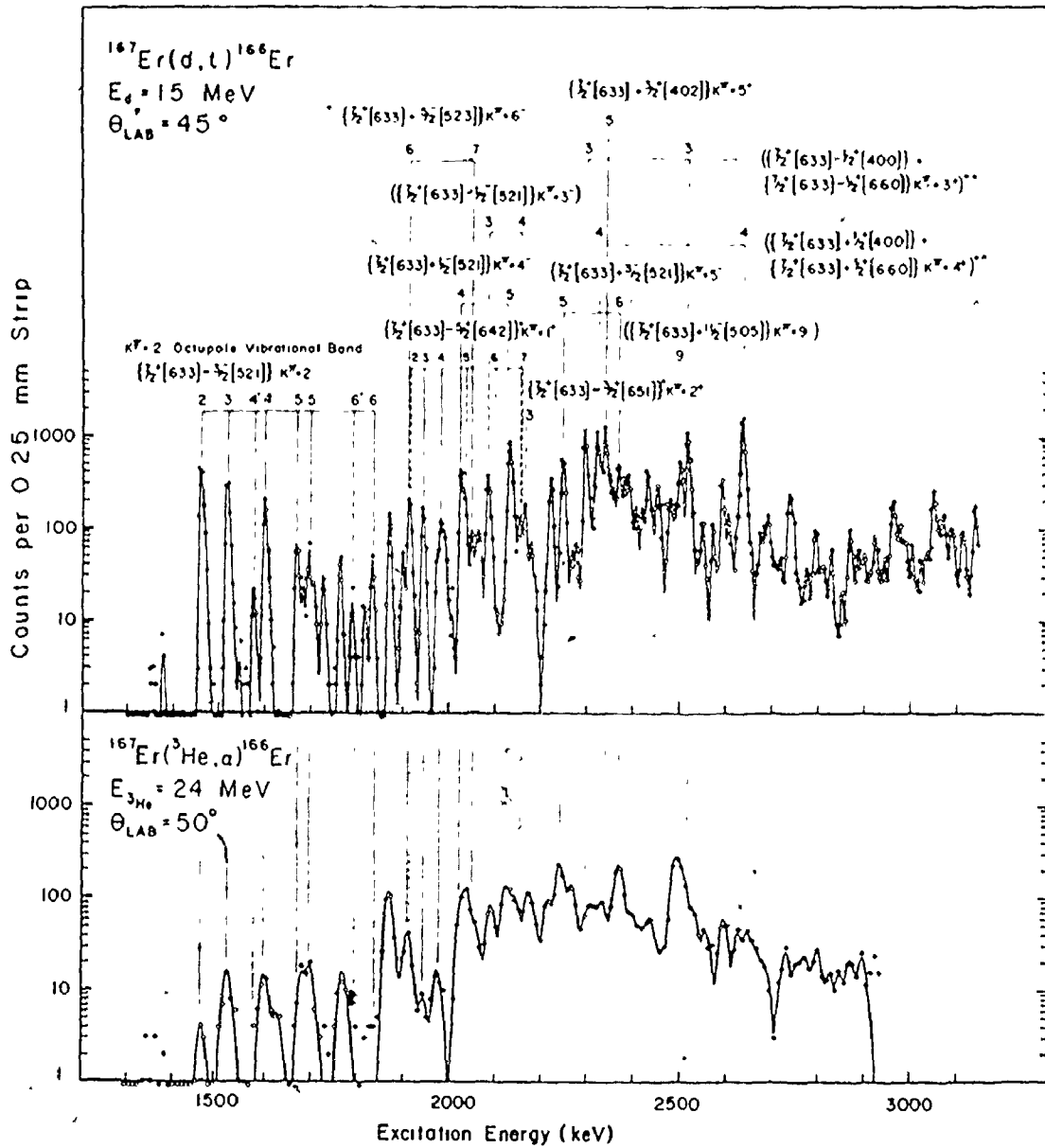
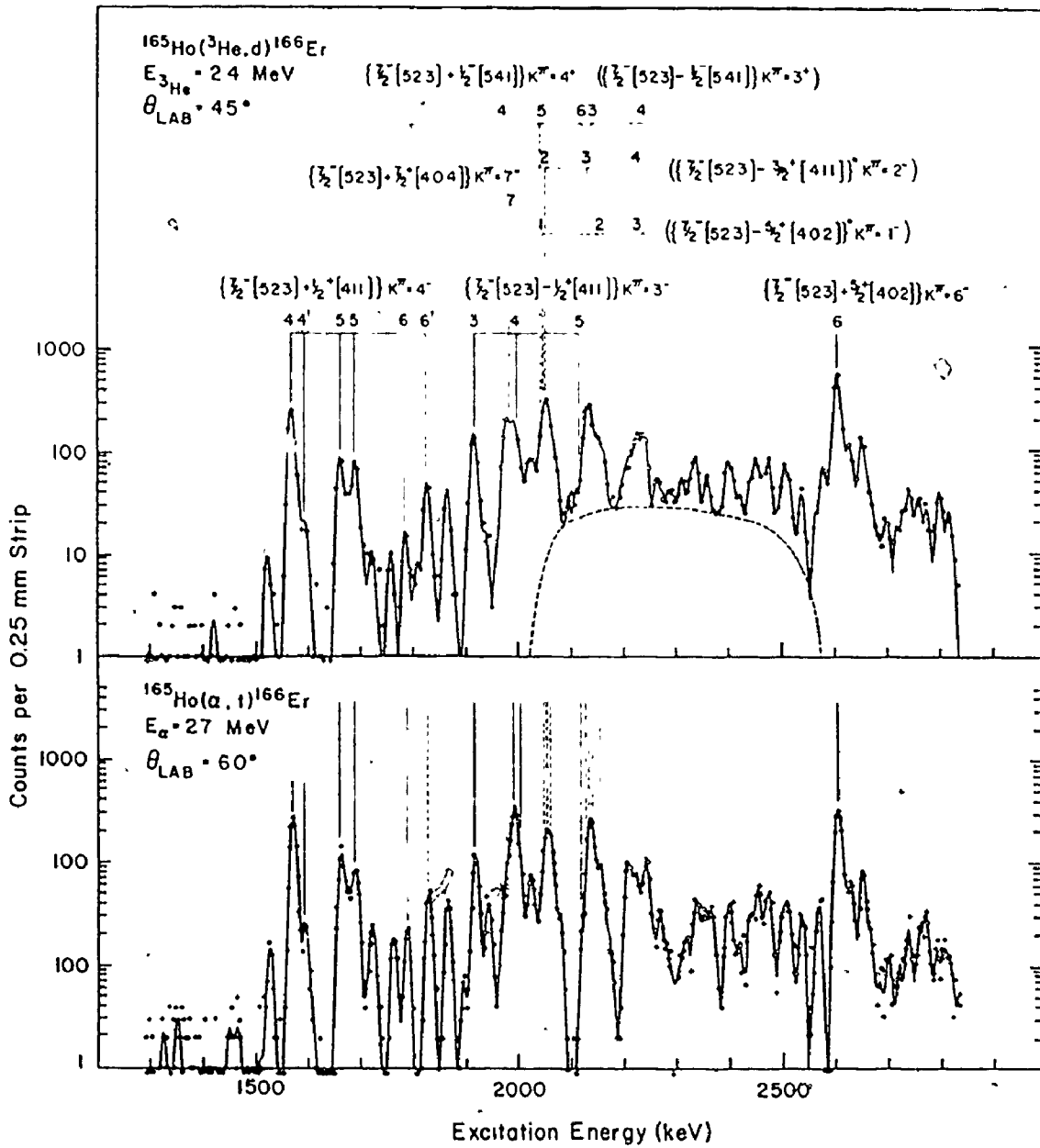


Fig. 4.1.2

Expanded portions of Fig. 2.4.1 showing the two-proton configurations. Tentative assignments are indicated by parentheses around the configuration labels. Tentatively assigned spins are indicated by broken lines.

The dagger (+) indicates that the state is primarily composed of the  $7/2^+[633]-3/2^-[521]$   $K^\pi = 2^-$  two neutron component of the  $K^\pi = 2^-$  octupole variational band.

The asterisk indicates that the label refers to the major component of this state, although the two configurations so marked are strongly mixed. Population of both configurations is almost entirely through the  $7/2^-[523]-5/2^+[402]$   $K^\pi = 1^-$  component.



parenthesis indicate tentative assignments. The (d,t) angular distributions are presented in Figs. 4.2.2 to 4.2.7 and the ( $^3\text{He},d$ ) angular distributions are presented in Figs. 4.3.2 to 4.3.7. For cases where assignments have been made to the levels, the observed distributions are compared with curves calculated for Coriolis mixed configurations. The comparisons are made by scaling the curves up or down until the best visual fit was obtained.

Ratios of the ( $^3\text{He},\alpha$ ) experimental cross sections at  $50^\circ$  to the (d,t) cross sections at  $45^\circ$  are presented in Fig. 4.2.1, and ratios of the ( $^3\text{He},d$ ) cross section at  $60^\circ$  to the ( $\alpha,t$ ) cross section at  $60^\circ$  are presented in Fig. 4.3.1. In both figures, the solid curves are predictions from the DWBA calculations for pure transitions of the  $l$ -values indicated.

## 4.2 States Populated in the Neutron Transfer Reactions

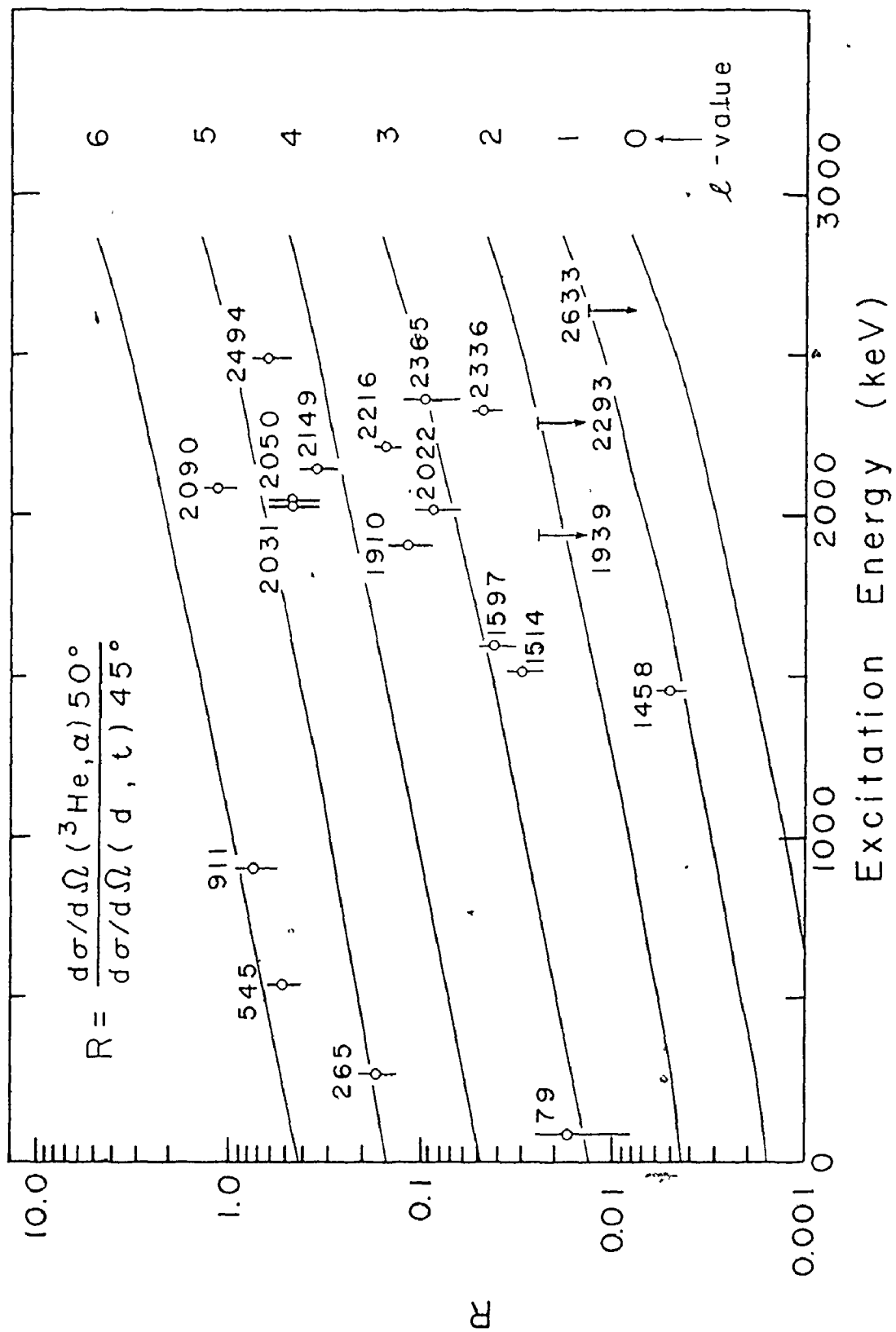
### (a) The Ground State Band

The  $K^\pi = 0^+$  ground state band is formed in the neutron pickup reactions by removing the  $7/2^+[633]$  neutron from the ground state of  $^{167}\text{Er}$ . The  $I = 0$  final ground state is predicted to have a vanishingly small cross section, but the spin 2, 4, 6 and 8 members of its rotational band are populated in the (d,t) reaction at energies of 79, 265, 545 and 911 keV (cf. Table 4.2.1) (Burke et al., 1969). These energies are in good agreement with the values from

Fig. 4.2.1

Ratios of differential cross sections for the  $(^3\text{He}, \alpha)_{50^\circ}$  and  $(d, t)_{45^\circ}$  reactions as a function of excitation energies in keV. The solid lines represent the predicted ratio for the transfer of a neutron with the  $\ell$ -values indicated. The points are the observed ratios for levels in  $^{166}\text{Er}$  labelled by their excitation energies. The predicted curves have been normalized to members of the ground state band (see text).

The short bars with downward pointing arrows are upper limits for the value of the ratio, R.



the decay studies of  $^{166}\text{Ho}$  and  $^{166}\text{Tm}$  (e.g. Reich and Cline, 1970). As the  $7/2^+[633]$  orbital originates from the  $i_{13/2}$  shell model state in the spherical limit; high  $\ell$ -value neutron transfers are expected. This is particularly true for the spin 6 and 8 states which are populated by almost pure  $\ell = 6$  transfers. These states are populated fairly strongly in the  $(^3\text{He}, \alpha)$  reaction, and are used to normalize the cross section ratio plot, Fig. 4.2.1, as discussed in Sect. 3.4.6. The  $(d, t)$  angular distributions, which are consistent with the high  $\ell$ -value transferred, are presented in Fig. 4.2.2.

If the ground state of  $^{166}\text{Er}$  is considered to be the two-quasiparticle configuration  $7/2^+[633]-7/2^+[633]$ , with  $V^2 = 0.72$ , the predicted  $(d, t)$  cross sections calculated without Coriolis mixing of the final states are smaller than the experimental values by an average of  $\sim 30\%$  for the ground state band. However, the ground state rotational band is more properly described as a highly complex combination of many two-quasiparticle configurations. Unfortunately, as the amplitudes of these configurations are unknown (Volkov, 1977), predicted cross sections, calculated taking all the configurations into account, are unobtainable. In Table 4.2.1, Coriolis mixed predicted cross sections are presented, but these were evaluated using the approximation that the unmixed ground state is populated solely through the  $7/2^+[633]-7/2^+[633]$   $K^\pi = 0^+$

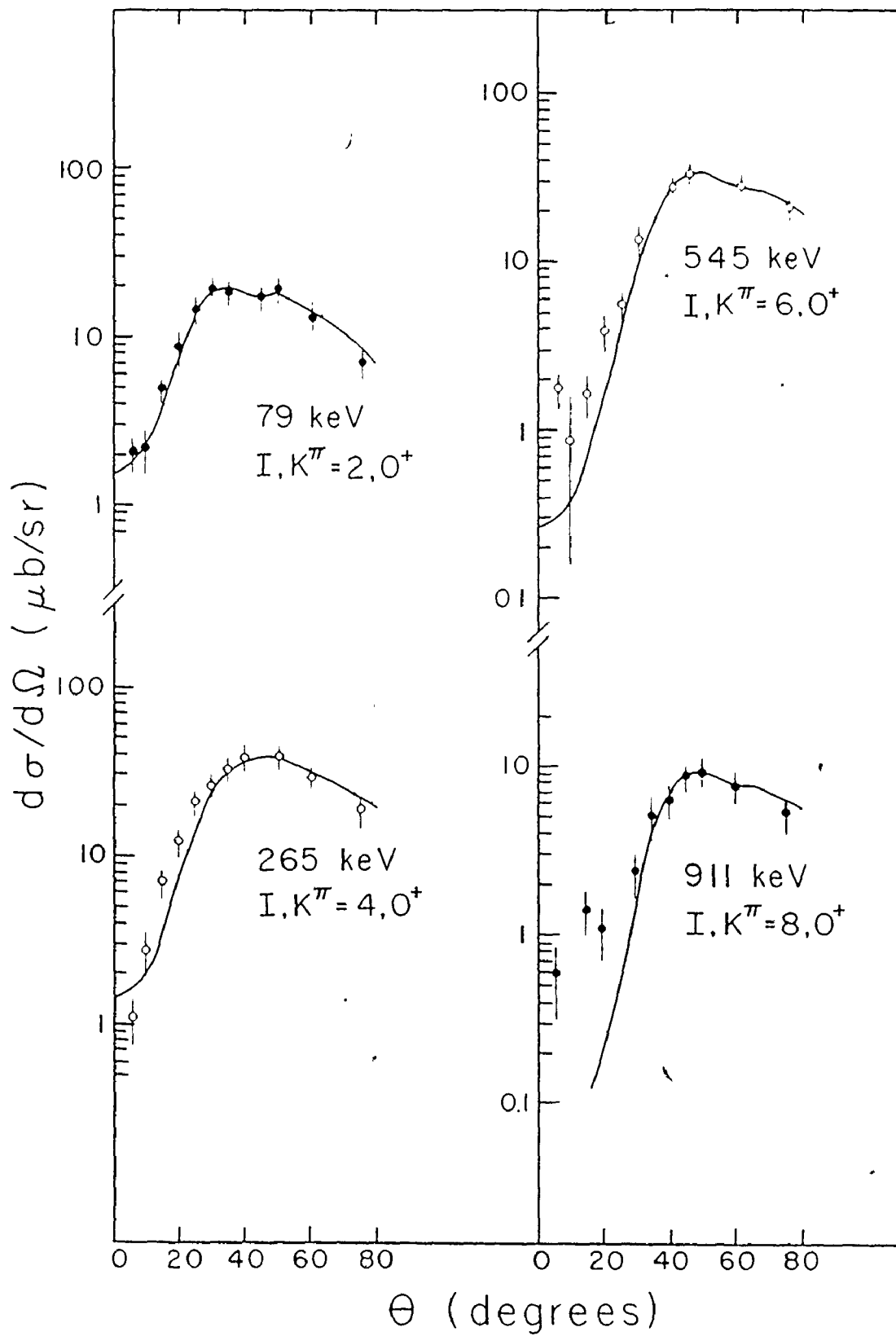
Table 4.2.1

## The Ground State Band, Neutron Transfer Reactions

Energy (keV)	(d,t) $d\sigma/d\Omega$ ( $\mu\text{b}/\text{sr}$ )		$(^3\text{He},\alpha)$ $d\sigma/d\Omega$ ( $\mu\text{b}/\text{sr}$ )		Assignment	
	Experiment $\theta=45^\circ$	Theory Pure Coriolis Mixed	Experiment $\theta=50^\circ$	Theory Pure Coriolis Mixed	I	K
0		0.1		0.0	0	0 <sup>+</sup>
79	17.3 $\pm$ 3.0	12.6	<1.0 $\pm$ 0.5	0.5	2	0 <sup>+</sup>
265	~39 $\pm$ 5	28.2	6.5 $\pm$ 1.2	7.1	4	0 <sup>+</sup>
545	34 $\pm$ 4	26.8	17.2 $\pm$ 2.8	12.7	6	0 <sup>+</sup>
911	8.2 $\pm$ 1	5.2	6.0 $\pm$ 1.1	3.3	8	0 <sup>+</sup>

Fig. 4.2.2

$^{167}\text{Er}(d,t)^{166}\text{Er}$  angular distributions to the spin 2,4,6 and 8 members of the ground state band. The solid lines are angular distributions generated by the computer code EVEPLT for mixed  $l$ -value neutron transfers. These generated shapes have been scaled up or down to produce the best visual fit.



configuration. Evidence that this approximation may not be so bad is found in that the Coriolis mixed values agree reasonably well with the experimental cross sections.

A further complication arises from the previously discussed admixture of the  $5/2^+[642]$  orbital into the  $^{167}\text{Er}$  ground state (Stott et al., 1975). It was originally hoped that the present work could provide additional tests for the degree of this admixture by studying the population of the ground state band in the neutron transfer reactions. However, the uncertainties in the structure of this ground state, as just discussed, precluded any such results. The amplitude of this admixture as reported by Stott et al. ( $\sim 0.2$ ) was therefore adopted for the  $5/2^+[642]$  orbital.

(b) The  $K^\pi = 2^+$   $\gamma$ -Vibrational Band

This band has been identified in decay studies up to spin 8 (Reich and Cline, 1970). Previously, the band had been observed up to spin 6 in the (d,t) reaction (Burke et al., 1969) and in the present work the known spin 7 member is also observed.

This band is weakly populated, the largest peak having only  $\sim 2\%$  of the intensity of the largest peaks in the (d,t) spectrum. As noted in the previous (d,t) study, these band members are expected to have small cross sections (Zheleznova et al., 1965). As with all such weakly populated states, uncertainties in the nature of the reaction

mechanism and in the theoretical composition of the wavefunctions preclude any definitive comments concerning their nuclear structure. The (d,t) angular distributions to the first four members of this band are included with the unfitted distributions in Fig. 4.2.8.

(c) The  $K^\pi = 2^-$  Octupole Vibrational Band and Transfer of the  $3/2^- [521]$  Neutron Orbital

From the previous decay studies of  $^{166}\text{Tm}$  and metastable  $^{166}\text{Ho}$  a series of negative parity states has been identified immediately above the energy gap in  $^{166}\text{Er}$ :  $I^\pi = 2^-$  at 1458.0 keV,  $I^\pi = 3^-$  at 1514.0 keV, two  $I^\pi = 4^-$  levels at 1572.1 and 1596.2 keV, two  $I^\pi = 5^-$  levels at 1665.8 and 1692.3 keV, and two with  $I^\pi = 6^-$  at 1786.9 and 1827.5 keV (Zylicz et al., 1966; Reich and Cline, 1970). Zylicz et al. suggested that the spin 2 and 3 levels were the lowest lying members of the  $K^\pi = 2^-$  octupole band, and this was confirmed in the previous (d,t) investigation by Burke et al. (1969, who proposed that the neutron transfer population of the band was via the  $7/2^+ [633] - 3/2^- [521]$   $K^\pi = 2^-$  component of the octupole vibration. The three pairs of states with spins 4, 5 and 6 were also populated in that (d,t) study, and with the aid of prepublication data from Reich and Cline, Burke et al. assigned the spin 4 state at 1597 keV to the octupole band. The other spin 4 state (1572 keV) had been tentatively assigned as the

two proton  $7/2^- [523] + 1/2^+ [411] K^\pi = 4^-$  bandhead by Zylicz et al., and this was confirmed by Kubo (1968) in the  $(^3\text{He}, d)$  reaction on a  $^{165}\text{Ho}$  target.

The two spin 5 states and the two spin 6 states were fairly weakly populated in the earlier  $(d, t)$  work. Therefore, while these levels were assumed to be associated with either the  $K^\pi = 2^-$  or the  $K^\pi = 4^-$  bands built on the 1458.0 and 1572.1 keV bandheads, respectively, evidence was not available to indicate which state belonged to which band.

The octupole band assignment was confirmed by the strong population of the  $I^\pi = 3^-$  member in inelastic scattering experiments (Tjøm and Elbek, 1968). In the earlier  $(d, t)$  study the cross sections to the first three band members were observed to be  $\sim 50\%$  of those predicted for a pure  $7/2^+ [633] - 3/2^- [521] K^\pi = 2^-$  configuration. Zheleznova et al. (1965) had predicted an admixture of  $\sim 58\%$  of this two neutron component into the octupole vibration.

In the present study, these states have all been observed in the neutron transfer reactions. (The pairs of states with spins 4, 5 and 6 have also been observed in the proton transfer reaction, but this point will be returned to later in this subsection and in Sect. 4.3.c.) With reference to Table 4.2.2, it appears at first glance as though the theoretical cross sections for the lower band

Table 4.2.2

The  $K^\pi = 2^-$  Octupole Vibrational Band and  $\{7/2^+ [633] \pm 3/2^- [521]\}$ 

Energy (keV)	$(d,t)$ $d\sigma/d\Omega$ (ub/sr)		Experiment $\theta=50^\circ$	$(^3\text{He},\alpha)$ $d\sigma/d\Omega$ (ub/sr)		Assignment I K		
	Experiment $\theta=45^\circ$	Pure Coriolis		Theory Coriolis	Mixed Coriolis			
1458	103±10	94	87	<1.0±0.5	1.8	1.9	2	2 <sup>-</sup>
1514	72±10	97	89	2.1±0.5	5.2	5.5	3	2 <sup>-</sup>
1572	5.0±1.5	89	78	1.9±0.5	8.2	8.4	4	2 <sup>-</sup>
1597	46±5							
1666	14.8±2.5	54	45	a)	7.6	7.3	5	2 <sup>-</sup>
1692	12.4±2.3							
1787	3.5±0.7	19.0	14.5	}	4.3	3.8	6	(2) <sup>-</sup>
1829	9.9±1.0							
2244	143±22	166	149	30±5 b)	6.0	5.7	5	5 <sup>-</sup>
2366	115±19	106	102	10.2±5.3	12.2	10.3	6	5 <sup>-</sup>

a) Obscured by peaks at 1679 and 1703 keV

b) Large ( $^3\text{He},\alpha$ ) cross section due to unresolved state

are reasonably well matched by the experimental values, while the higher spin states ( $I = 4, 5$  and  $6$ ), taken all together, have a predicted strength which is larger than the experimental value by roughly a factor of 2. However, if it is recalled that according to Zheleznova et al. the theoretical cross section should be larger than the experimental value by just this factor, it is now realized that the agreement for the higher spin states is reasonable, while the spin 2 and 3 members are deficient in theoretical intensity.

This can be explained by referring to the  $(d,t)$  angular distributions (Fig. 4.2.3) where a deficiency of  $\ell=1$  strength is noted in the predicted shapes of the lower spin band members. (The  $\ell = 1$  component results in the maximum seen between  $\theta = 10^\circ$  and  $\theta = 15^\circ$ ). The  $\ell = 1$  component of the calculated cross section comes from the  $C_{3/2, 1}$  coefficient in the wavefunction (cf. eq. 3.4.1, 3.4.2), and it would appear as though this coefficient, which was obtained from a Nilsson calculation with reasonable parameters, is too small. While the  $C_{3/2, 1}$  coefficient is fairly small ( $C_{3/2, 1}^2 \sim 0.07$ ), the  $\ell = 1$   $(d,t)$  cross section can be quite substantial, and a reduction in the size of this coefficient can markedly reduce the predicted cross section. As the lower spin members are the ones which should have large parts of their intensities produced by the  $\ell = 1$  contribution, it is reasonable that

Fig. 4.2.3

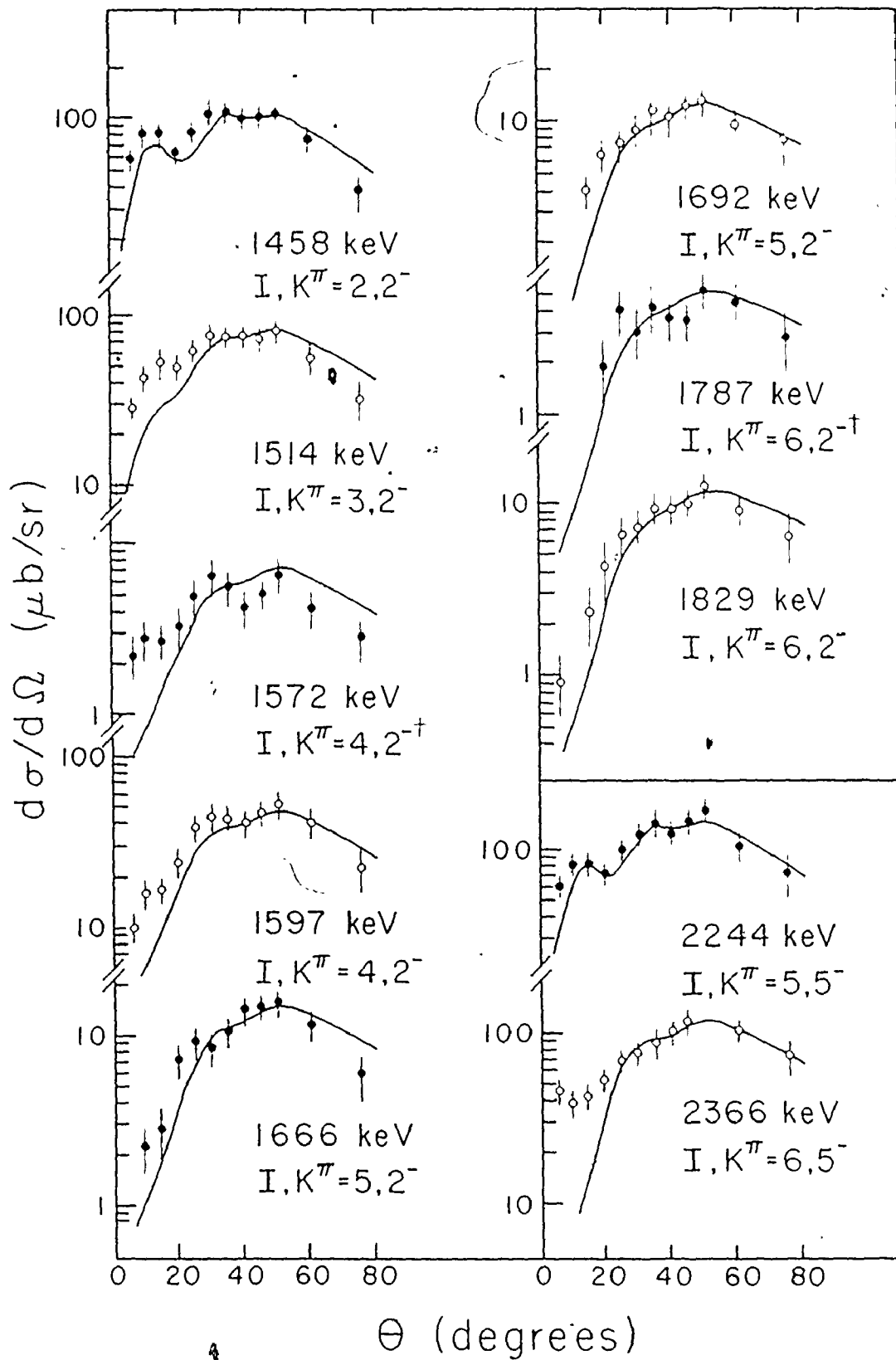
$^{167}\text{Er}(d,t)^{166}\text{Er}$  angular distributions to states of the  $7/2^+[633]-3/2^-[521]$  two neutron configuration.

The  $K_{<}^{\pi} = 2^{-}$  band is mixed with the  $K^{\pi} = 2^{-}$  octupole vibrational band; further mixing with the predominantly  $7/2^-[523]+1/2^+[411]$  two proton configuration gives rise to two states each for spins 4, 5 and 6. (Note the similar experimental distribution shape for both states of each spin.)

The first two members of the  $7/2^+[633]+3/2^-[521]$   $K_{>}^{\pi} = 5$  band are also shown.

The dagger (+) indicates that the state is primarily composed of the  $7/2^-[523]+1/2^+[411]$   $K^{\pi} = 4^{-}$  two proton configuration.

The solid lines are angular distributions generated by the computer code EVEPLT for mixed  $\ell$ -value neutron transfers. These generated shapes have been scaled up or down to produce the best visual fit.



primarily they, but not the higher spin members, should exhibit the reduced theoretical cross sections.

This effect is not completely unexpected, as in the odd Er nuclei the experimental value of  $C_{3/2, 1}^2$  is seen to fluctuate by a factor of two or more. In  $^{161}\text{Er}$  it agrees with the predicted value of 0.10 while it rises to 0.23 for  $^{169}\text{Er}$ . In contrast, for all the odd Er nuclei, the experimental  $C_{7/2, 3}^2$  coefficient (the largest coefficient for this orbital) is seen to remain in good agreement with the predicted value of 0.53.

The Nilsson parameters which were used to generate the  $C_{j, \ell}$ 's used in the present study were from Lamm (1969), and they produced a theoretical value of  $C_{3/2, 1}^2 = 0.07$  as noted above. From the study of the odd Er nuclei, it can be seen that it is reasonable to expect this coefficient to fluctuate by more than a factor of two (implying fluctuations in the Nilsson parameters or perturbations to the model itself). Further calculations were thus made to see how sensitive the  $C_{3/2, 1}^2$  coefficient was to reasonable variations in the Nilsson parameters. For example, with  $\kappa$  changed from 0.0637 to 0.050 and  $\mu$  changed from  $\mu = 0.42$  to 0.45 (Chi, 1967) one obtains  $C_{3/2, 1}^2 = 0.11$ . This raised the predicted intensity of the spin 3 state so that the Zheleznova et al. prediction is roughly satisfied and the predicted angular distribution is in better agreement with the experimental one. However, the theoretical

strength for the spin 2 state is still ~35% too small at  $\theta = 45^\circ$ . The theoretical values obtained with the larger  $C_{3/2\ 1}$  coefficient are not listed in Table 4.2.2 as it is possible that a more complete parameter search may produce still larger values of  $C_{3/2\ 1}^2$ . However, this search has not been attempted as it is still not clear that these variations are the only ones contributing to the effect. For example, it is possible that higher order effects in the reaction mechanism may also be important.

In conclusion, it should be noted that in the previous (d,t) study the experimental cross sections were ~50% of the theoretical values for all the states (completely supporting the Zheleznova et al. predictions). However, empirical values of  $C_{j\ell} \sigma_\ell$  from neighbouring Yb nuclei were used, thereby avoiding the present problem of obtaining a correct  $C_{3/2\ 1}$  value. It thus appears that the admixture of the  $7/2^+[633] - 3/2^-[521]$   $K^\pi = 2^-$  configuration in the octupole vibration is of the order of 50% as calculated.

As noted above, the pairs of states with spins 4, 5 and 6 were observed in both the proton transfer and neutron transfer reactions. While the spin 4 state at 1572 keV is primarily the two proton  $7/2^-[523] + 1/2^+[411]$   $K^\pi = 4^-$  bandhead, and the state at 1597 keV is mainly the two neutron  $7/2^+[633] - 3/2^-[521]$   $K^\pi = 2^-$  configuration, mechanisms for the population of the 1572 keV level in the

(d,t) and ( $^3\text{He},\alpha$ ) reactions, and of the 1597 keV level in the ( $^3\text{He},d$ ) and ( $\alpha,t$ ) reactions were not proposed.

The present study suggests a possible explanation for these populations. In addition, the outlined scheme accounts for the equal populations of the two spin 5 states at 1665 and 1692 keV in both the neutron transfer and proton transfer reactions, and certain qualified comments can be made regarding the association of the two spin 6 states with the two bands.

It is this equal population of the spin 5 levels which provides the impetus for explaining the paired nature of the spin 4, 5 and 6 states. The assumption is made that the spin 5 levels are mixed states which were approximately degenerate prior to mixing, one state being the two neutron configuration, the other the two proton configuration. This not only implies that a neutron-proton mixing interaction (like the Massmann type type) is present (cf. Sect. 3.3.h.3), but the separation of the two spin 5 levels yields an effective matrix element of  $\sim 13$  keV. Substantial support for this idea is found in the (d,t) angular distributions, where similar shapes are found for both members of each pair with a given spin. This would be the case if for both members of the pair the nuclear structure, and hence the population, is the same.

Some possible mixing schemes are as follows:



or



where

$$\begin{aligned}
 \text{A} &\equiv 7/2^+ [633]^n - 3/2^- [521]^n \quad K^\pi = 2^- \\
 \text{B} &\equiv 7/2^+ [633]^n - 1/2^- [521]^n \quad K^\pi = 3^- \\
 \text{C} &\equiv 7/2^+ [633]^n + 1/2^- [521]^n \quad K^\pi = 4^- \\
 \text{D} &\equiv 7/2^- [523]^p + 1/2^+ [411]^p \quad K^\pi = 4^- \\
 \text{E} &\equiv 7/2^- [523]^p - 1/2^+ [411]^p \quad K^\pi = 3^- \\
 \text{and F} &\equiv 7/2^- [523]^p - 3/2^+ [411]^p \quad K^\pi = 2^-.
 \end{aligned}$$

In these schemes the two-quasiparticle configurations which are connected by the double-headed arrows may be mixed by the interaction indicated; CI is a Coriolis interaction, and np is a neutron-proton (possibly Massmann type) interaction. (Note that all the orbitals involved in the mixing lie near the Fermi surface. cf. Sect. 3.3.h.3.)

The couplings shown in the first two schemes would introduce admixtures into the  $7/2^+ [633] \pm 1/2^- [521]$   $K^\pi = 3^-, 4^-$  two neutron configurations which would cause the spin 4 and higher band members to be populated in the single proton transfer reactions. This is supported by

the observation of the spin 4 states of these configurations (at 2022 and 2149 keV, cf. Sect. 4.3.e) in the proton transfer studies. Conversely, the two proton  $7/2^- [523] - 1/2^+ [411]$   $K^\pi = 3^-$  spin 4 state at 2002 keV (cf. below) is observed in the (d,t) study, particularly supporting the second scheme. The spin 5 level of the  $7/2^+ [633] + 1/2^- [521]$   $K^\pi = 4$  two neutron configuration falls at the edge of a large multiplet in the proton transfer study. Therefore, its energy in the proton transfer spectrum cannot be determined accurately enough to allow comparisons with peak energies in the (d,t) spectrum.

The third mechanism is proposed as the octupole vibration is predicted to have a 36% intensity admixture of the  $7/2^- [523] - 3/2^+ [411]$   $K^\pi = 2^-$  two proton configuration (Zheleznova et al., 1965). However, no significant population of the spin 2 state at 1458 keV is observed in the present proton transfer reactions. Assuming  $U^2 = 0.236$  for the  $3/2^+ [411]$  state in  $^{165}\text{Ho}$  (cf. Table 4.1.2), an upper limit of  $\sim 4\%$  can be given for this admixture. Thus the Zheleznova et al. calculation of the microscopic structure of the  $K^\pi = 2^-$  octupole vibration is successful in predicting the  $\sim 50\%$   $7/2^+ [633] - 3/2^- [521]$  component, but predicts a much larger  $7/2^- [523] - 3/2^+ [411]$  component than is observed.

The association of the higher lying  $I^\pi = 6^-$  state

with the octupole band is based upon the comparison of its cross section with the theoretically predicted value. This theoretical value is  $\sim 15 \mu\text{b}/\text{sr}$ , for a pure  $7/2^+[633] - 3/2^-[521]$  configuration and it is unaffected by any shortcomings in the  $C_{3/2, 1}$  coefficient, as the Clebsch-Gordan coefficient for the  $j = 3/2$  contribution to the cross section of this state is identically zero. Considering the expected 58% admixture of the pure two-quasiparticle state in the octupole vibration a cross section of  $\sim 9 \mu\text{b}/\text{sr}$  should be expected for the spin 6 state(s). The  $I^\pi = 6^-$  levels at 1787 and 1829 keV have cross sections of 3.5 and  $9.9 \mu\text{b}/\text{sr}$ , respectively, so the latter appears to be a more likely candidate for the octupole band. However, some uncertainty remains as the intensities of such weak transitions may be affected by multistep processes in the reaction mechanism.

The  $7/2^+[633] + 3/2^-[521] K^\pi = 5^-$  bandhead is assigned to a peak at 2244 keV and the spin 6 band member is assigned to a peak at 2366 keV. This excitation energy is in keeping with the known relative energies of this band with respect to others in the region (Tjøm and Elbek, 1969; O'Neil and Burke, 1972; Burke et al., 1966). The calculated splitting energy between the  $K = 2$  and  $K = 5$  bands is 170 keV, but the  $K_2$  band's interaction with the octupole vibration has greatly reduced its energy and

noticeably increased this figure.

The experimental cross section for these states is very well matched by the predicted values (Table 4.2.2), but as with the  $K_1$  band the angular distributions indicate an  $\nu = 1$  theoretical strength deficiency (Fig. 4.2.3). Apart from this small deficiency, the bandhead distribution is well fitted by the predicted shape, as is the spin 6 level.

A large ( $^3\text{He}, \alpha$ ) peak is observed at  $\sim 2244$  keV, at about the energy of the spin 5 level. This is due to the presence of an unresolved state populated by a high  $\ell$ -value neutron transfer and it obscures the ( $^3\text{He}, \alpha$ ) peak of the bandhead. Thus, the ratio of the ( $^3\text{He}, \alpha$ ) and (d, t) cross sections was unobtainable for this level. However, this ratio was available for the spin 6 state and it is consistent with the predominantly  $\ell = 3$  neutron transfer expected.

(d) The  $7/2^+[633] \pm 5/2^-[523]$  Bands

As the Fermi level is placed between the  $5/2^-[523]$  and  $7/2^+[633]$  neutron orbitals in  $^{166}\text{Er}$ , these two orbitals coupled to  $K^\pi = 6^-$  are expected to form the lowest lying two-quasiparticle state above the pairing gap. The  $K^\pi = 6^-$  band is predicted to be populated significantly with most of the strength in the spin 6 and 7 levels (cf. Table 4.2.3). Suitable candidates for these states are found at 1910 and 2050 keV. The spin 6 state is

Table 4.2.3

The  $7/2^+ [633] + 5/2^- [523]$  Bands

Energy (keV)	(d,t) $d\sigma/d\Omega$ ( $\mu\text{b}/\text{sr}$ )		$(^3\text{He}, \alpha)$ $d\sigma/d\Omega$ ( $\mu\text{b}/\text{sr}$ )		Assignment			
	Experiment $\theta=45^\circ$	Theory	Pure	Mixed	Experiment $\theta=50^\circ$	Theory	I	K
1910	$47 \pm 5$	74	70	74	$5.3 \pm 1.0$	8.7	6	$6^-$
2050	$22 \pm 4$	48	49	48	$8.8 \pm 3.5$	14.2	7	$6^-$

Table 4.2.4

The  $7/2^+ [633] + 1/2^- [521]$  Bands

Energy (keV)	(d,t) $d\sigma/d\Omega$ ( $\mu\text{b}/\text{sr}$ )		$(^3\text{He}, \alpha)$ $d\sigma/d\Omega$ ( $\mu\text{b}/\text{sr}$ )		Assignment			
	Experiment $\theta=45^\circ$	Theory	Pure	Mixed	Experiment $\theta=50^\circ$	Theory	I	K
2023	$96 \pm 15$	117	125	117	$8.0^{\text{a}}$	1.4	4	$4^-$
2122	$28 \pm 6$	22	26	22	b)	1.6	(5)	$4^-$
2080	$88 \pm 10$	87	95	87	b)	1.2	(3)	$3^-$
2149	$33 \pm 8$	27	31	27	b)	1.5	(4)	$3^-$

a) Unresolved multiplet with spin 5 member of  $7/2^+ [633] - 5/2^+ [642]$   $K^\pi = 1^+$  band  
b) Obscured by another peak, cf. Section 4.2.3

expected to be populated by a mixture of  $\ell = 3$  and  $\ell = 5$  neutron transfers, and this is consistent with the  $(^3\text{He}, \alpha)$  to  $(d, t)$  cross section ratio for the 1910 keV state (Fig. 4.2.1). The  $(d, t)$  angular distribution is also well matched by the predicted shape for this state (Fig. 4.2.4). The spin 7 band member is assigned to the level at 2050 keV on the basis of its  $\ell = 3$  and  $\ell = 5$  mixed angular distribution (Fig. 4.2.4) and cross section ratio (Fig. 4.2.1). Small Coriolis interaction effects are expected for this band as the only configurations having reasonably sized matrix elements with it are the  $7/2^+[633] + 3/2^-[532]$   $K^\pi = 5^-$  and  $7/2^+[633] + 7/2^-[514]$   $K^\pi = 7^-$  couplings, and these are far away in energy. Thus, the assignment of the spin 6 and 7 levels implies a rotational parameter of  $\sim 10.0$  keV, consistent with the value of  $\sim 9.7$  keV obtained from the lower states of the  $K^\pi = 2^-$  octupole band.

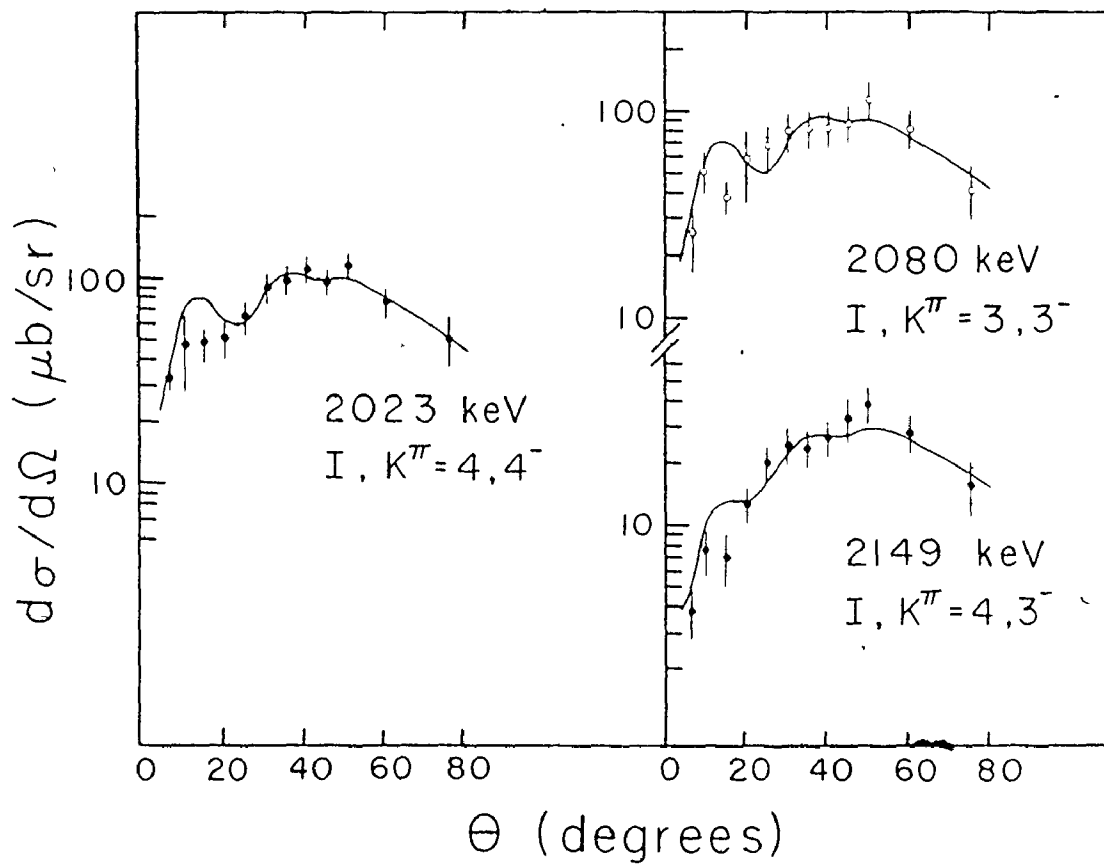
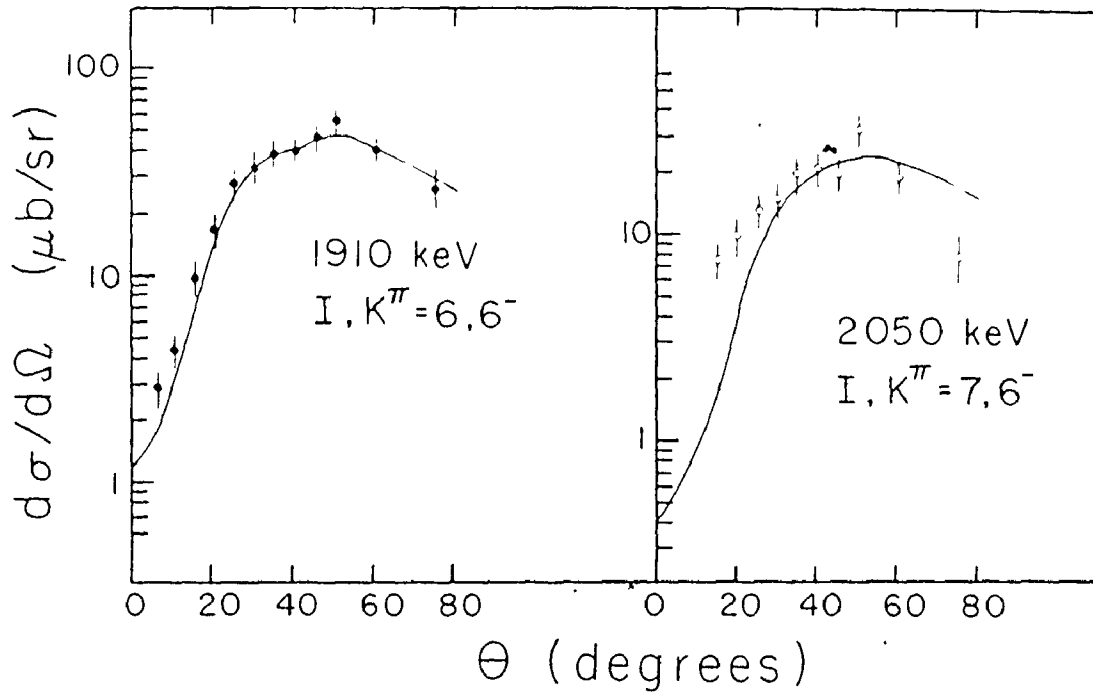
For both the  $K^\pi = 6^-$  states, the experimental cross sections are only  $\sim 55\%$  of the predicted strength. A similar effect is noted for the transfer of the  $5/2^-[523]$  orbital in  $^{165}\text{Er}$  (Tjøm and Elbek, 1969) where the experimental cross sections to the spins  $7/2$ ,  $9/2$  and  $11/2$  levels are only  $\sim 55\%$  of the predicted values. In both nuclei,  $^{165}\text{Er}$  and  $^{166}\text{Er}$ , the major components of the wavefunction of the respective states are provided by the  $C_{9/2}^5$  spherical expansion coefficient. Thus, the discrepancies

Fig. 4.2.4

$^{167}\text{Er}(d,t)^{166}\text{Er}$  angular distributions to states of the  $7/2^+[633]+5/2^-[523]$   $K^\pi = 6^-$  configuration. The first two band members are shown. The solid lines are angular distributions generated by the computer code EVEPLT for mixed  $\ell$ -value neutron transfers. These generated shapes have been scaled up or down to produce the best visual fit.

Fig. 4.2.5

$^{167}\text{Er}(d,t)^{166}\text{Er}$  angular distributions to states of the  $7/2^+[633]\pm 1/2^-[521]$  configuration. The  $K^\pi_{<} = 4^-$  band head, and the first two members of the  $K^\pi_{>} = 3^-$  band are shown. The solid lines are angular distributions generated by the computer code EVEPLT for mixed  $\ell$ -value neutron transfers. These generated shapes have been scaled up or down to produce the best visual fit.



between the observed and calculated strengths are likely a result of too large a value for this coefficient being used in the theoretical calculations. As the same effect is observed in these neighbouring nuclei, the present assignment appears to be reasonable.

The splitting energy between the  $K_{<}^{\pi} = 6^{-}$  and the  $K_{>}^{\pi} = 1^{-}$  bandheads is predicted to be  $\sim 450$  keV. As the strength to the upper band is spread among several members, the largest single cross section is predicted to be  $\sim 15$   $\mu\text{b}/\text{sr}$  and the splitting energy would put these states in a region where there are many strongly populated levels. Hence, the  $K^{\pi} = 1^{-}$  band has not been identified. Reich and Cline (1965) have tentatively assigned the  $1^{-}$  state at 1830.5 keV as the  $K = 1$  bandhead; however, this would place it below the  $K_{<}^{\pi} = 6^{-}$  bandhead, violating the Gallagher-Moszkowski rule.

(e) The  $7/2^{+}[633] \pm 1/2^{-}[521]$  Bands

The  $1/2^{-}[521]$  Nilsson orbital has a single particle energy only about 100 keV above that of the  $7/2^{+}[633]$  orbital. (cf. Table 4.1.1). Therefore, in spite of their designation as "particle states" in  $^{166}\text{Er}$ , some of the  $7/2^{+}[633] \pm 1/2^{-}[521]$  band members are predicted to have appreciable (d,t) cross sections. In addition, the only significant Coriolis mixing involving these states should occur between the parallel and antiparallel couplings.

Since this interaction matrix element is quite small (typically  $\sim 20$  keV) the two bands, with  $K_{<}^{\pi} = 4^{-}$  and  $K_{>}^{\pi} = 3^{-}$ , should be readily identifiable.

The state at 2023 keV is assigned as the spin 4 bandhead on the basis of its excitation energy, cross section (cf. Table 4.2.4), and (d,t) angular distribution (Fig. 4.2.5). The ratio of the ( $^3\text{He},\alpha$ ) to (d,t) cross sections was found to be somewhat higher than the value expected for the mixed  $\ell = 1$  and 3 neutron transfer to this state. This, however, is probably because in the ( $^3\text{He},\alpha$ ) spectra this level is not well resolved from the spin 5 state of the  $7/2^{+}[633] - 5/2^{+}[642]$   $K^{\pi} = 1^{+}$  band (tentatively assigned at  $\sim 2034$  keV in Section 4.2.g). The spin 5 level is predicted to have a much smaller cross section and is expected to lie at  $\sim 2122$  keV if a rotational parameter of  $\sim 9.7$  keV is assumed. A peak at that energy, only partially resolved from the multiplet at  $\sim 2128$  keV, is tentatively assigned as this spin 5 level. The higher spin states of this band are predicted to have very small cross sections, and they are not expected to be observed.

The most likely assignment for the  $K_{>}$  bandhead is the level at 2080 keV which has the correct cross section and (d,t) angular distribution (cf. Table 4.2.4, Fig. 4.2.5). The spin 4 band member is tentatively assigned at 2149 keV on the basis of its cross section,

(d,t) angular distribution and rotational spacing above the bandhead. The cross section ratios for these spin 3 and 4 levels are not available as the states are expected to be very weakly populated in the ( $^3\text{He},\alpha$ ) reaction and are obscured by the spin 6 and 7 members respectively of the  $7/2^+[633] - 5/2^+[642] K^\pi = 1^+$  band (cf. Sect. 4.2.g).

A problem with these tentative assignments for the  $K^\pi = 3^-$  band is that while the Gallagher-Moszkowski rule is not violated, the experimentally observed splitting energy is only  $\sim 60$  keV instead of the predicted  $\sim 260$  keV. A possible  $K^\pi = 3^-$  bandhead assignment more in keeping with this calculated splitting energy is the level at 2216 keV. However, while the (d,t) cross section at  $45^\circ$  agrees with the predicted value, the (d,t) angular distribution is definitely deficient in  $\ell = 1$  strength. Moreover, the ( $^3\text{He},\alpha$ ) cross section to this level is considerably too large. On the basis of a rotational parameter of  $\sim 9.7$  keV the spin 4 member should be found at  $\sim 2293$  keV. In the (d,t) reaction, any peak at that energy would be obscured by the large  $\ell = 0$  neutron transfer state, while in the ( $^3\text{He},\alpha$ ) reaction, the observed cross section far exceeds the predicted strength precluding any meaningful comments about the validity of this selection for the spin 4 member.

The first choice for the  $K^\pi = 3^-$  band is preferred because differences of this magnitude between the predicted

and observed splitting energies do not seem to be unusual. In the proton transfer studies (cf. Sect. 4.3) similar discrepancies are also observed.

(f) The  $7/2^+[633] \pm 11/2^-[505]$  Bands

For the  $K^\pi = 9^-$  band, the angular momentum coupling rules allow population of only the spin 9 bandhead. The  $11/2^-[505]$  orbital is found at  $\sim 600$  keV in  $^{165}\text{Er}$  and at  $\sim 1000$  keV in  $^{167}\text{Er}$ , and so with a pairing gap of 1.76 MeV for  $^{166}\text{Er}$ , this bandhead is expected to be observed at  $\sim 2560$  keV in the present study. With reference to Table 4.2.5 this level should appear as one of the strongest peaks in the  $(^3\text{He}, \alpha)$  spectrum, and such a peak at 2496 keV exhibits the required  $\ell = 5$  cross section ratio. In the  $(d, t)$  spectrum this state is found in a doublet with another populated by a stronger  $\ell = 0$  neutron transfer, and so the  $(d, t)$  angular distribution is unavailable, particularly at the forward angles. However, the  $(d, t)$  experimental cross section at  $45^\circ$  agrees with the predicted value to within experimental error.

None of the states populated by removing a neutron from an  $i_{13/2}$  orbital are predicted to have unmixed  $(^3\text{He}, \alpha)$  cross sections with even half of the value of the cross section for this  $K^\pi = 9^-$  bandhead. Nonetheless, this bandhead assignment is considered to be tentative, as it is conceivable that  $i_{13/2}$  states with substantial unmixed

Table 4.2.5

The  $7/2^+ [633] + 11/2^- [505] K^\pi = 9^-$  Band

Energy (keV)	(d,t) $d\sigma/d\Omega$ ( $\mu\text{b/sr}$ )		$(^3\text{He},\alpha) d\sigma/d\Omega$ ( $\mu\text{b/sr}$ )		Assignment
	Experiment $\theta=45^\circ$	Theory Coriolis Mixed	Experiment $\theta=50^\circ$	Theory Pure Coriolis Mixed	
2496	57±17	43	34±6	34	(9 9 <sup>-</sup> )

cross sections could mix in some complex manner so as to produce a state with the characteristics of the 2496 keV level.

The cross section to the  $K_{\pi}^{\pi} = 2^{-}$  band is spread among several states with the largest single ( ${}^3\text{He}, \alpha$ ) cross section predicted to be only  $\sim 10 \mu\text{b}/\text{sr}$ . The calculated splitting energy of  $\sim 160$  keV would place these levels in a region of high density of states and they would not stand out, thus making their identification difficult. The identification of these states in the (d,t) reaction would be even more difficult, as the cross sections would be  $\sim 10 \mu\text{b}/\text{sr}$  at most. There are many peaks in this region with much larger cross sections, cf. Fig. 4.1.1.

(g) The  $\ell = 0$  Neutron Transfers and the  $7/2^{+}[633] \pm 1/2^{+}[400]$ ,  $7/2^{+}[633] \pm 3/2^{+}[402]$ ,  $7/2^{+}[633] \pm 1/2^{+}[660]$ ,  $7/2^{+}[633] - 3/2^{+}[651]$  and  $7/2^{+}[633] - 5/2^{+}[642]$  Bands

Of the approximately seventy-five angular distributions studied in the (d,t) reaction, about a dozen had large cross sections at forward angles indicative of  $\ell = 0$  neutron transfers (Fig. 4.2.6). These states had energies of 1939, 1979, 2161, 2293, 2318, 2386, 2438, 2499, 2514, 2588, 2633 and 2734 keV (Fig. 4.2.7). The only configuration in this mass region which would be expected to generate large  $\ell = 0$  (d,t) cross sections is the  $7/2^{+}[633] \pm 1/2^{+}[400]$  coupling. From comparisons with the odd Er nuclei (Tjøm and Elbek, 1969) this configuration is likely

Fig. 4.2.6

$^{167}\text{Er}(d,t)^{166}\text{Er}$  angular distributions to states populated with prominent  $\ell=0$  neutron transfer components. The  $\ell=0$  transfer is due to admixtures of the  $7/2^+[633]\pm 1/2^+[400]$  configuration into these states. For a pure configuration, only three states ( $I, K^\pi = 3, 3^+, 4, 3^+, \text{ and } 4, 4^+$ ) would be expected to be populated by  $\ell=0$  neutron transfers; the dozen states observed in this work are accounted for by a complex mixing scheme (see text).

The solid lines are pure  $\ell=0$  angular distributions from the DWBA calculation with a  $Q$  value of  $-2.0$  MeV. They have been scaled up or down to produce the best visual fit.

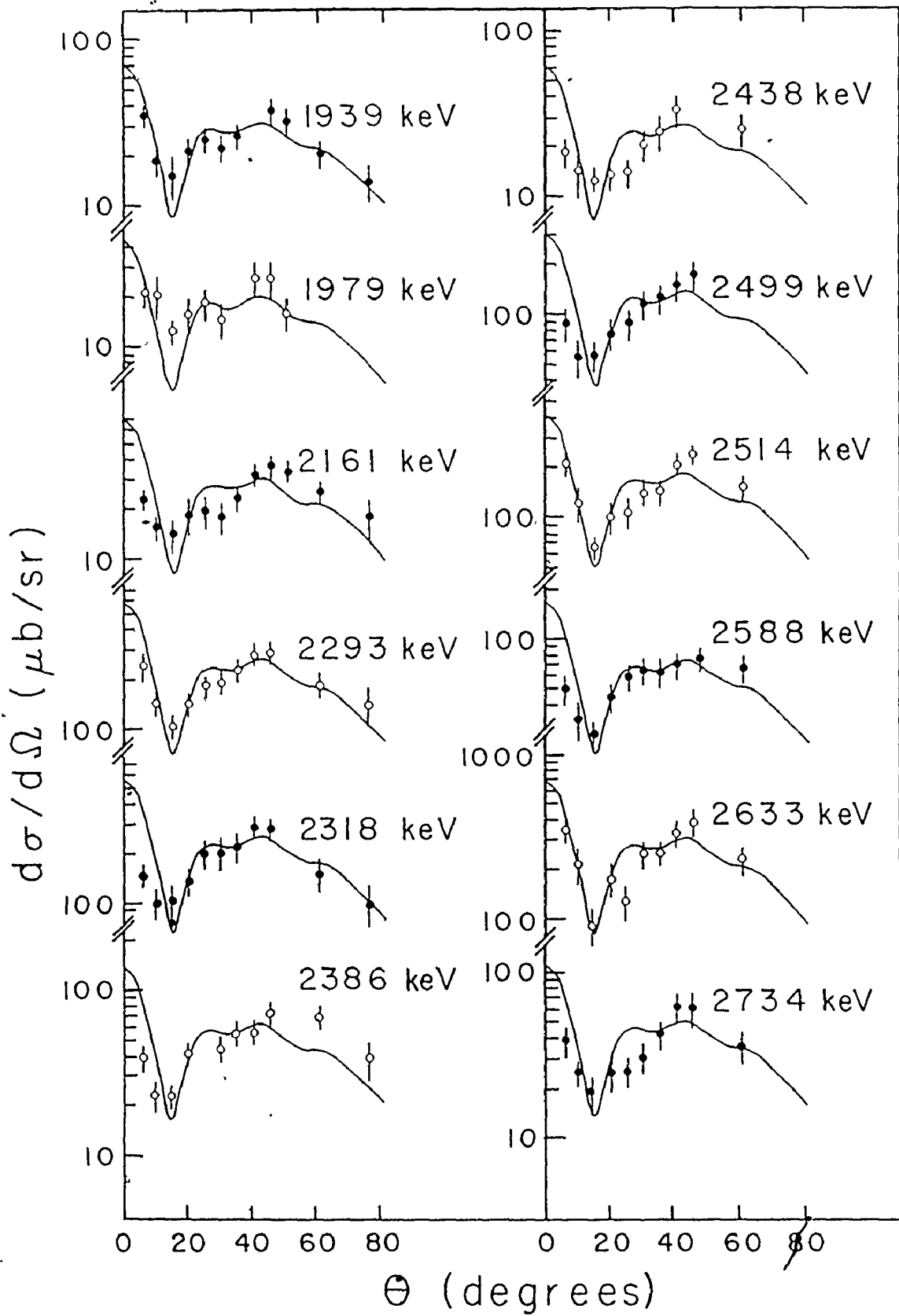
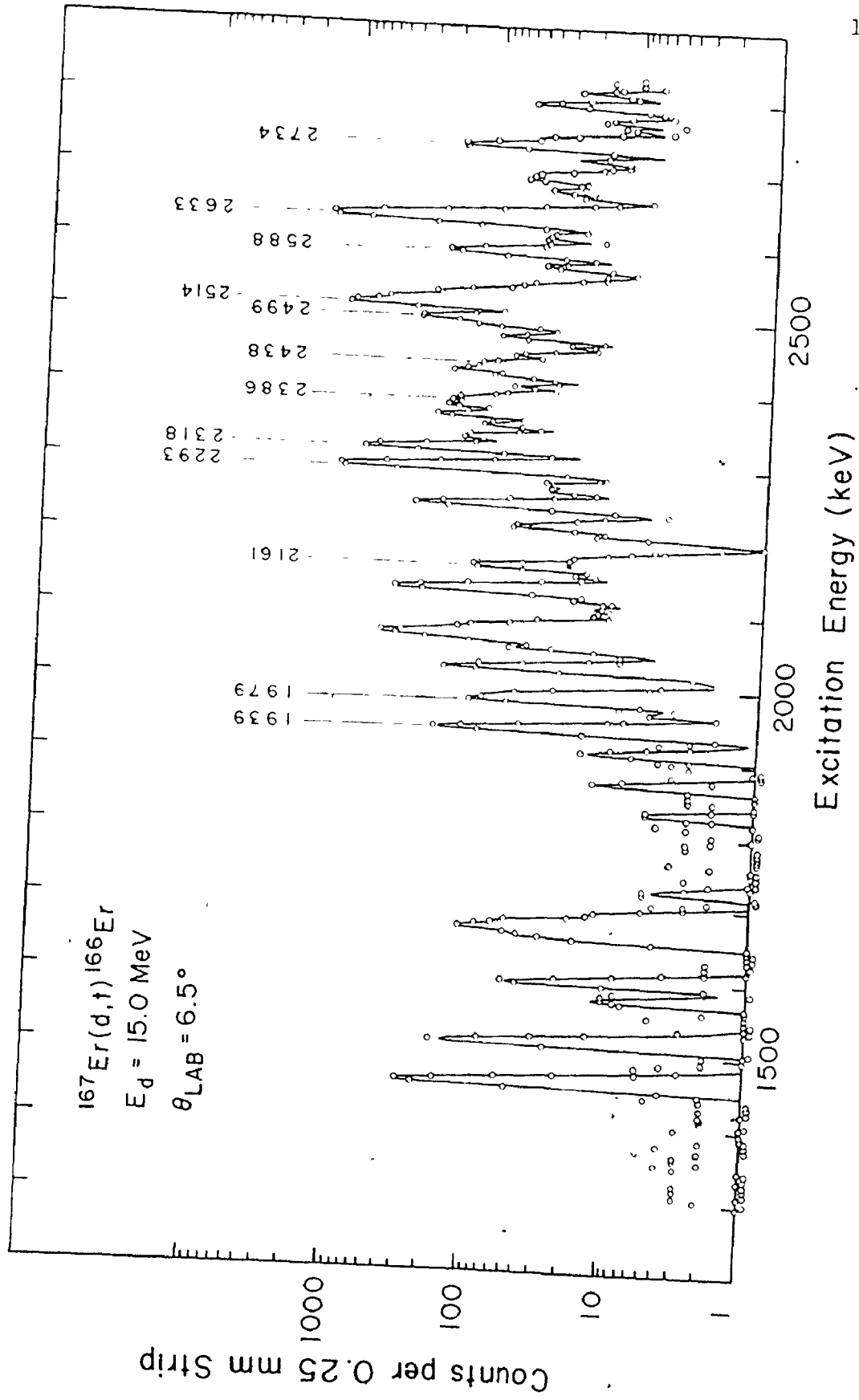


Fig. 4.2.7

The  $^{167}\text{Er}(d,t)^{166}\text{Er}$  spectrum at  $6\ 1/2^\circ$  from  $\sim 1300$  to  $\sim 2800$  keV. The energies denote the positions of peaks populated by neutron transfers displaying  $\ell=0$  characters. The four labels raised above the others are for levels with configurations which are predominantly a mixture of the  $7/2^+[633]\pm 1/2^+[400]$  and the  $7/2^+[633]\pm 1/2^+[660]$  couplings.



to be found at about 2400 to 2800 keV in  $^{166}\text{Er}$ . Considering only the two bands from this coupling, three states populated by  $\ell = 0$  transitions should be found viz. the spin 3 and 4 states of the "antiparallel"  $K^\pi = 3^+$  band, and the "parallel"  $K = 4^+$  bandhead. To account for the additional  $\ell = 0$  transfers, various mixing interactions need to be invoked.

Coriolis mixing between the  $7/2^+[633] - 1/2^+[400]$  and  $7/2^+[633] - 3/2^+[402]$  bands can give rise to two more states populated by  $\ell = 0$  transfers, the spin 3 and 4 members of the  $K^\pi = 2^+$  band. This mixing is not expected to be strong, however, as the  $1/2^+[400]$  and  $3/2^+[402]$  orbitals originate from different shell model states resulting in small Coriolis matrix elements ( $\lesssim 30$  keV). Thus, this Coriolis interaction is probably not responsible for the large cross section of many of the states populated by  $\ell = 0$  neutron transfers. Moreover, the number of such transfers generated by this interaction is insufficient to account for the observed data.

To explain similar multiple strong  $\ell = 0$  neutron transfers, previous works have introduced  $\Delta N = 2$  mixings between states involving the orbitals  $1/2^+[400]$  and  $1/2^+[660]$ , and the orbitals  $3/2^+[402]$  and  $3/2^+[651]$ . (e.g. Jolly, 1976; Tjømm and Elbek, 1969). To investigate the effects of all these mixings quantitatively in the present study, a symme-

tric interaction matrix was set up. In this matrix, the diagonal elements were the pre-mixing energies of the states involved, and the off diagonal terms were the Coriolis and  $\Delta N = 2$  interaction strengths. These were all treated as input parameters. The matrix was diagonalized with the routine EAOLB, acquired from the McMaster University Computer Program Library (Milis, 5.3.265, 1974). Eigenvalues and eigenvectors were obtained as output, and the latter were used with DWBA cross sections to obtain predicted cross sections for the mixed states. Calculations were performed separately for spin 3 and spin 4, the former with a 5 x 5 matrix, the latter with an 8 x 8 matrix. The input matrices labelled with the relevant configurations for each column are presented in Table 4.2.6 and 4.2.7 for spins 3 and 4, respectively. The eigenvectors and cross sections at  $6\frac{1}{2}^\circ$  are presented in Tables 4.2.8 and 4.2.9, again for spins 3 and 4, respectively. The experimental cross sections at  $6\frac{1}{2}^\circ$  are also presented for comparison.

Many attempts to reproduce the experimentally observed spectrum were tried by changing, first, the pre-mixing order and spacings of the states, and second, the values of the interaction matrix elements. While the effects of varying the interaction matrix-elements were quite considerable, they were not as drastic as the results of the first changes. In fact, the schemes presented in

Table 4.2.6

Input Matrix, I = 3 a)

$7/2^+$ [633] $-1/2^+$ [400]	$7/2^+$ [633] $-3/2^+$ [402]	$7/2^+$ [633] $-1/2^+$ [660]	$7/2^+$ [633] $-3/2^+$ [651]	$7/2^+$ [633] $-5/2^+$ [642]
K = 3	K = 2	K = 3	K = 2	K = 1
2393	-15	-110	0	0
-15	2600	0	-65	0
-110	0	2397	-60	0
0	-65	-60	2270	-116
0	0	0	-116	2250

a) All matrix elements in keV.

Table 4.2.7

Input Matrix, I = 4 a)

$7/2^+ [633]$ $-1/2^+ [400]$	$7/2^+ [633]$ $+1/2^+ [400]$	$7/2^+ [633]$ $-3/2^+ [402]$	$7/2^+ [633]$ $-1/2^+ [660]$	$7/2^+ [633]$ $+1/2^+ [660]$	$7/2^+ [633]$ $-3/2^+ [651]$	$7/2^+ [633]$ $-5/2^+ [642]$	$7/2^+ [633]$ $-7/2^+ [633]$
K = 3	K = 4	K = 2	K = 3	K = 4	K = 2	K = 1	K = 0
2480	-5	-22	-110	0	0	0	0
-5	2520	0	0	-107	0	0	0
-22	0	2583	0	0	-20	0	0
-107	0	0	2470	-134	-177	0	0
0	-110	0	-134	2440	0	0	0
0	0	-20	-177	0	2240	-196	0
0	0	0	0	0	-196	2060	222
0	0	0	0	0	0	222	265

a) All matrix elements in keV.

Table 4.2.8

Eigenvectors and Eigenvalues for I = 3

$7/2^+ [633]$ $-1/2^+ [400]$ K = 3	$7/2^+ [633]$ $-3/2^+ [402]$ K = 2	$7/2^+ [633]$ $-1/2^+ [660]$ K = 3	$7/2^+ [633]$ $-3/2^+ [651]$ K = 2	$7/2^+ [633]$ $-5/2^+ [642]$ K = 1	Calculated $d\sigma/d\Omega, \theta=6\frac{1}{2}^\circ$ ( $\mu\text{b}/\text{sr}$ )	Calculated Energy (keV)	Experimental $d\sigma/d\Omega, \theta=6\frac{1}{2}^\circ$ ( $\mu\text{b}/\text{sr}$ )	Experimental Energy (keV)
-.124	-.956	-.123	.224	-.071	28	2617	50	2591
-.646	-.217	.713	-.153	.068	334	2509	210	2514
-.087	-.099	-.193	-.696	-.679	9	2131	36	1939
.380	-.163	.093	-.658	.623	131	2372	24	2161
-.645	-.050	-.656	-.097	.376	415	2280	241	2293

Table 4.2.9  
Eigenvectors and Eigenvalues for I = 4

$7/2^+ [633]$ $-1/2^+ [400]$ K = 3	$7/2^+ [633]$ $+1/2^+ [400]$ K = 4	$7/2^+ [633]$ $-3/2^+ [402]$ K = 2	$7/2^+ [633]$ $-1/2^+ [660]$ K = 3	$7/2^+ [633]$ $+1/2^+ [660]$ K = 4	$7/2^+ [633]$ $-3/2^+ [651]$ K = 2	$7/2^+ [633]$ $-5/2^+ [642]$ K = 1	$7/2^+ [633]$ $-7/2^+ [633]$ K = 0	Calc. $d\sigma/d\Omega$ , $\theta = 60^\circ$ ( $\mu\text{b}/\text{sr}$ )	Calc. Energy (keV)	Exp. $d\sigma/d\Omega$ , $\theta = 60^\circ$ , ( $\mu\text{b}/\text{sr}$ )	Exp. Energy (keV)
.000	.000	.000	.001	.000	.012	.122	-.992	0	238	1	265
.046	.012	.020	.224	.062	.607	.752	.100	2	1931	NOT OBSERVED	
.254	.165	.034	.588	.440	.341	-.499	-.056	87	2219	22	1979
-.353	.295	.117	.673	-.469	-.304	.190	.009	25	2701	39	2734
.834	-.234	.085	.208	-.183	-.358	.190	.019	7	2452	19	2441
.276	.697	.459	-.327	-.272	.202	-.083	-.008	621	2561	345	2633
-.190	-.364	.875	.031	.239	-.084	.032	.003	172	2590	89	2499
-.010	.462	-.047	-.022	.647	-.496	.344	.036	248	2366	147	2318

Tables 4.2.6 and 4.2.7 were basically the only ones which / came even close to reproducing the observed data.

In comparing the predicted energies and cross sections to the observed data, the great complexity of the mixings lead to two problems: first, the states can become so thoroughly mixed that they cannot be meaningfully labelled by any given Nilsson configuration; and second, where one configuration is expected to predominate and labelling is possible, if the predicted cross section is fairly small and several small peaks exhibiting  $\ell = 0$  populations are present it is often difficult to decide just which experimental state should be matched to this predicted state. Generally, for the very large peaks characterized by  $\ell = 0$  transfers, neither problem really exists.

Four large peaks are observed in the  $6\frac{1}{2}^0$  (d,t) spectrum (Fig. 4.2.7) at 2293, 2318, 2514 and 2633 keV, all with the requisite  $\ell = 0$  angular distributions, and these have been tentatively assigned. The level at 2633 keV is the most strongly populated, and on that basis it is assigned as being predominantly the  $7/2^+[633] + 1/2^+[400]$   $IK^\pi = 44^+$  state; the level at 2318 keV is suspected to be predominantly the  $7/2^+[633] + 1/2^+[660]$   $IK^\pi = 44^+$  state. These two states mix mainly with each other. The equally intensely populated states at 2293 and 2514 keV are

tentatively assigned as the pair of  $IK^\pi = 33^+$  levels both predominantly being composed of the same two configurations. Their roughly equal populations imply that, barring any further significant mixings with other states, they were nearly degenerate prior to mixing. This provides an estimate of the  $\Delta N = 2$  matrix element, and the value of  $\sim 110$  keV is consistent with similar matrix elements for  $^{165}\text{Er}$  ( $\sim 117$  keV, Tjøm and Elbek, 1969) and  $^{163}\text{Dy}$  ( $\sim 107$  keV, Grotdal et al. 1970).

These mixings can also account for the other  $\ell = 0$  neutron transfers. Once the  $\ell = 0$  strength is injected into the  $7/2^+[633] \pm 1/2^+[660]$  bands, the Coriolis interaction will pass it on to the  $7/2^+[633] - 3/2^+[651]$   $K^\pi = 2^+$  band and the  $7/2^+[633] - 5/2^+[642]$   $K^\pi = 1^+$  band. A further  $\Delta N = 2$  mixing can transfer  $\ell = 0$  strength between the  $7/2^+[633] - 3/2^+[651]$   $K^\pi = 2^+$  band and the  $7/2^+[633] - 3/2^+[402]$   $K^\pi = 2^+$  band. In all these cases only spin 3 and 4 band members will share in the  $\ell = 0$  character.

A level previously labelled as  $I^\pi = 3^{(+)}$  at 2160.2 keV in the decay study of  $^{166}\text{Tm}$  (Zylicz et al., 1966) is associated in this (d,t) work with the state populated by an  $\ell = 0$  transfer at 2161 keV. It is assigned as being the  $I = 3$  member of the  $7/2^+[633] - 3/2^+[651]$   $K^\pi = 2^+$  band, although its population in the (d,t) reaction is primarily through the  $7/2^+[633] - 1/2^+[400]$   $K^\pi = 3^+$  admixture. The

$I = 4$  band member has not been identified.

The  $I = 3$  and 4 members of the  $7/2^+[633] - 5/2^+[642]$   $K^\pi = 1^+$  band have been assigned to the levels at 1939 and 1979 keV, respectively. The level at 1938.2 keV was previously assigned as  $I^\pi = 2^+$  or  $3^+$  (Zylicz et al., 1966), and its  $\ell = 0$  population demands the  $I^\pi = 3^+$  label. The same study ascribed  $I^\pi = 2^+$  or  $3^+$  or  $4^+$  to the state at 1979.0 keV, consistent with the present  $I^\pi = 4^+$  assignment. The spin 5, 6 and possibly the spin 7 members of this  $K^\pi = 1^+$  band are tentatively assigned to the levels at 2031, 2090 and 2149 keV mainly on the basis of their ( $^3\text{He}, \alpha$ ) to (d,t) cross section ratios (cf. Fig. 4.2.1) and their conformation to the expected rotational pattern. The experimentally observed rotation parameter of  $\sim 5$  keV for this band is based on the spin 3 and 4 members.

In comparing the data involving  $\ell = 0$  transfers to the predicted values (Tables 4.2.8 and 4.2.9), it is noteworthy that while an exact reproduction of the observed spectrum was not obtainable, most of the strongly populated states were reasonably well matched by the calculation, both in energy and intensity. In addition, the  $\ell = 0$  strength was, in fact, brought down into the lower energy bands in agreement with experiment. In some of the attempted calculations with different input matrices, this effect was far more spectacular, but in those cases, the fit to the

higher lying levels was not as good. The results presented in Tables 4.2.8 and 4.2.9 show the best overall agreement between calculation and experiment that was achieved by manual variations in the input matrices.

One of the largest peaks in the (d,t) spectrum was the level at 2336 keV, and on the basis of its intensity, strong  $\ell = 2$  angular distribution (Fig. 4.2.6) and  $\ell = 2$  cross section ratio (Fig. 4.2.1) it has been assigned as the  $K_{\zeta}^{\pi} = 5^{+}$  bandhead of the  $7/2^{+}[633] + 3/2^{+}[402]$  configuration. The predicted splitting energy of 185 keV is consistent with the placing of the  $K_{\zeta}^{\pi} = 2^{+}$  bandhead (prior to any mixings) at  $\sim 2535$  keV. This is the energy for the  $K^{\pi} = 2^{+}$  bandhead that is obtained from the "best fit" energies of the  $I^{\pi} = 3^{+}$  and  $4^{+}$  band members (prior to mixing) in the complex mixing calculation. They were used as input parameters (diagonal matrix elements) for that calculation. Thus, the mixing calculation is compatible with the placement of the  $K_{\zeta}^{\pi} = 5^{+}$  bandhead.

#### (h) Miscellaneous States

The level at 1868 keV is observed in both the neutron transfer and proton transfer reactions. Its (d,t) angular distribution (Fig. 4.2.8b) and cross section ratio imply an  $\ell = 5$  neutron transfer. As no unassigned states populated by high  $\ell$  neutron transfers are expected to be found in this energy region, the appearance of this peak

in the (d,t) and ( $^3\text{He},\alpha$ ) spectra remains unexplained.

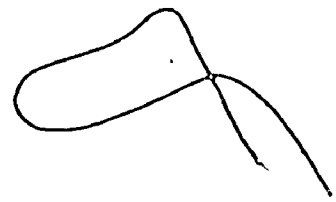
Another peak observed in both the neutron transfer and proton transfer reactions is found at  $\sim 2128$  keV. In the proton transfer study this peak is a multiplet assigned to at least three individual states with different spins. (cf. Table 2.4.1). This multiplet nature is also evident in the (d,t) study, and its population in the neutron pickup experiment remains unexplained.

In the region between  $\sim 1950$  and  $\sim 2650$  keV there are approximately fourteen levels which appear in both the proton transfer and the neutron transfer spectra, at excitation energies that are identical within the experimental uncertainty of  $\pm 2$  keV. Four or five other levels exhibit less certain "coincidences". If the number of random "coincidences" that might be expected between such states is calculated, the probability peaks at about twelve with a standard deviation of about three. Thus, while some "coincidences" are possibly due to a form of n-p interaction, most are probably accidental and so in general it is not assumed that the levels populated in the neutron transfer processes have to be the same ones as observed in the proton transfer reactions.

The angular distributions to the remaining unassigned states observed in this study are shown in Fig. 4.2.8. Their (d,t) cross sections range from a few  $\mu\text{b}/\text{sr}$

Fig. 4.2.8a

$^{167}\text{Er}(d,t)^{166}\text{Er}$  angular distributions for miscellaneous states observed in the present study. The first four states (786, 859, 957 and 1075 keV) are the first four members of the  $\gamma$ -vibrational band. The other angular distributions are for states unassigned in this work.



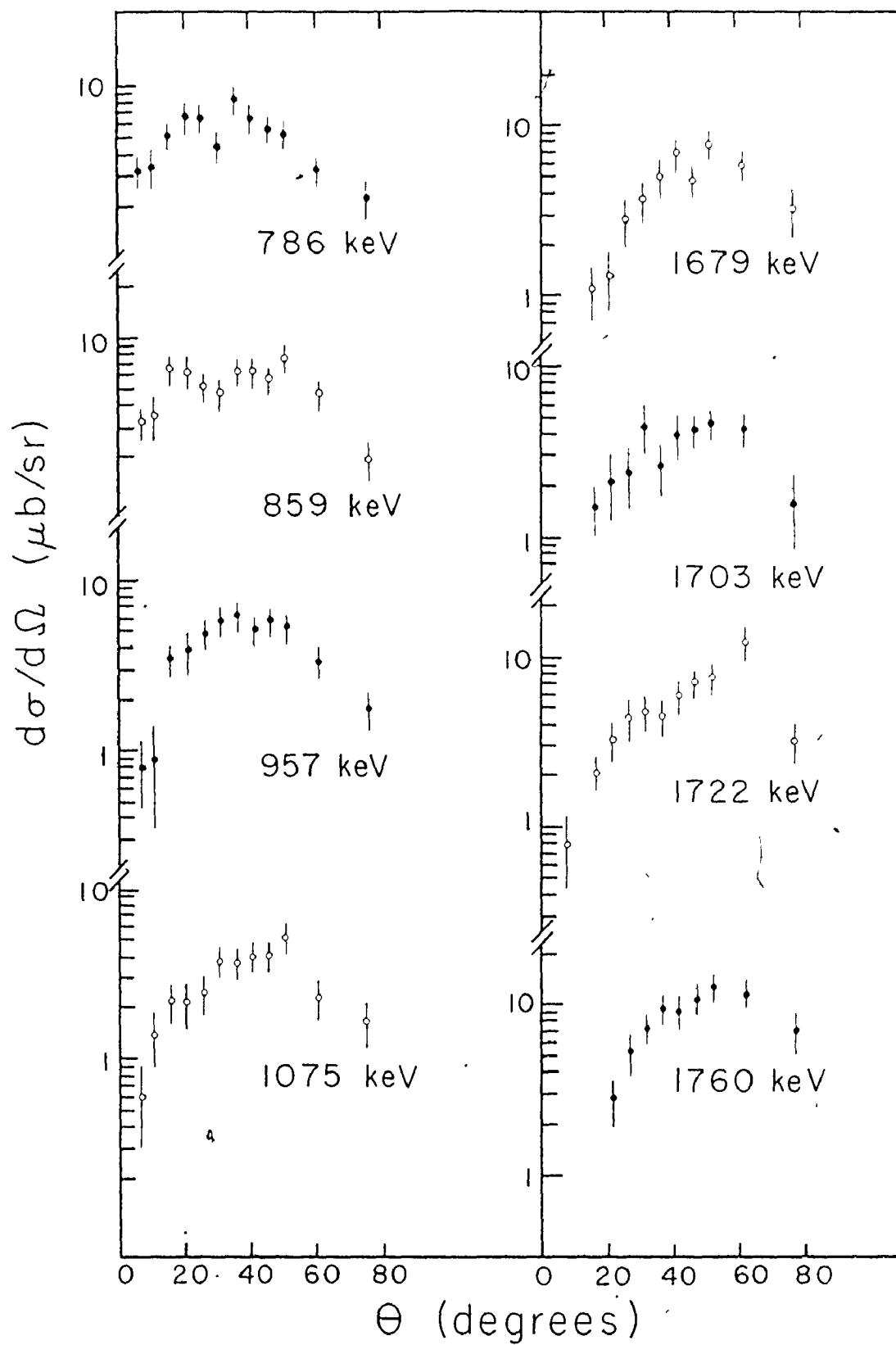


Fig. 4.2.8b

$^{167}\text{Er}(d,t)^{166}\text{Er}$  angular distributions for miscellaneous states observed in the present study. Assignments have not been made for these states in this work.

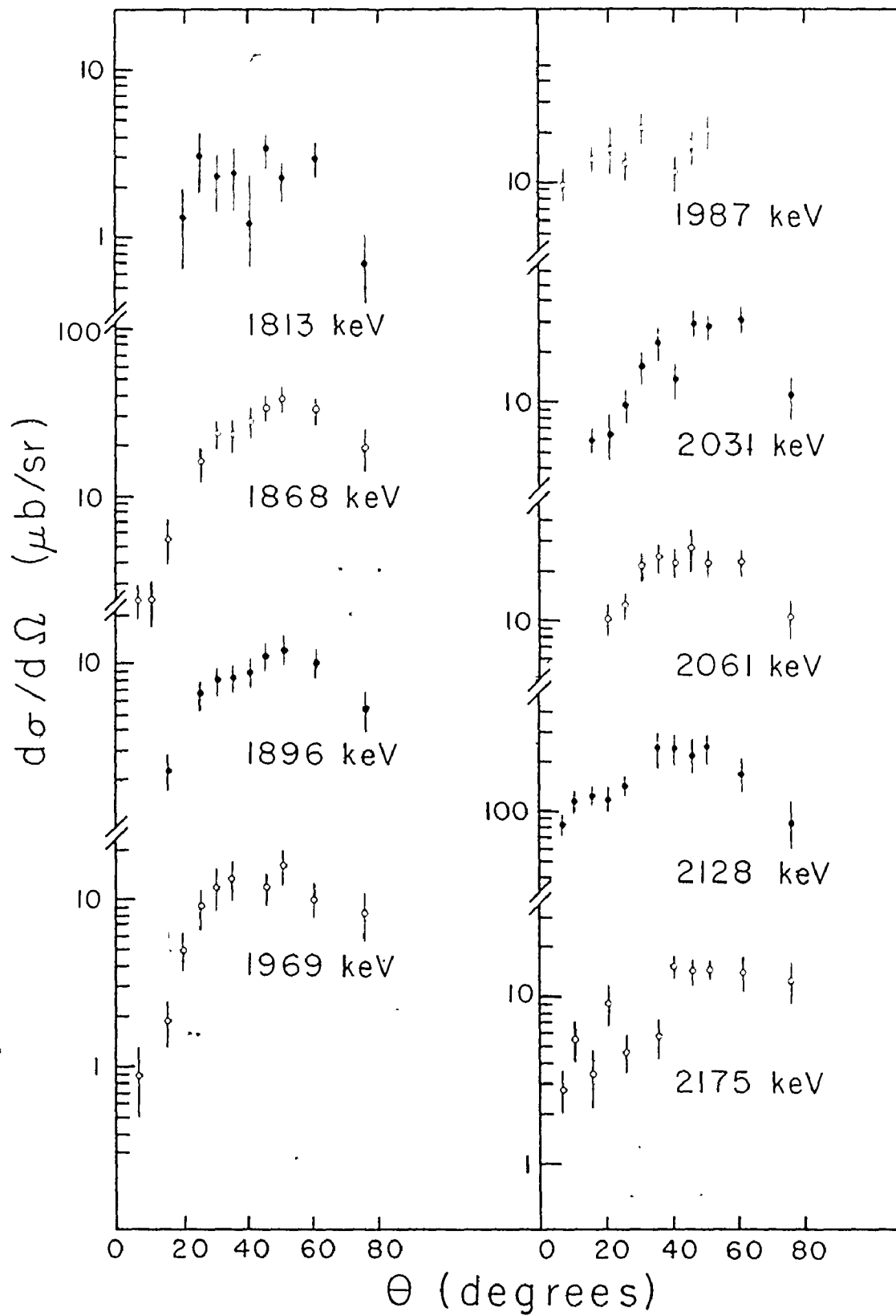


Fig. 4.2.8c

$^{167}\text{Er}(d,t)^{166}\text{Er}$  angular distributions for miscellaneous states observed in the present study. Assignments have not been made for these states in this work.

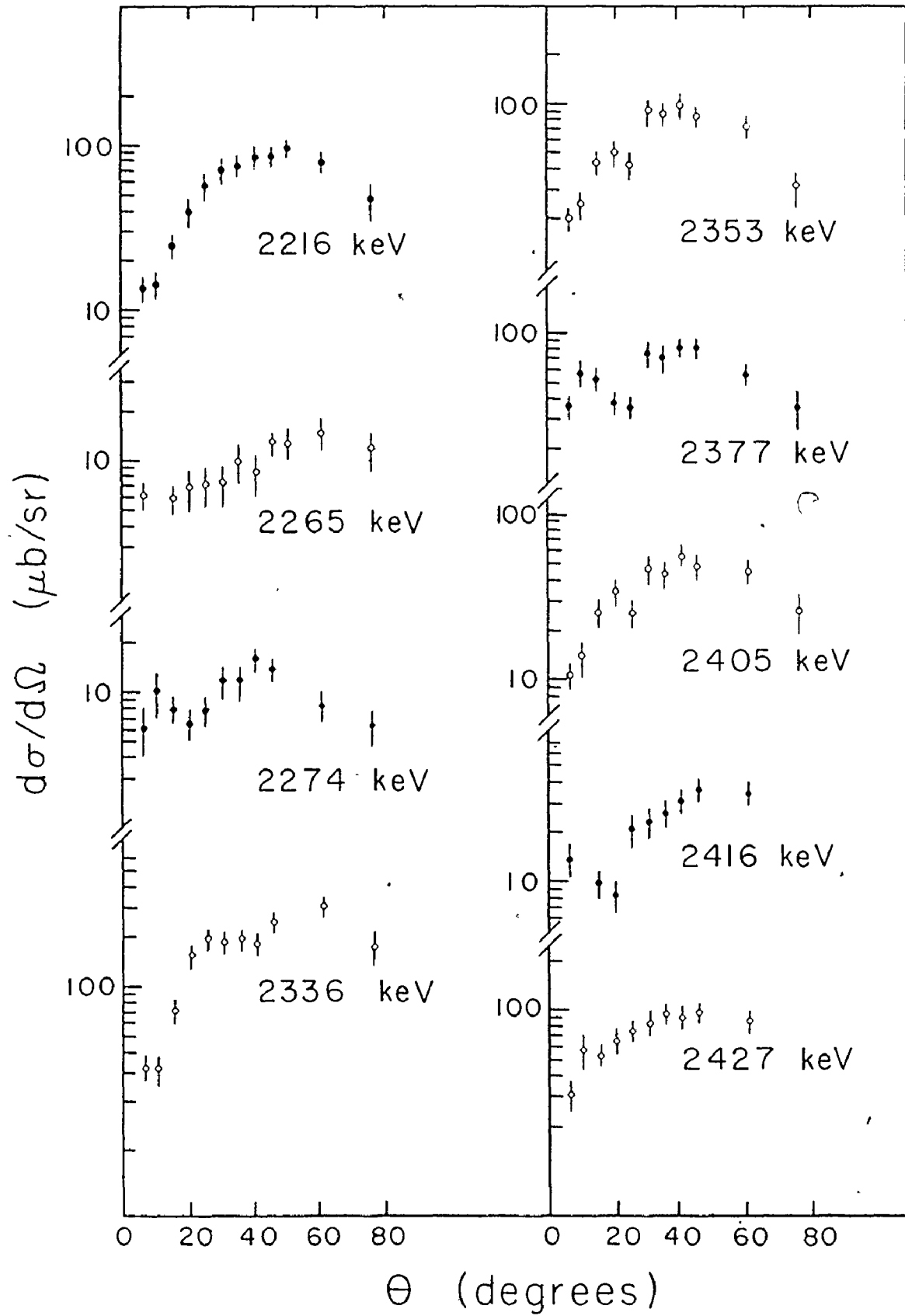
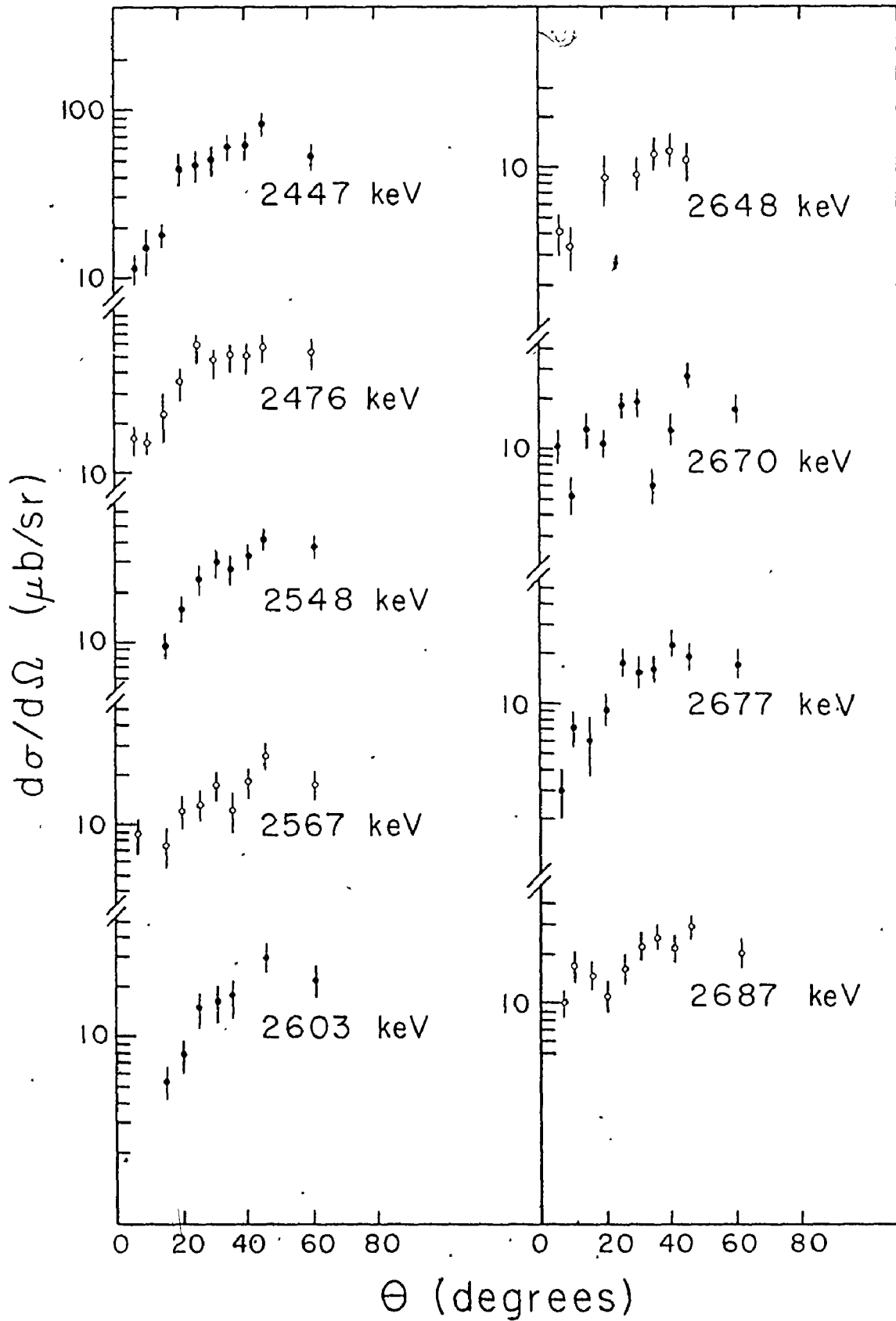


Fig. 4.2.8d

$^{167}\text{Er}(d,t)^{166}\text{Er}$  angular distributions for miscellaneous states observed in the present study. Assignments have not been made for these states in this work.



to almost 100 $\mu$ b/sr. While some of these states may be due to predominantly one two-quasiparticle configuration, many are doubtless states formed by second order mixing effects between the states already described. Others likely come from particle-vibration interactions similar to those described in Section 4.2.c, or from  $\gamma$ -vibrations built upon particle states as seen in the odd Ho and Tm nuclei (Wagner, et al., 1975; Panar et al., 1977; Cheung, et al., 1974). These states do not, however, comprise a large fraction of the total cross section. In the  $45^\circ$  (d,t) spectrum almost 80% of the strength has been either tentatively or definitely assigned in the above sections.

#### 4.3 States Populated in the Proton Transfer Reactions

##### (a) The Ground State Band

The  $K^\pi = 0^+$  ground state band of  $^{166}\text{Er}$  is formed in the ( $^3\text{He},d$ ) and ( $\alpha,t$ ) reactions by adding a proton in the  $7/2^- [523]$  orbital to the  $7/2^- [523]$  proton already present in the  $^{165}\text{Ho}$  target ground state. Peaks corresponding to rotational band members up to spin 8 are observed in both reactions (cf. Fig. 2.4.1, Table 4.3.1) (cf. also Kubo, 1968). In agreement with the cross section prediction, the spin 0 and 8 members of the band are weakly populated, while for the other observed band members, where comparisons between the experimental and predicted cross sections can be made, the agreement is reasonably good.

Table 4.3.1

## The Ground State Band, Proton Transfer Reactions

Energy (keV)	$(^3\text{He}, d) \, d\sigma/d\Omega \, (\mu\text{b/sr})$		$(\alpha, t) \, d\sigma/d\Omega \, (\mu\text{b/sr})$		Assignment I K $\pi$	
	Experiment $\theta=45^\circ$	Pure Theory Coriolis Mixed	Experiment $\theta=60^\circ$	Pure Theory Coriolis Mixed		
0	$1.0 \pm 0.5$	0.2	$< 1.0 \pm 0.5$	0.4	0	0 <sup>+</sup>
79	$2.2 \pm 0.5$	0.9	$6.1 \pm 1.0$	4.0	2	0 <sup>+</sup>
264	$6.4 \pm 1.2$	3.9	$24 \pm 4$	18.1	4	0 <sup>+</sup>
543	$2.8 \pm 0.6$	2.2	$10.7 \pm 1.7$	9.9	6	0 <sup>+</sup>
910	$< 1.0 \pm 0.5$	0.2	$< 1.0 \pm 0.5$	0.7	8	0 <sup>+</sup>

Fig. 4.3.1

Ratios of differential cross sections for the  $(^3\text{He},d)_{60^\circ}$  and  $(\alpha,t)_{60^\circ}$  reactions as a function of excitation energies in keV. The solid lines represent the predicted ratio for the transfer of a proton with the  $\ell$ -value indicated. The points are the observed ratios for levels in  $^{166}\text{Er}$  labelled by their excitation energies. The predicted curves have been normalized to members of the ground state band (see text).

The short bar with an upward pointing arrow is a lower limit for the value of the ratio, R.

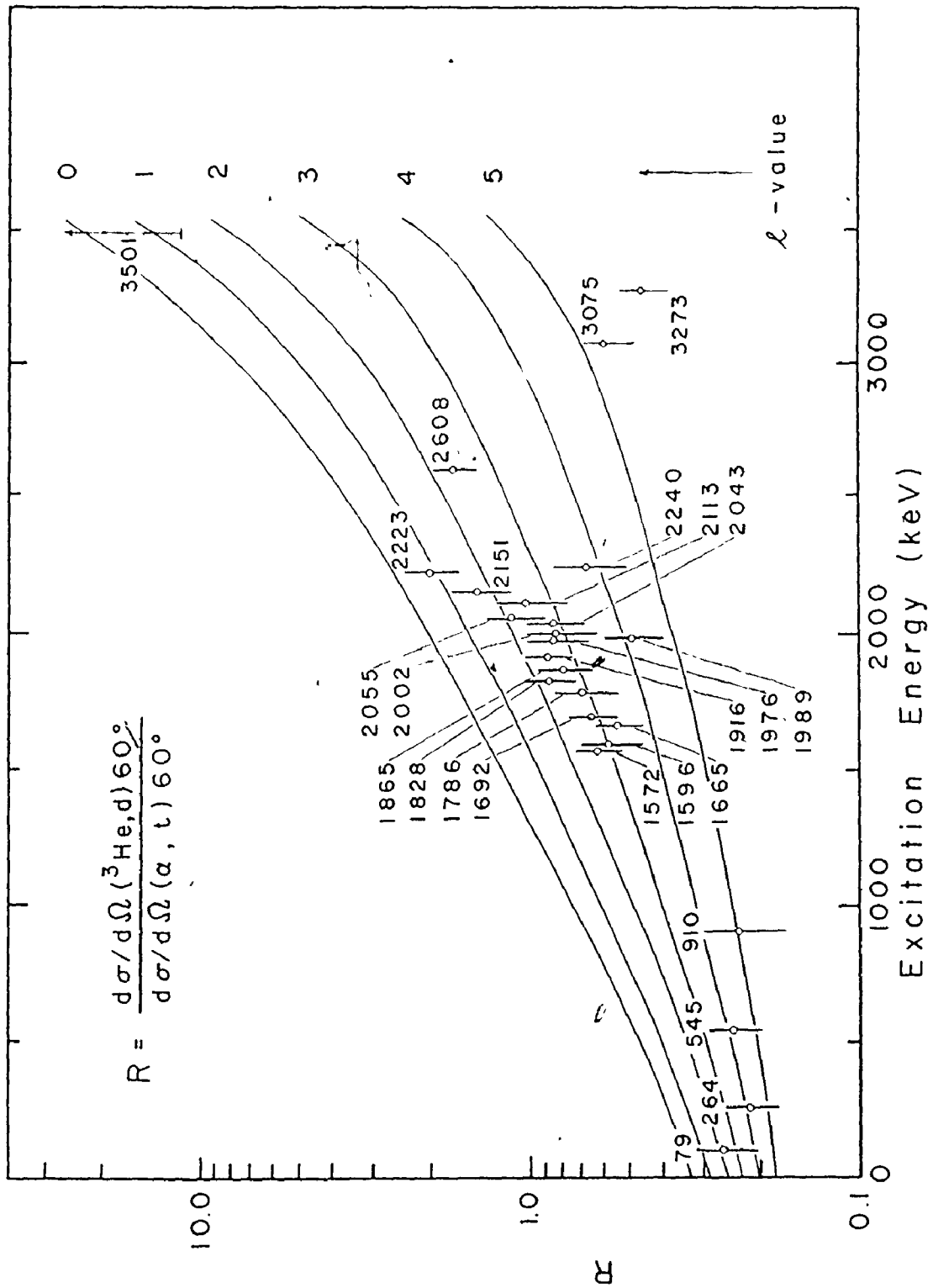
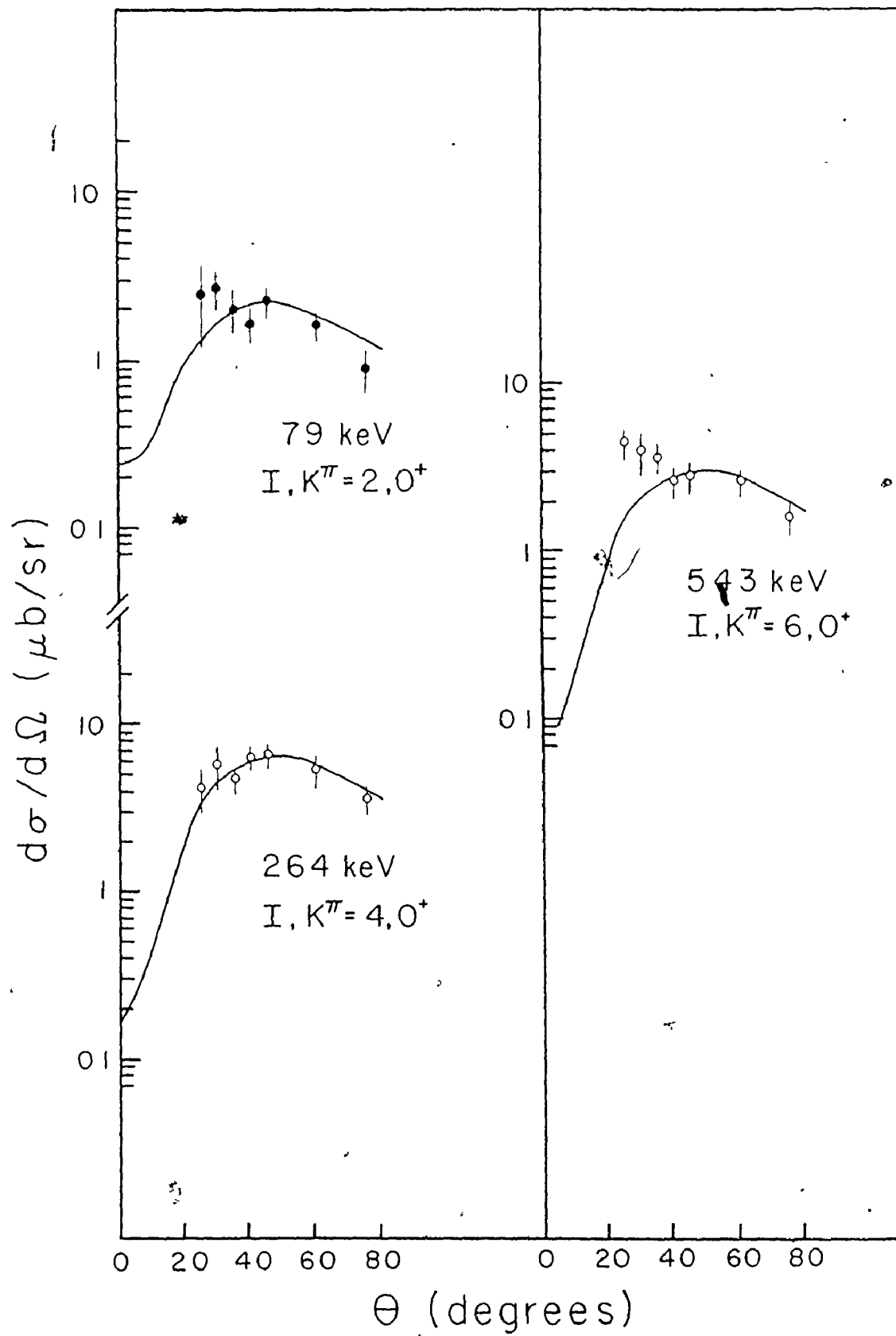


Fig. 4.3.2

$^{165}\text{Ho}(^3\text{He},d)^{166}\text{Er}$  angular distributions to the spins 2, 4 and 6 members of the ground state band. The solid lines are angular distributions generated by the computer code EVEPLT for mixed  $l$ -value proton transfers. These generated shapes have been scaled up or down to produce the best visual fit.



This band will be predominantly populated by higher  $\ell$ -value transfers ( $\ell \sim 5$ ) as the  $7/2^- [523]$  orbital originates from the  $h_{11/2}$  shell model state and  $C_{11/2 5}$  is expected to be the largest  $C_{j\ell}$  coefficient. The  $(^3\text{He},d)$  angular distributions, shown in Fig. 4.3.2 are consistent with the calculated mixed  $\ell = 3$  and 5 transfer to the spin 2 and 4 levels. From the angular distribution it is evident that an impurity peak obscures the spin 6 state at forward angles, destroying the almost pure  $\ell = 5$  shape which is predicted by the theory. The ratio of  $(^3\text{He},d)$  and  $(\alpha,t)$  cross sections for levels with spins 2 to 8 are presented in Fig. 4.3.1. The ratio plot is normalized using the ground state band, with the  $(\alpha,t)$  DWBA normalization being 78 for a  $(^3\text{He},d)$  DWBA normalization of 6 (cf. also Sect. 3.4.b).

(b) The  $K^\pi = 2^+$   $\gamma$ -Vibrational Band

The members of this band have been observed in this study up to spin 6 in the  $(^3\text{He},d)$  reaction, and up to spin 5 in the  $(\alpha,t)$  reaction (cf. Fig. 2.4.1). All the band members are very weakly populated in these reactions, typical cross sections being  $\sim 1\%$  of those for the largest peaks in the spectra. Thus, as in the neutron transfer studies, the structure of the band has not been investigated.

(c) The  $7/2^- [523] \pm 1/2^+ [411]$  Bands

The  $1/2^+ [411]$  orbital forms the lowest lying "particle" state in  $^{165}\text{Ho}$  (Wagner et al., 1975). Therefore,

the band built on the  $K_{\pi}^{\pi} = 4^{-}$  coupling of the  $7/2^{-}[523] + 1/2^{+}[411]$  configuration should be the first one observed above the pairing gap in  $^{166}\text{Er}$ . It was discussed in Section 4.2.c along with the  $K^{\pi} = 2^{-}$  octupole band, which was populated in the neutron transfer reactions through an admixture of the  $7/2^{+}[633] - 3/2^{-}[521]$   $K^{\pi} = 2^{-}$  configuration. In that section "pairs" of levels were noted:  $I^{\pi} = 4^{-}$  at 1572 and 1596 keV,  $I^{\pi} = 5^{-}$  at 1665 and 1692 keV, and  $I^{\pi} = 6^{-}$  at 1786 and 1828 keV (cf. Fig. 4.1.2). It was also noted that the  $K_{\pi}^{\pi} = 4^{-}$  bandhead assignment for the 1572 keV state was suggested by Zylicz et al. (1966). This assignment was confirmed in a previous ( $^3\text{He},d$ ) study of  $^{166}\text{Er}$  (Kubo, 1968), and while this suggestion is still considered to be essentially correct, a small admixture of the two neutron  $7/2^{+}[633] - 3/2^{-}[521]$   $K^{\pi} = 2^{-}$  configuration into this state is proposed in the present study. This admixture is the result of a form of mixing between this  $K^{\pi} = 2^{-}$  two neutron configuration and the  $7/2^{-}[523] + 1/2^{+}[411]$   $K^{\pi} = 4^{-}$  two proton configuration. As noted in Section 4.2.c, the mixing gives rise to the pairs of states for spins 4, 5 and 6 observed in both the neutron transfer and proton transfer reactions.

The similarity in the shapes of the ( $^3\text{He},d$ ) angular distributions for each pair (Fig. 4.3.3) is also considered, along with the coincident excitation energies for the

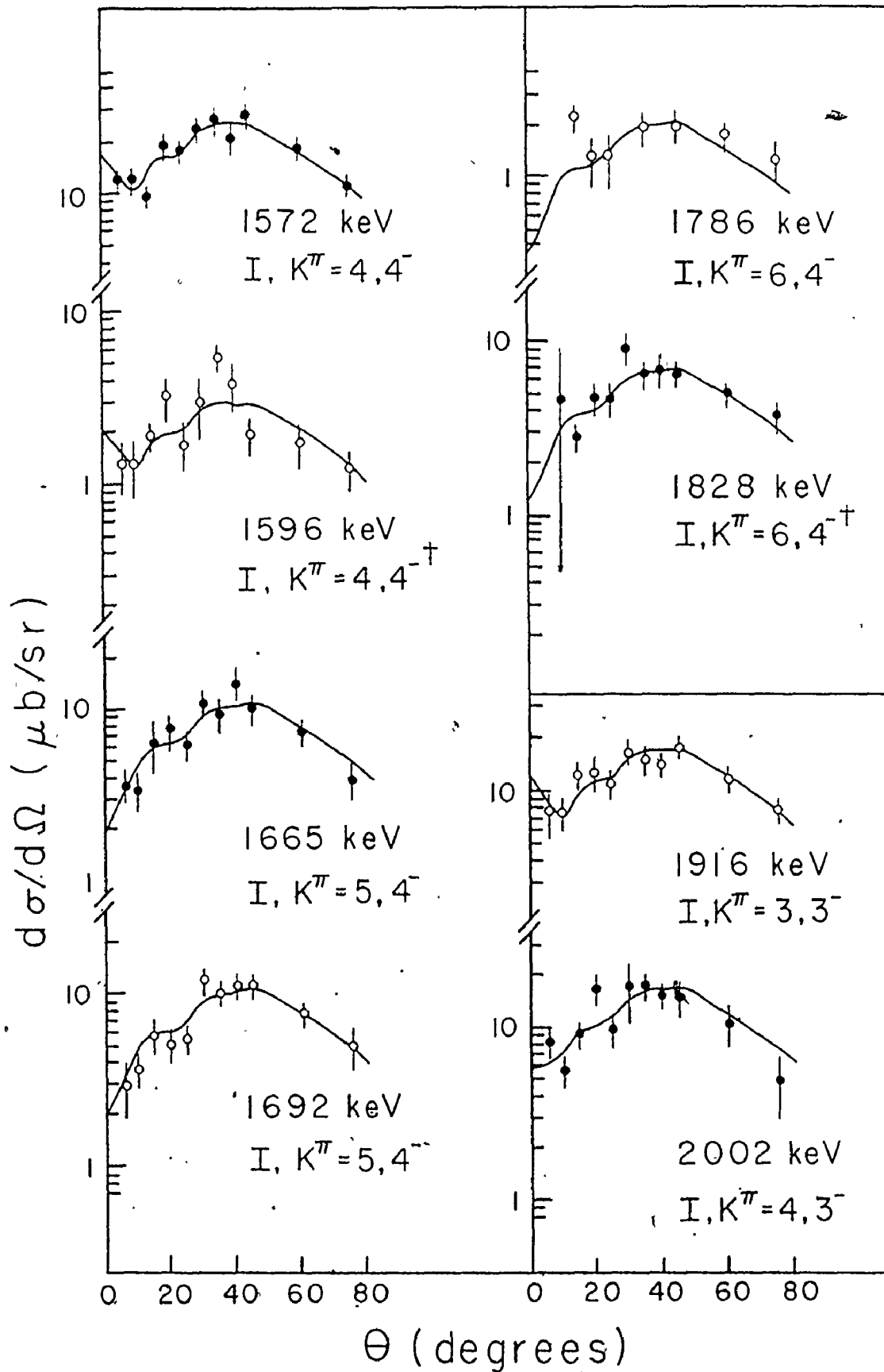
Fig. 4.3.3

$^{165}\text{Ho}(^3\text{He},d)^{166}\text{Er}$  angular distributions to states of the  $7/2^- [523]+1/2^+ [411]$  two proton configuration. Mixing with the  $K^\pi = 2^-$  octupole bands produces two states each for the spins 4, 5 and 6. (Note the similar experimental distribution shape for both states of each spin.)

The first two members of the  $7/2^- [523]-1/2^+ [411]$   $K^\pi = 3^-$  band are also shown.

The dagger ( $\dagger$ ) indicates that the state is primarily composed of the  $K^\pi = 2^-$  octupole vibrational band.

The solid lines are angular distributions generated by the computer code EVEPLT for mixed  $\ell$ -value proton transfers. These generated shapes have been scaled up or down to produce the best visual fit.



states in the neutron transfer and proton transfer reactions, to be evidence for the n-p mixing discussed in Section 3.3.h.3 (cf. Tables 4.2.2 and 4.3.2).

With reference to Table 4.3.2, the experimental cross sections are well matched by the predicted values for the spin 4 states. The only appreciable Coriolis interaction matrix elements for this band are between members of the  $K_{<}^{\pi} = 4^{-}$  and  $K_{>}^{\pi} = 3^{-}$  bands of this configuration (typically 30 to 40 keV), and between both these bands and those of the  $7/2^{-}[523] \pm 3/2^{+}[402]$  configurations. The latter mixings are highly suppressed due to the large energy separation between the  $7/2^{-}[523] + 1/2^{+}[411]$  and  $7/2^{-}[523] + 3/2^{+}[402]$  levels. Thus, the Coriolis interaction does not play a large part in the current discussion. From the table it can be seen that the spin 5 and 6 levels have experimental cross sections which are somewhat greater than the predicted values, possibly due to an as yet undetermined mixing. However, as these are relatively small peaks, this is not considered to be a serious discrepancy.

Upon closer inspection of the cross sections to the spin 6 levels, it is seen that the value to the upper state is considerably too large in the proton transfer reaction, while the cross section is reasonably well matched by the lower state. The implication here is that the upper state

Table 4.3.2

The  $7/2^- [523] \pm 1/2 [411]$  Bands

Energy (keV)	$(^3\text{He}, d) \, d\sigma/d\Omega \, (\mu\text{b}/\text{sr})$		$(\alpha, t) \, d\sigma/d\Omega \, (\mu\text{b}/\text{sr})$		Assignment K $\pi$			
	Experiment $\theta=45^\circ$	Pure	Coriolis Mixed	Experiment $\theta=60^\circ$		Pure		
1572	27 $\pm$ 5	28.3	28.2	29 $\pm$ 5	26.1	26.8	4	4 $^-$
1596	1.9 $\pm$ 0.5			3.0 $\pm$ 0.6			4	4 $^-$ a)
1665	9.8 $\pm$ 2.0			13.5 $\pm$ 2.4	13.1	13.3	5	4 $^-$
1692	8.2 $\pm$ 1.5	13.0	12.7	$\sim$ 12.8 $\pm$ 3.0			5	4 $^-$
1786	1.9 $\pm$ 0.4	2.3	2.5	2.5 $\pm$ 0.5	2.8	2.8	6	4 $^-$
1828	6.4 $\pm$ 1.2			5.7 $\pm$ 0.9			6	(4) $^-$
1916	18.0 $\pm$ 3.1	26.6	26.7	13.8 $\pm$ 2.2	18.2	18.3	3	3 $^-$
2002	14.9 $\pm$ 8.9	16.3	15.8	12.7 $\pm$ 6.4	12.1	11.5	4	3 $^-$
2113	2.2 $\pm$ 0.8	5.4	5.4	2.2 $\pm$ 1.0	4.4	4.2	(5	3 $^-$ )

a) Minor component; major component is  $7/2^+ [633] - 3/2^- [521]$  two neutron configuration.

is considerably mixed and the lower level is thus predominantly the  $7/2^- [523] + 1/2^+ [411]$  configuration. This is consistent with the results of the neutron transfer study where the upper spin 6 level is considered to be associated predominantly with the  $K^\pi = 2^-$  octupole band.

The assignment of these states to the  $K^\pi = 4^-$  band yields an average rotational parameter of  $\sim 10.6$  keV for the two-proton states of  $^{166}\text{Er}$ .

As the three pairs of states with spins 4, 5 and 6 have been discussed both in this section and the neutron transfer, a brief summary of the main conclusions concerning their make-up is in order. The  $I^\pi = 4^-$  state at 1572 keV is predominantly the  $7/2^- [523] + 1/2^+ [411]$   $K^\pi = 4^-$  two proton configuration as is the  $I^\pi = 6^-$  state at 1786 keV. Both states have small admixtures of the  $7/2^+ [633] - 3/2^- [521]$   $K^\pi = 2^-$  two neutron configuration. Conversely, the higher lying  $I^\pi = 4^-$  state at 1596 keV and the higher lying  $I^\pi = 6^-$  state at 1828 keV are both predominantly the two neutron configuration with a small admixture of the two proton component. On the other hand, the two  $I^\pi = 5^-$  states (1665 and 1692 keV) appear to have equal admixtures of the two proton and the two neutron configurations.

Before discussing the  $K_>$  band, a digression is made concerning the multiplet nature of many of the states observed in the proton transfer reactions. The presence of at

least four multiplets, all with substantial total cross sections and having at least three components per multiplet, greatly increased the complexity of the proton transfer data analysis. During the course of the analysis, many schemes were hypothesized to interpret particularly the peaks and multiplets with large cross sections; it was found, however, that the scheme finally settled upon and presented in this study (cf. Fig. 4.1.2) was the only one which afforded any degree of credibility. Not only were all the states which were expected to have large cross sections accounted for, but the total cross section observed for each multiplet was well matched by the total predicted cross section for the states in that multiplet. This was true for both the ( $^3\text{He},d$ ) and ( $\alpha,t$ ) spectra. In Table 2.4.1, these multiplets are indicated by brackets beside the differential cross sections. It should be further noted that even though from Fig. 4.1.2 it is hard to pick out the individual members of the various multiplets, the peak fitting program consistently did so at the different angles studied.

The  $K_{>}^{\pi} = 3^{-} \quad 7/2^{-}[523] - 1/2^{+}[411]$  bandhead is predicted by the splitting calculation to lie  $\sim 340$  keV above the  $K_{<}^{\pi} = 4^{-}$  spin 4 state. The level at 1916 keV is at the right energy to be this  $K_{>}$  state, and Zylicz et al. (1966) identified the state as  $I^{\pi} = 3^{-}$  and tentatively

assigned it as the  $K_2$  bandhead. The present work confirms this suggestion. The level at 2002 keV was tentatively assigned in the 1966 study as the spin 4 member of the  $K_2$  band on the basis of its preferential decay to the 1916 keV level and the present study also confirms this. The spin 5 member is tentatively assigned to the barely resolved peak at 2113 keV.

The ( $^3\text{He},d$ ) angular distributions for these states are well matched by the predicted shapes, although the spin 4 distribution had to be extracted from a rather complex multiplet (Fig. 4.3.3). The ratios of the ( $^3\text{He},d$ ) to ( $\alpha,t$ ) cross sections also agree with the predicted value, indicating a mixed  $\ell = 0$  and 2 transfer for the bandhead, and a predominantly  $\ell = 2$  transfer for the spin 4 and 5 members.

The cross section to the bandhead is  $\sim 30\%$  lower than predicted for both reactions (cf. Table 4.3.2), but this deficiency may be due to mixing of this state with the two-proton components of the  $K^\pi = 2^-$  octupole band. Evidence for this comes from the preferential  $\gamma$ -decay of the 1916 state to the octupole bandhead observed in the  $^{166}\text{Tm}$  electron capture decay (Zyllicz et al., 1966).

The energies for the three states in the  $K_2$  band results in a rotational parameter of  $\sim 10.7$  keV, consistent with the average observed spacings of the

$K_{<}^{\pi} = 4^{-}$  band discussed above.

(d) The  $7/2^{-}[523] + 7/2^{+}[404]$  Band

A barely resolved peak at 1989 keV, located in the same multiplet as the spin 4 state of the  $7/2^{-}[523] + 1/2^{+}[411]$   $K_{>}^{\pi} = 3^{-}$  band, was noted as having the largest cross section in the  $60^{\circ}$   $(\alpha, t)$  spectrum. (cf. Table 4.3.3). In addition, the ratio of  $({}^3\text{He}, d)$  and  $(\alpha, t)$  cross sections was indicative of an  $\ell = 4$  proton transfer. (cf. Fig. 4.3.1) As the  $7/2^{-}[523] + 7/2^{+}[404]$   $K_{<}^{\pi} = 7^{-}$  bandhead is expected to be the most strongly populated state in the  $(\alpha, t)$  reaction at that angle, and as it is expected to be populated by a pure  $\ell = 4$  transition (the  $7/2^{+}[404]$  orbital originates with the  $g_{7/2}$  shell model state in the spherical limit), the peak at 1989 keV is assigned as this bandhead. The  $({}^3\text{He}, d)$  angular distribution to this state is consistent with this assignment (Fig. 4.3.4).

The only state having an appreciable Coriolis matrix element ( $\sim 60$  keV) with this state is in the  $7/2^{-}[523] + 5/2^{+}[413]$   $K_{<}^{\pi} = 6^{-}$  band. However, in  ${}^{165}\text{Ho}$  the  $5/2^{+}[413]$  "hole" bandhead is located at 995 keV while the  $7/2^{+}[404]$  "particle" bandhead is found at 716 keV. The hole state band, formed by coupling the  $5/2^{+}[413]$  orbital to the target ground state orbital, will be further removed from the  $K_{<}^{\pi} = 7^{-}$  bandhead in  ${}^{166}\text{Er}$  as a result of the shift in the Fermi level in going from  ${}^{165}\text{Ho}$  to  ${}^{166}\text{Er}$ .

Table 4.3.3

The  $7/2^- [523] + 7/2^+ [404] K^\pi = 7^-$  Band

Energy (keV)	$(^3\text{He}, d) \, d\sigma/d\Omega \, (\mu\text{b}/\text{sr})$		$(\alpha, t) \, d\sigma/d\Omega \, (\mu\text{b}/\text{sr})$		Assignment $K^\pi$			
	Experiment $\theta=45^\circ$	Pure	Theory Coriolis Mixed	Experiment $\theta=60^\circ$		Theory Coriolis Mixed		
1989	19.4±6.2	12.5	13.3	35±11	30.1	29.4	7	7 <sup>-</sup>

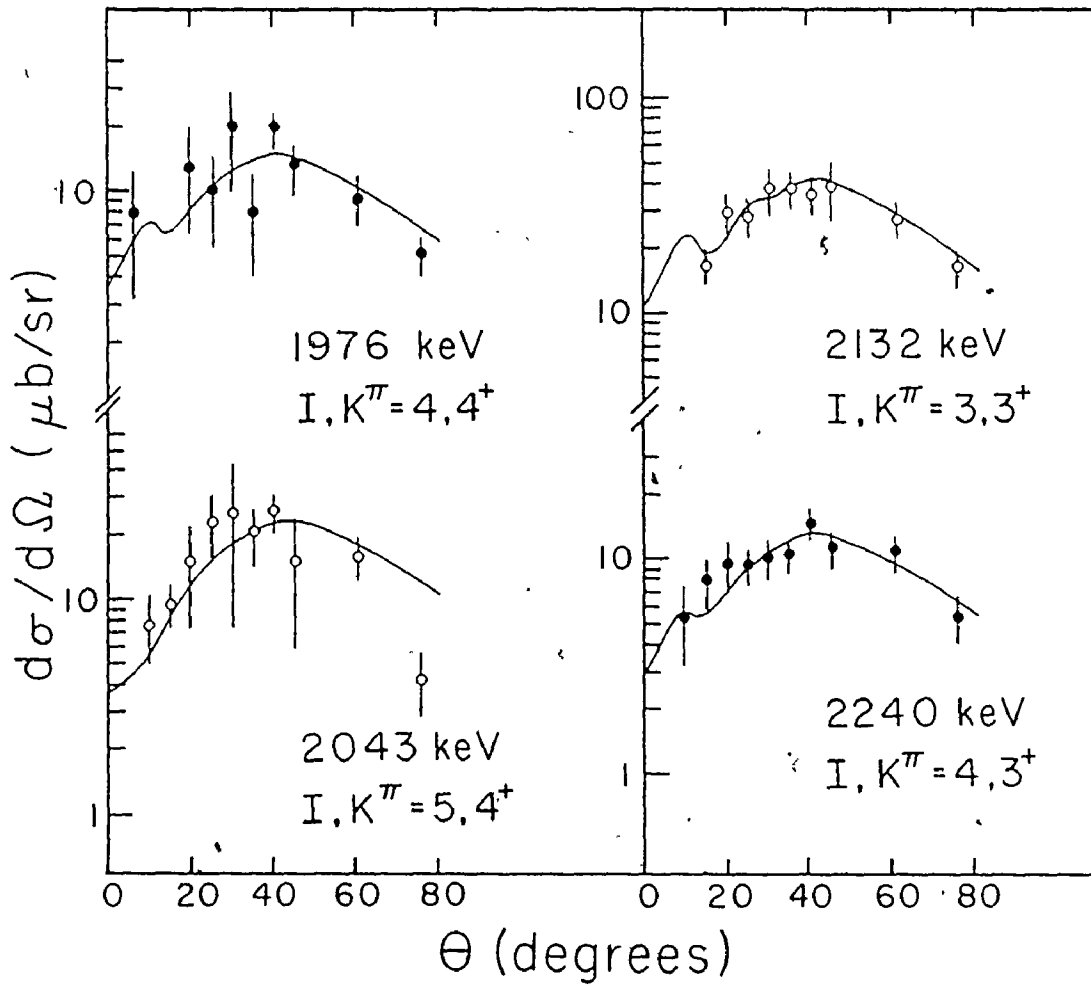
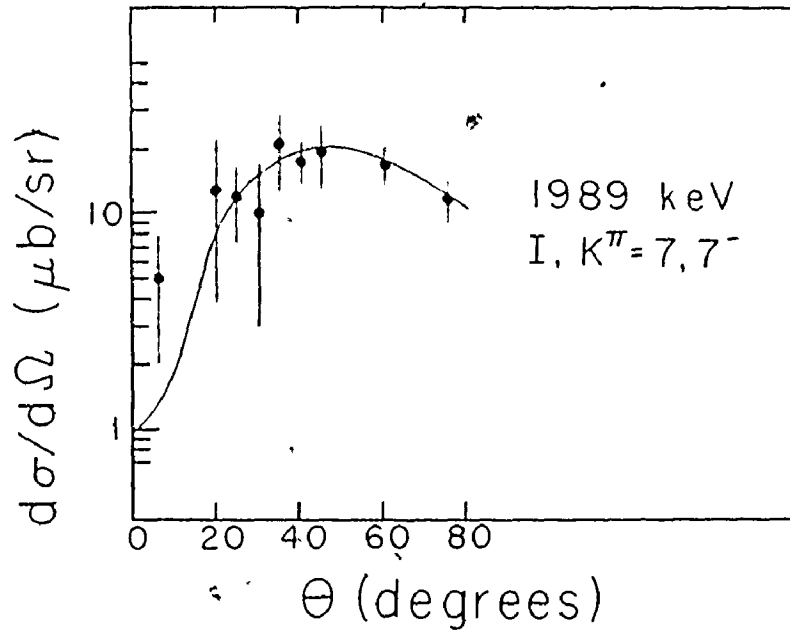
9

Fig. 4.3.4

$^{165}\text{Ho}(^3\text{He},d)^{166}\text{Er}$  angular distributions to the  $7/2^- [523] + 7/2^+ [404]$   $K^\pi$  bandhead. The solid lines are angular distributions generated by the computer code EVEPLT for mixed  $\ell$ -value proton transfers. These generated shapes have been scaled up or down to produce the best visual fit.

Fig. 4.3.5

$^{165}\text{Ho}(^3\text{He},d)^{166}\text{Er}$  angular distributions to the  $7/2^- [523] \pm 1/2^- [541]$   $K^\pi = 4^+, 3^+$  bands. The first two members of each band are shown. The solid lines are angular distributions generated by the computer code EVEPLT for mixed  $\ell$ -value proton transfers. These generated shapes have been scaled up or down to produce the best visual fit.



Thus, very little Coriolis mixing is expected for this level at 1989 keV, and the full strength is expected to be observed consistent with the experimental results (cf. Table 4.3.3).

Almost no single proton transfer cross section to the higher members of the  $K_{<}^{\pi} = 7^{-}$  band is expected for either reaction. Consequently, these states have not been identified in this study.

In the Katori et al. (1974) study, because of the poor resolution obtained, the peak at 1989 keV was not resolved from the multiplet (in fact, the multiplet nature of this peak was not recognized). This led to their assigning it as the  $7/2^{-}[523] - 1/2^{+}[411] K_{>}^{\pi} = 3^{-}$  bandhead, despite the fact that this designation would imply a low  $\ell$ -value for the transferred proton whereas the large  $(\alpha, t)$  population implies a high  $\ell$ -value transfer. The  $K_{<}^{\pi} = 7^{-}$  bandhead was instead assigned in their work to a state at 2611 keV which was strongly populated in the  $({}^3\text{He}, d)$  reaction. In the present study both the  $({}^3\text{He}, d)$  angular distribution and the ratio of the  $({}^3\text{He}, d)$  to  $(\alpha, t)$  cross sections support an  $\ell=2$  proton transfer to the state at 2608 keV (presumed to be the state to which Katori et al. refer) disallowing the  $\ell=4$  transfer required by the  $K^{\pi}=7^{-}$  assignment. The origin of these errors in determining the transferred  $\ell$ -values is not clear from their paper.

A second problem with their study of these  $K_{<}^{\pi} = 7^{-}$  and  $K_{>}^{\pi} = 0^{-}$  bands is their assignment of the  $K^{\pi} = 0^{-}$  bandhead at 2005 keV, well below the  $K^{\pi} = 7^{-}$  bandhead. This violates the Gallagher-Moszkowski coupling rule (cf. Section 3.3.h). In the present study, the majority of the intensity of the  $K_{>}^{\pi} = 0^{-}$  band is predicted to be divided among the first five band members. The predicted splitting energy of  $\sim 420$  keV implies that these states will lie in a region where they would be obscured by many larger peaks. Hence, they have not been identified.

(e) The  $7/2^{-}[523] \pm 1/2^{-}[541]$  Bands

Another configuration expected to produce large proton transfer cross sections at energies just above the pairing gap is the coupling of the  $7/2^{-}[523]$  and  $1/2^{-}[541]$  orbitals. Substantial Coriolis mixing between the  $K_{<}^{\pi} = 4^{+}$  and the  $K_{>}^{\pi} = 3^{+}$  bands is expected to increase the cross sections to the lower band, while the strong Coriolis matrix elements between the upper band and the much higher lying  $7/2^{-}[523] - 3/2^{-}[532]$   $K^{\pi} = 2^{+}$  configuration are expected to slightly enhance the  $K_{>}^{\pi} = 3^{+}$  cross sections.

The bandhead and spin 5 members of the  $K_{<}^{\pi} = 4^{+}$  band are tentatively assigned to states at 1976 and  $\sim 2043$  keV, respectively. The spin 6 member is probably located at  $\sim 2132$  keV. The first two band members are resolved (barely) from the multiplets in which they are found while

the spin 6 state is found in an unresolved multiplet, hence its more tentative assignment (cf. Fig. 4.1.2, Table 2.4.1).

For the two "resolved" levels the experimental ( $^3\text{He},d$ ) cross sections agree quite well with the predicted values, and both the ( $^3\text{He},d$ ) angular distributions and the ratio of the ( $^3\text{He},d$ ) and ( $\alpha,t$ ) cross sections support the predicted mixed  $\ell = 3$  and  $\ell = 1$  proton transfer to the bandhead and the primarily  $\ell = 3$  transfer to the spin 5 state. (cf. Fig. 4.3.5, Table 4.3.4). The observed rotational parameter from the spins 4 and 5 states is  $\sim 7$  keV which is in good agreement with the value of  $\sim 6.7$  keV predicted by the Coriolis mixing calculation (the value prior to mixing was input as  $\sim 10.7$  keV, in accordance with the value from the preceding subsections).

Possible support for the assignment of the 1976 keV state as a bandhead comes from the decay studies of  $^{166}\text{Tm}$  (Zylicz et al., 1966) where a level at 1979.0 keV, assigned as  $I^\pi = (2, 3, 4)^+$ , (and conceivably the level considered here) has no confirmed coincidence decays to any possible lower band members. Rather, it decays to states of the  $\gamma$ -vibrational band, suggesting that it is itself the lowest member of a band.

The observed rotational parameter from the lower band members placed the spin 6 members in the multiplet at  $\sim 2132$  keV. For this multiplet, as well as for others

Table 4.3.4

The  $7/2^- [523] \pm 1/2^- [541]$  Bands

Energy (keV)	$(^3\text{He}, d) \, d\sigma/d\Omega \, (\mu\text{b/sr})$		Experiment		$(\alpha, t) \, d\sigma/d\Omega \, (\mu\text{b/sr})$		Theory Coriolis Mixed	Theory Coriolis Mixed	Assignment K $\pi$
	Experiment $\theta=45^\circ$	Pure	Coriolis Mixed	$\theta=60^\circ$	Pure	Pure			
1976	13.2±3.4	15.3	16.3	11.2±2.1	11.0	14.7	4	4 <sup>+</sup>	
2043	14.9±8.9	9.9	14.9	19.0±3.2	11.6	22.2	5	4 <sup>+</sup>	
2132	36±11	4.8	9.4 <sup>a)</sup>	38±9	8.8	21.1 <sup>b)</sup>	(6)	4 <sup>+</sup>	
2132	36±11	13.3	14.5 <sup>a)</sup>	38±9	7.9	9.3 <sup>b)</sup>	(3)	3 <sup>+</sup>	
2240	11.2±2.2	10.3	11.2	12.9±3.3	9.4	9.1	(4)	3 <sup>+</sup>	

a) Total predicted cross section from Tables 4.3.4 and 4.3.5 is 38.8  $\mu\text{b/sr}$ b) Total predicted cross section from Tables 4.3.4 and 4.3.5 is 37.5  $\mu\text{b/sr}$

as noted above, the total predicted cross sections from all the components of the multiplet match the total experimental cross sections very well both in the ( $^3\text{He},d$ ) and ( $\alpha,t$ ) reactions. Thus, the assignments are supported for each component of each multiplet. For the spin 6 state, the unresolved nature of the level prevents the generation of either a cross section ratio or a ( $^3\text{He},d$ ) angular distribution to provide further tests for the interpretation. Thus, a firm assignment would be premature..

The first two members of the  $K_{\pi}^{\pi} = 3^{+}$  band have been tentatively identified (Table 4.3.4). It is proposed that the spin 3 bandhead lies in the multiplet at 2132 keV, consistent with the predicted splitting energy of  $\sim 160$  keV. The spin 4 state is tentatively assigned as the state at 2240 keV.

As in the case of the spin 6 state (noted above as being part of the same multiplet), the bandhead's predicted cross section is consistent with the predicted values for the other members of the multiplet and the total experimental cross section. Again, no ( $^3\text{He},d$ ) angular distribution or cross section ratio was available. For the spin 4 state, the ratio of the ( $^3\text{He},d$ ) and ( $\alpha,t$ ) cross sections indicates a mixed  $\ell = 3$  and  $\ell = 5$  proton transfer, consistent with the assignment, and the ( $^3\text{He},d$ )

angular distribution is reasonably well fitted by the predicted shape. (Fig. 4.3.1, 4.3.5).

(f) The  $7/2^- [523] \pm 5/2^+ [402]$  and the  $7/2^- [523] \pm 3/2^+ [411]$  Bands

Although many levels had been assigned thus far in the present proton transfer study, not only did an appreciable amount of experimental strength still remain unassigned below  $\sim 2650$  keV, but it was spread among several different multiplets and individual levels. The only unassigned configurations with appreciable cross sections in this energy region were the  $7/2^- [523] \pm 5/2^+ [402]$  couplings. With reference to Table 4.3.5 the states expected to have large unmixed cross sections were the  $K_{>}^{\pi} = 6^-$  bandhead and the spin 1, 2 and 3 members of the  $K_{<}^{\pi} = 1^-$  band. These two-quasiparticle bands were expected to be at  $\sim 2500$  keV in  $^{166}\text{Er}$ , based on the excitation energy of the  $5/2^+ [402]$  band in  $^{165}\text{Ho}$  (Wagner et al., 1975), and the predicted splitting energy was  $\sim 150$  keV.

The identification of the  $K_{>}^{\pi} = 6^-$  bandhead as the peak at 2608 keV was readily accomplished as this bandhead is predicted to form the largest peak in the  $(^3\text{He}, d)$  spectrum at  $45^\circ$ . The angular distribution and the ratios of the cross sections indicate that the proton transfer to this state is predominantly  $\ell = 2$ , as expected since the  $5/2^+ [402]$  orbital originates from a  $d_{5/2}$  shell model state.

Table 4.3.5

The  $7/2^- [523] \pm 5/2^+ [402]$   $K^\pi = 6^-$  and  $1^-$ , and the  $7/2^- [523] - 3/2^+ [411]$   $K^\pi = 2^-$  Bands

Energy (keV)	$(^3\text{He}, d)$ $d\sigma/d\Omega$ ( $\mu\text{b}/\text{sr}$ )		$(\alpha, t)$ $d\sigma/d\Omega$ ( $\mu\text{b}/\text{sr}$ )		Assignment $K^\pi$
	Experiment $\theta=45^\circ$	Pure Coriolis Mixed	Experiment $\theta=60^\circ$	Pure Coriolis Mixed	
2608	$74 \pm 11$	76.5	$34 \pm 7$	29.1	$6^-$
2055	$33 \pm 20$	26.7	$17.2 \pm 3.1$	12.4	$1^-$
2151	$\sim 13 \pm 7$	25.3	$\sim 8 \pm 4$	11.4	$1^-$
2223	$11.7 \pm 3.5$	14.6	$\sim 5 \pm 2$	6.4	$1^-$
2055	$33 \pm 20$	4.4	$17.2 \pm 3.1$	2.1	$2^-$
2132	$36 \pm 11$	6.2	$38 \pm 9$	2.9	$2^-$
2223	$11.7 \pm 3.5$	4.1	$\sim 5 \pm 2$	1.9	$2^-$

a) Total predicted cross section is 40.1  $\mu\text{b}/\text{sr}$

b) Total predicted cross section is 18.9  $\mu\text{b}/\text{sr}$

c) Total predicted cross section is 13.5  $\mu\text{b}/\text{sr}$

d) Total predicted cross section is 6.1  $\mu\text{b}/\text{sr}$

e) Total predicted cross section from Tables 4.3.4 and 4.3.5 is 38.8  $\mu\text{b}/\text{sr}$

f) Total predicted cross section from Tables 4.3.4 and 4.3.5 is 37.5  $\mu\text{b}/\text{sr}$

in the spherical limit. (Fig. 4.3.6, 4.3.1). The observed cross sections are in excellent agreement with predictions for this state (cf. Table 4.3.5). The cross sections to the higher band members are all predicted to be very small.

As noted in Section 4.3.d, the large ( $^3\text{He}, d$ ) peak observed by Katori et al. (1974) at 2611 keV was erroneously assigned to be the  $7/2^- [523] + 7/2^+ [404]$   $K^\pi = 7^-$  bandhead. No consideration of the  $7/2^- [523] \pm 5/2^+ [402]$  configuration was taken in their work, and this omission contributes to the many discrepancies in the assignments noted between that study and the present one.

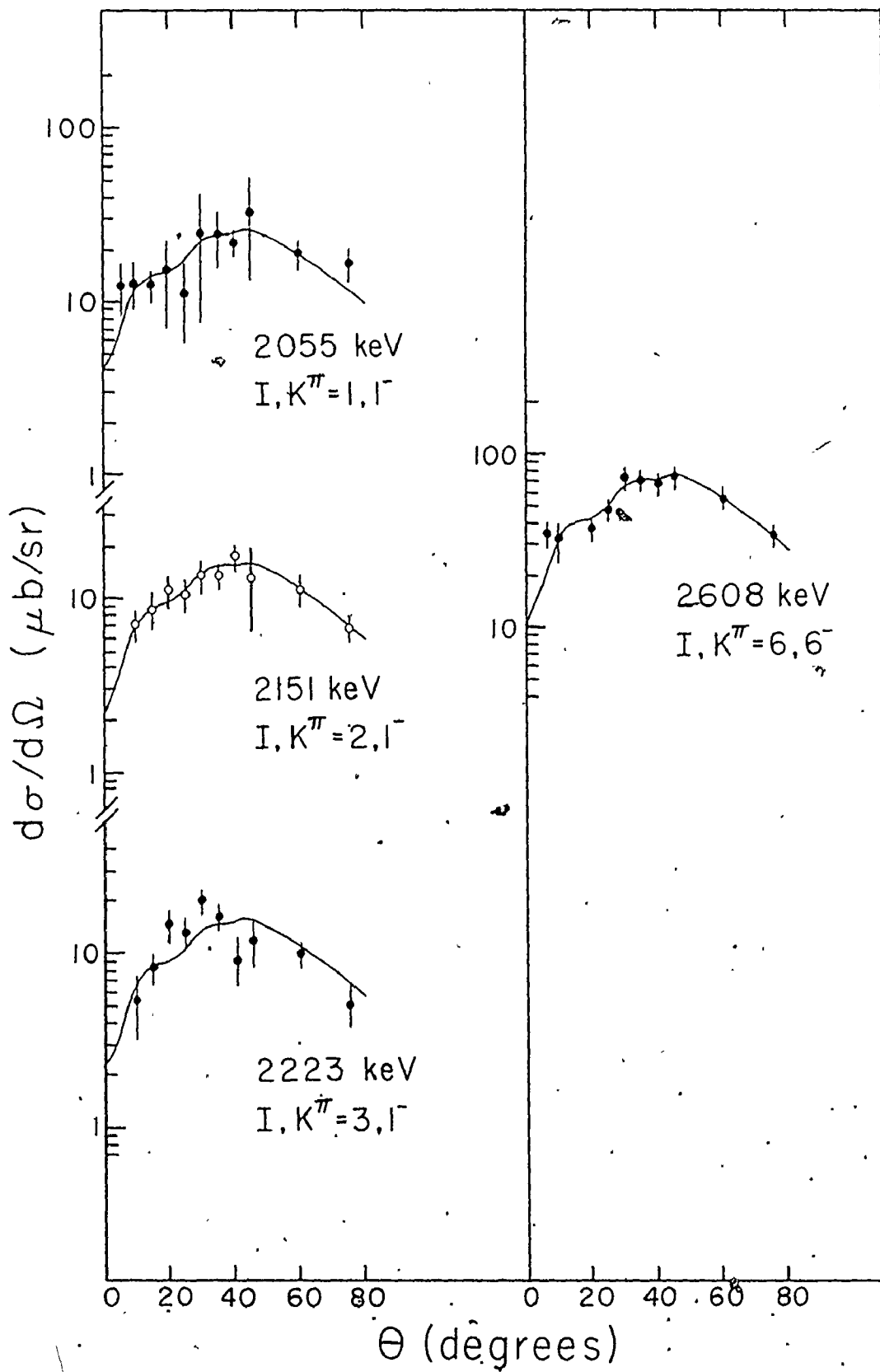
The assignment of the  $K^\pi = 1^-$  band presented more of a problem: no large peaks appear in the spectra at  $\sim 160$  keV below the  $K^\pi = 6^-$  bandhead, as predicted by the splitting calculation, and in fact, no unassigned peaks of the strength required to be the lower spin members of the  $K^\pi = 1^-$  band appear at all, particularly not in a  $I(I+1)$  rotational pattern.

A possible explanation for the deviation from the unmixed predictions is available by noting that in  $^{165}\text{Ho}$  the  $3/2^+ [411]$  "hole" state bandhead is located  $\sim 700$  keV below the  $5/2^+ [402]$  "particle" state bandhead (Wagner, et al., 1975). If in going from  $^{165}\text{Ho}$  to  $^{166}\text{Er}$  the Fermi level moves upwards by  $\sim 400$  keV, the  $7/2^- [523] \pm 3/2^+ [411]$

146(a)

Fig. 4.3.6

$^{165}\text{Ho}({}^3\text{He},d){}^{166}\text{Er}$  angular distributions to the  $7/2^- [523]-5/2^+ [402]$   $K^\pi = 1^-$  band and the  $7/2^- [523]+5/2^+ [402]$   $K^\pi = 6^-$  bandhead. The spin 1 and 3 levels form doublets with levels of the  $7/2^- [523]-3/2^+ [411]$   $K^\pi = 2^-$  configuration but the proton transfer population is almost entirely through the  $K^\pi = 1^-$  components (cf. also Fig. 4.1.2). The solid lines are angular distributions generated by the computer code EVEPLT for mixed  $l$ -value proton transfers. These generated shapes have been scaled up or down to produce the best visual fit.



configuration will lie very near to the  $7/2^- [523] + 5/2^+ [402]$  configuration prior to any mixing. As the splitting energy for the former is predicted to exceed that of the latter configuration, it is quite possible that the  $7/2^- [523] - 3/2^+ [411] K_{<}^{\pi} = 2^-$  bandhead will lie below the spin 2 member of the  $7/2^- [523] - 5/2^+ [402] K_{<}^{\pi} = 1^-$  band, and the spin 6 member of the  $7/2^- [523] + 3/2^+ [411] K_{>}^{\pi} = 5^-$  band will lie above the  $7/2^- [523] + 5/2^+ [402] K_{>}^{\pi} = 6^-$  bandhead. Although these  $K_{<}$  bands do not have large Coriolis matrix elements (typically  $\sim 30$  keV) for the spin 2 and 3 states, the Coriolis mixing interaction can transfer much of the strength from the  $K_{<}^{\pi} = 1^-$  band to the  $K_{<}^{\pi} = 2^-$  band (cf. Table 4.3.5).

A possible interpretation is presented involving the association of these mixed levels with the unassigned strength in the aforementioned multiplets. The peak at 2055, barely resolved from the spin 5 state at 2043 keV (cf. Fig. 4.1.2), is attributed to a combination of the  $K_{<}^{\pi} = 1^-$  bandhead and the  $K_{<}^{\pi} = 2^-$  bandhead. The total observed cross section for this multiplet (cf. Table 2.4.1) is reasonably well matched by the predicted values for both the  $(^3\text{He}, d)$  and  $(\alpha, t)$  reactions (cf. Table 4.3.5). The cross section ratio is consistent with the required  $\ell = 2$  proton transfer (Fig. 4.3.1), and the  $(^3\text{He}, d)$  angular distribution is quite well matched by the predicted

shape (Fig. 4.3.6).

The spin 3 member of the  $K_{<}^{\pi} = 2^{-}$  band is assigned as the third member of the multiplet at 2132 keV. With its inclusion, the total predicted cross section agrees very well with observed values for both the ( $^3\text{He},d$ ) and ( $\alpha,t$ ) reactions. The spin 2 members of the  $K_{<}^{\pi} = 1^{-}$  band is assigned to the state at 2151 keV on the basis of its intensity (cf. Table 4.3.5) and its  $\ell = 2$  cross section ratio (Fig. 4.3.1). In addition, the angular distribution is very well matched by the predicted shape for this state (Fig. 4.3.6). The spin 3 member of the  $K_{<}^{\pi} = 1^{-}$  band and the spin 4 member of the  $K_{<}^{\pi} = 2^{-}$  band have the correct predicted mixed cross sections to be located in an unresolved doublet at 2223 keV. The ( $^3\text{He},d$ ) angular distribution is fitted well by the expected  $\ell = 2$  shape for these states (Fig. 4.3.6) and the cross section ratio is consistent with the  $\ell = 2$  proton transfer assignment.

The  $K_{>}^{\pi} = 5^{-}$  coupling of the  $7/2^{-}[523] + 3/2^{+}[411]$  band is not identified in this study as it is expected to be quite weakly populated. As noted above, it is logical to expect that the spin 6 member of this band will lie above the  $K_{>}^{\pi} = 6^{-}$  bandhead of the  $7/2^{-}[523] + 5/2^{+}[402]$  configuration, a position supported by the fact that the latter state is observed with its complete strength.

The reason for the splitting energies being  $\sim 400$  keV

larger than expected for these bands is not completely understood. Interactions with vibrational configurations may be responsible for these effects as noted in the neutron transfer study where the  $7/2^+[633] - 3/2^-[521] K_{\zeta}^{\pi} = 2^-$  band is depressed  $\sim 590$  keV more than predicted by the splitting energy calculation (cf. Section 4.2.c). In spite of this only partially explained difficulty, the total scheme is supported by the fact that the cross sections are so well matched for the several highly complex multiplets observed in both the ( $^3\text{He},d$ ) and ( $\alpha,t$ ) reactions.

(g) The  $7/2^-[523] + 9/2^-[514]$  Bands

Two states have been assigned in this study for the two members of the  $7/2^-[523] + 9/2^-[514] K_{\zeta}^{\pi} = 8^+$  band, at 3075 and 3273 keV (Table 4.3.6). Their ratio of ( $^3\text{He},d$ ) and ( $\alpha,t$ ) cross sections indicates  $\ell = 5$  proton transfers (Fig. 4.3.1) consistent with the  $h_{11/2}$  shell model state origin in the spherical limit for the  $9/2^-[514]$  orbital. No Coriolis mixing is expected for the spin 8 state, and only very little is expected for the spin 9 level, the  $7/2^-[523] + 11/2^-[505] K = 9^+$  band being considerably higher in energy.

The  $K_{\zeta}^{\pi} = 1^+$  band is not identified in the present study as the strength is predicted to be spread among several band members, and they are expected to lie in a region where they would be obscured by many larger peaks.

Table 4.3.6

The  $7/2^- [523] + 9/2^- [514] K^\pi = 8^+$  Band

Energy (keV)	$(^3\text{He}, d) d\sigma/d\Omega$ ( $\mu\text{b}/\text{sr}$ )		$(\alpha, t) d\sigma/d\Omega$ ( $\mu\text{b}/\text{sr}$ )		Assignment $K^\pi$
	Experiment $\theta=45^\circ$	Pure Theory Coriolis Mixed	Experiment $\theta=60^\circ$	Pure Theory Coriolis Mixed	
3075	6.7±1.5	4.7	6.9±1.3	9.7	8 <sup>+</sup>
3273	11.2±2.4	7.5	13.7±2.2	13.8	8 <sup>+</sup>

## (h) Miscellaneous States

The state observed in the neutron transfer study at 1868 keV may be the same one found at 1865 keV in the proton transfer reaction (cf. Tables 2.3.1 and 2.4.1). The  $(^3\text{He},d)$  to  $(\alpha,t)$  cross section ratio indicates an  $\ell \sim 3$  proton transfer (or mixed  $\ell = 2, \ell = 4$ ) while the  $(^3\text{He},d)$  angular distribution shows an  $\ell = 2$  shape if the point at  $6\frac{1}{2}^0$  is attributed to an impurity (Fig. 4.3.7a). The level is not assigned in this study.

The peak at 3501 keV is seen to have a large  $(^3\text{He},d)$  cross section and a small  $(\alpha,t)$  cross section yielding an  $\ell = 0$  (or possibly  $\ell = 1$ ) cross section ratio. In addition, the  $(^3\text{He},d)$  angular distribution is fitted by an  $\ell = 0$  shape (Fig. 4.3.7a), and so this peak is associated with the  $7/2^- [523] \pm 1/2^+ [400]$  configuration. Despite the fact that the observed  $(^3\text{He},d)$  cross section is quite large, it is still only a fairly small fraction of the total strength expected for this configuration and the peak at 3501 keV is likely due to an admixture of one of the strongly populated bandheads into a vibrational state. As the Gallagher-Moszkowski rule predicts that the  $K^\pi = 3^-$  state will lie lowest and this is the lowest lying state populated by an  $\ell = 0$  transition, it is possible that the level is populated by an admixture of this spin 3 state. However, this should be regarded as a highly tentative

Fig. 4.3.7a

$^{165}\text{Ho}(^3\text{He},d)^{166}\text{Er}$  angular distributions for miscellaneous states observed in the present study. The state at 1865 keV is compared with an  $\ell=2$  shape, scaled to produce the best visual fit, while the state at 3501 keV is similarly compared with an  $\ell=0$  shape. The other angular distributions are for states unassigned in this work.

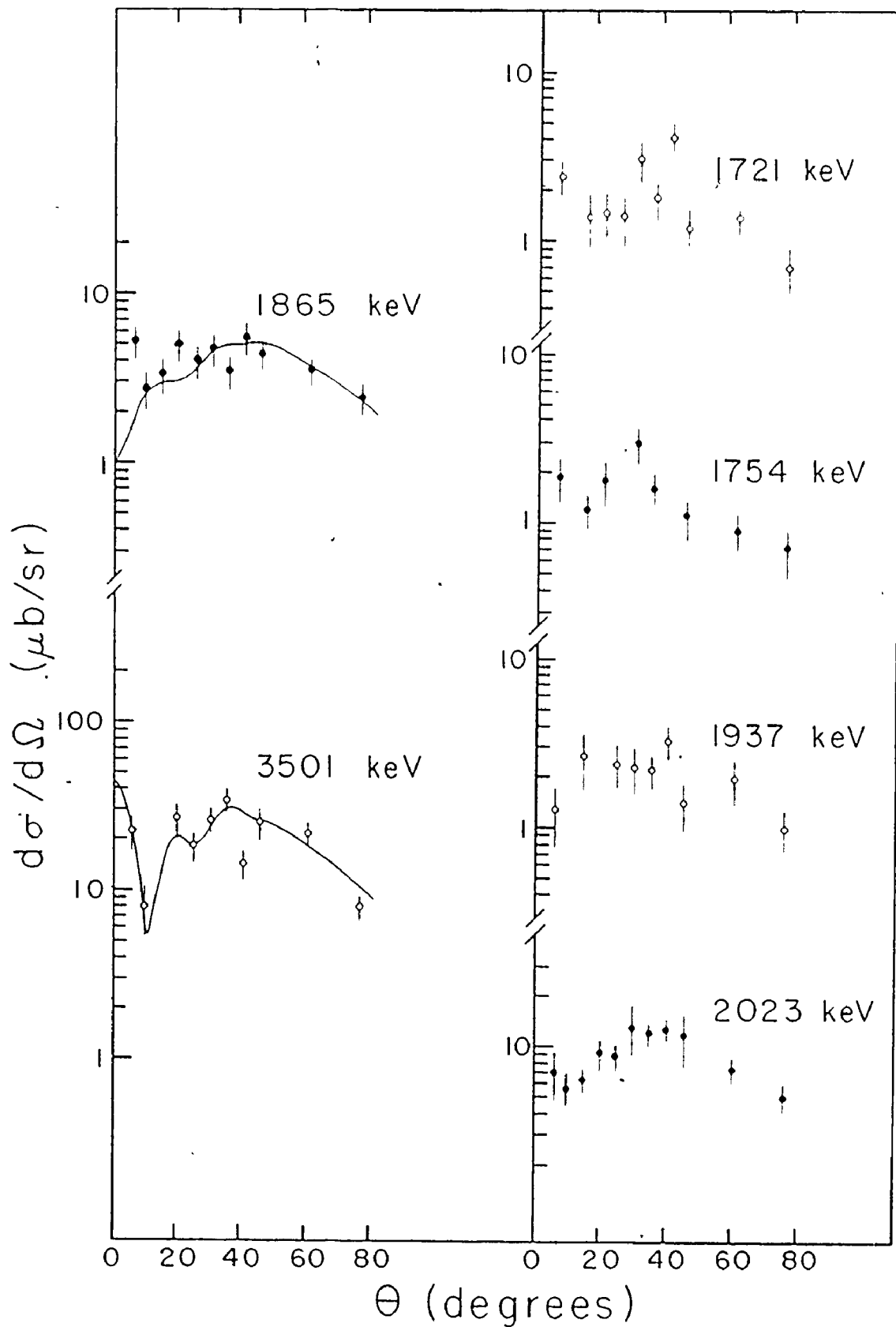


Fig. 4.3.7b

$^{165}\text{Ho}({}^3\text{He},d)^{166}\text{Er}$  angular distributions for miscellaneous states observed in the present study. Assignments have not been made for these states in this work.

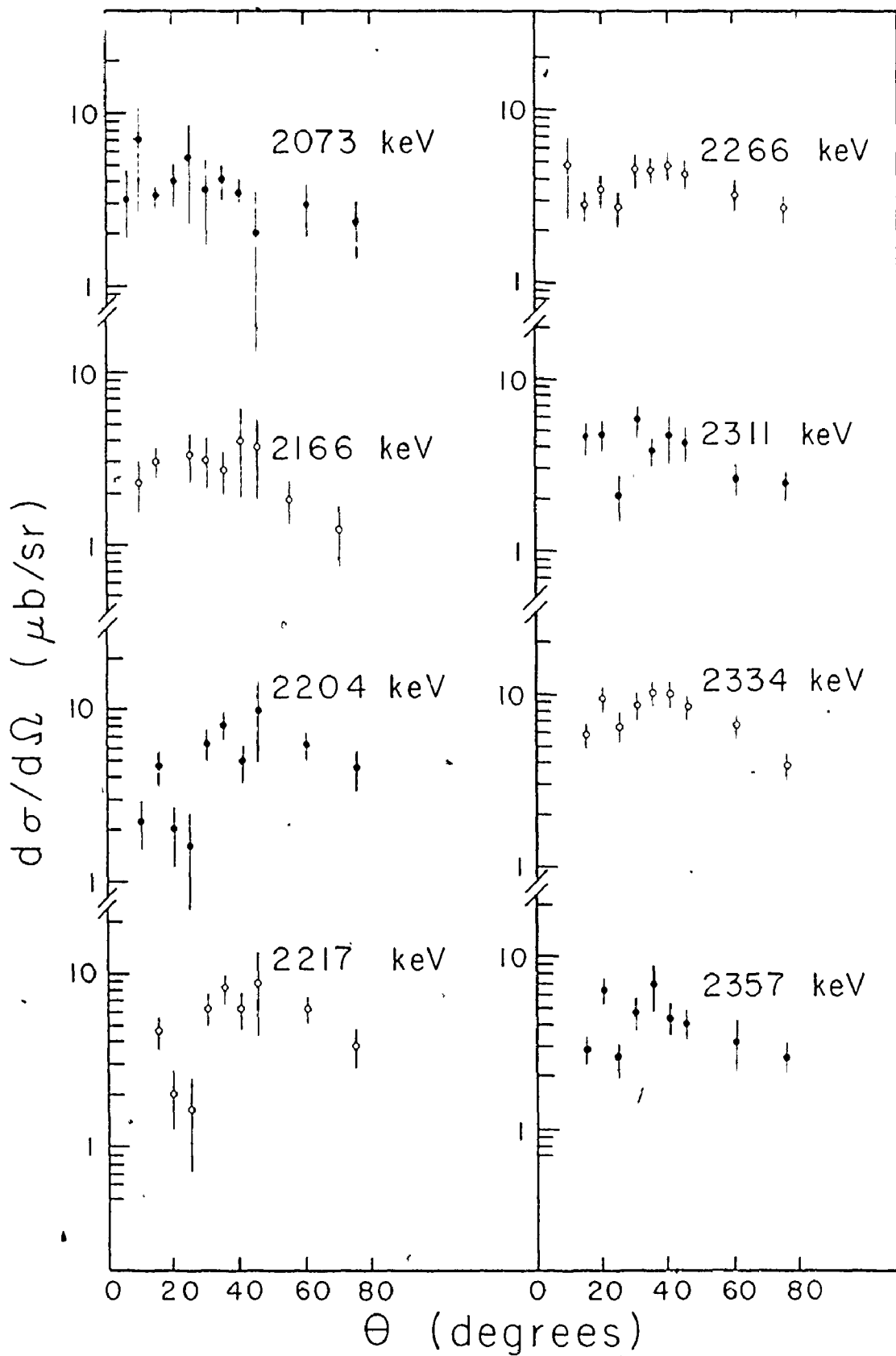


Fig. 4.3.7c

$^{165}\text{Ho}(^3\text{He},d)^{166}\text{Er}$  angular distributions for miscellaneous states observed in the present study. Assignments have not been made for these states in this work.

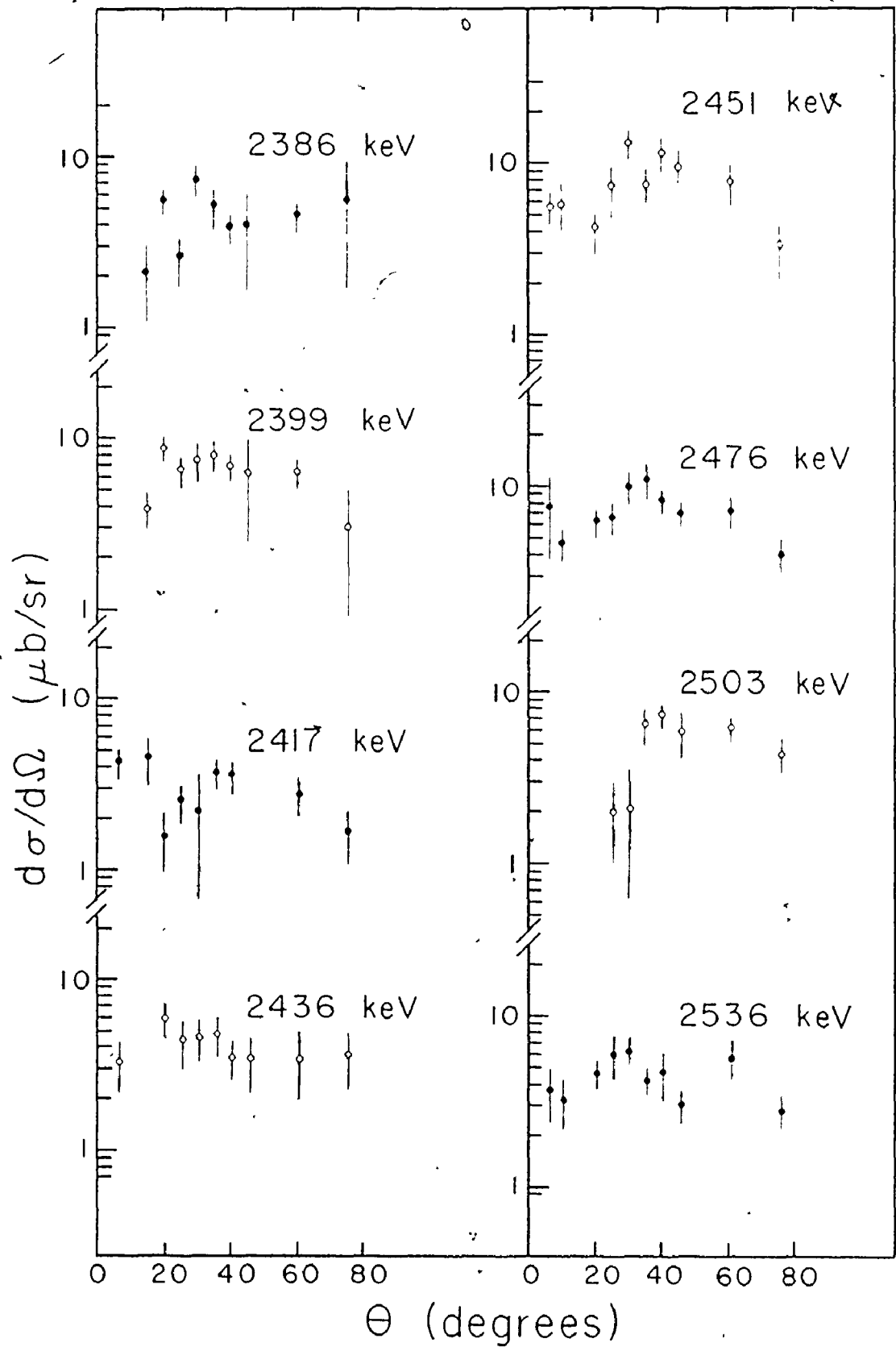
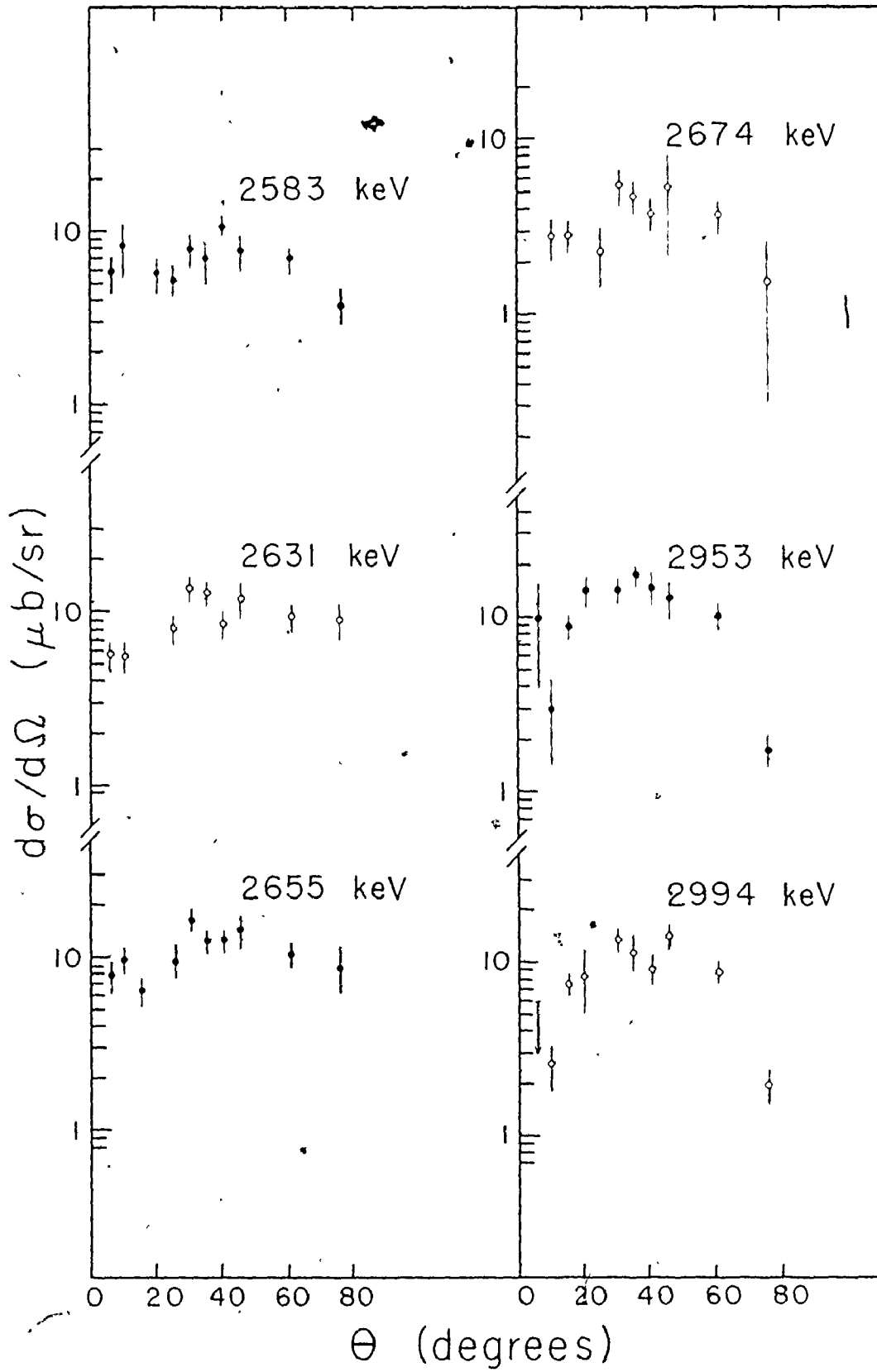


Fig. 4.3.7d

$^{165}\text{Ho}(^3\text{He},d)^{166}\text{Er}$  angular distributions for miscellaneous states observed in the present study. Assignments have not been made for these states in this work.



assignment.

The ( $^3\text{He},d$ ) angular distributions for the unassigned states, where available, are also shown in Fig. 4.3.7. As in the neutron transfer study many of these levels are probably due to higher order mixing interactions between the states already considered, or between those states and various vibrational configurations. Again, as in the neutron transfer study, these states do not comprise a large fraction of the total observed cross section. In the  $45^\circ$  ( $^3\text{He},d$ ) spectrum,  $\sim 80\%$  of the total observed strength has been accounted for up to an energy of  $\sim 2610$  keV.

CHAPTER 5  
CONCLUSIONS

This nuclear structure study of the rare earth deformed nucleus  $^{166}\text{Er}$  has used the  $^{167}\text{Er} (d,t) ^{166}\text{Er}$ ,  $^{167}\text{Er} (^3\text{He},\alpha) ^{166}\text{Er}$ ,  $^{165}\text{Ho} (^3\text{He},d) ^{166}\text{Er}$  and  $^{165}\text{Ho} (\alpha,t) ^{166}\text{Er}$  reactions.

In the neutron transfer study the  $(d,t)$  reaction was studied at twelve angles and sixty-six angular distributions were generated. The  $(^3\text{He},\alpha)$  reaction was investigated at three angles and ratios of the  $(^3\text{He},\alpha)$  and  $(d,t)$  cross sections were obtained for twenty states. Up to an excitation energy of  $\sim 2650$  keV, almost 80% of the strength has been accounted for.

In the proton transfer study the  $(^3\text{He},d)$  reaction was studied at ten angles and forty-eight angular distributions were generated. The  $(\alpha,t)$  reaction was investigated at two angles and ratios of the  $(^3\text{He},d)$  and  $(\alpha,t)$  cross sections were obtained for twenty-five states. Up to an excitation energy of  $\sim 2610$  keV, almost 80% of the strength has been accounted for.

A great deal of new information on the structure of  $^{166}\text{Er}$  has been assembled in this work, with many new assignments being proposed for two-quasiparticle states. In addition, several previous assignments were confirmed,

and in some cases, other earlier labellings were refuted. Generally, the results of the decay studies of Zylicz et al. (1966), and Reich and Cline (1970) were confirmed, as were the results of the (d,t) study of Burke et al. (1969) and those of the ( $^3\text{He},d$ ) study of Kubo (1968). In contrast, almost all the results from the ( $^3\text{He},d$ ) study by Katori et al., (1974) were disputed.

Substantial amounts of evidence for both  $\Delta N = 2$  and neutron-proton interactions in  $^{166}\text{Er}$  have also been presented. These, combined with the new information regarding the two-quasiparticle assignments have helped to increase the understanding of  $^{166}\text{Er}$  in the context of the Nilsson model.

Future work with this nucleus could follow three major lines. First, a better theoretical understanding of the ground state band structure of even-even nuclei could aid in the determination of the  $^{167}\text{Er}$  target nucleus configuration. This, of course, implies an adequate knowledge of the multistep processes which populate lower lying states in the single particle transfer reactions. Second, a  $\gamma$ -ray study of the higher lying states by, typically, the ( $\alpha, xn\gamma$ ) reaction may possibly shed still more light on the configurations above  $\sim 2$  MeV in excitation energy. And finally, a more rigorous theoretical treatment of this nucleus which fully incorporates the many vib-

rational excitations believed to be present, would likely prove to be most valuable.

## REFERENCES

- Andersen, B.L., 1968. Nucl. Phys. A, 112, 443.
- Bardeen, J., Cooper, L.N., and Schrieffer, J.R., 1957.  
Phys. Rev. 108, 1175.
- Bogoliubov, N.N., 1958. Zh. Eksperim. I. Teor. Fiz. 34, 58.
- Bohr, A., 1952. Mat. Fys. Medd. Dan. Vid. Selsk. 26, #14.
- Bohr, A., Mottelson, B., and Pines, D., 1958. Phys. Rev. 110,  
936.
- Bunker, M.E. and Reich, C.W., 1971. Rev. Mod. Phys. 43, 348.
- Burke, D.G., Zeidman, B., Elbek, B., Herskind, B., and  
Olesen, M., 1966. Mat. Fys. Medd. Dan. Vid. Selsk. 35, #2.
- Burke, D.G., Nelson, D.E. and Reich, C.W., 1969. Nucl. Phys.  
A, 124, 683.
- Burke, D.G., Alford, W.P. and O'Neil, R.A., 1971. Nucl. Phys.  
A, 161, 129.
- Burke, D.G., Waddington, J.C., Nelson, D.E. and Buckley, J.,  
1973. Can. J. Phys. 51, 455.
- Burke, D.G., 1974. Private Communication.
- Burke, D.G., 1977. Private Communication.
- Buyrn, A., 1975. Nucl. Data Sheets 14, 471.
- Cairns, J.E., Greene, M.W. and Kuehner, J.A., 1974. Nucl.  
Inst. and Meth. 114, 489.
- Cheung, H., 1974. Unpublished computer program SPLIT.
- Cheung, H., Burke, D.G. and Løvholden, G., 1974. Can. J. Phys.  
52, 2108.

- Chi, B.E., 1967. Single-Particle Energy Levels in a Nilsson Well.  
Physics Department Publication, S.U.N.Y..
- Dunmore, P., 1976. McMaster University Computer Program Library,  
MILIS 5.3.265, computer program EA01B.
- Elbek, B. and Tjøm, P.O., 1967. Mat. Fys. Medd. Dan. Vid.  
Selsk. 36, #8.
- Elbek, B. and Tjøm, P.O., 1969. Advances in Nuclear Physics,  
3, 759. Ed. M. Baranger and E. Vogt. Plenum Press, New York-  
London
- Elton, L.R.B., 1966. Introductory Nuclear Theory. W. B.  
Saunders Company, Philadelphia, Pa.
- Gallagher, C.J. and Moszkowski, S.A., 1958. Phys. Rev. 111, 1282.
- Gallagher, C.J., 1962. Phys. Rev. 126, 1525.
- Gallagher, C.J. and Soloviev, V.G., 1962. Mat. Fys. Skr. Dan.  
Vid. Selsk. 2, #2.
- Gove, N.B. and Wapstra, A.H., 1972. Nuclear Data Tables 11, 127.
- Grotdal, T., Nybø, K. and Elbek, B., 1970. Mat. Fys. Medd. Dan.  
Vid. Selsk. 37, #12.
- Hirning, C.R., 1975. Computer program documentation, code EVE,  
Tandem Accelerator Laboratory, McMaster University.
- Hirning, C.R. and Pánar, J.D., 1976. Unpublished computer  
program EVEPLT.
- Hjorth, S.A., Ryde, H., Hagemann, K.A., Løvholden, G. and  
Waddington, J.C., 1970. Nucl. Phys. A, 144, 513.

- Immele, J.D. and Struble, G.L., 1977. Phys. Rev. C, 15, 1103.
- Jaskola, M., Nybø, K., Tjøm, P.O., Elbek, B., 1967. Nucl. Phys. A, 96, 52.
- Jolly, O.P., 1975. Private communication.
- Jolly, O.P., 1976. "Nuclear Structure of Two Transition Nuclei:  $^{154}_{64}\text{Gd}_{90}$  and  $^{152}_{63}\text{Lu}_{89}$ ", (McMaster University) Thesis.
- Jones, H.D., 1969. "Nuclear Reaction Studies of Odd-Odd Deformed Nuclei", (Florida State University) Thesis.
- Kanestrøm, I. and Løvholden, G., 1971. Nucl. Phys. A, 160, 665.
- Katori, K., Medsker, L.R. and Yntema, J.L., 1974. Phys. Rev. C, 9, 360.
- Kubo, H., 1968. "A Study of Levels Populated in  $^{166}\text{Er}$  by the ( $^3\text{He}, d$ ) Reaction", (McMaster University) Thesis.
- Künz, P.D., 1974. University of Colorado unpublished computer program DWUCK4.
- Lamm, I.-L., 1969. Nucl. Phys. A, 125, 504.
- Lederer, C.M., Hollander, J.M. and Perlman, I., 1968. Table of Isotopes, 6th Edition, John Wiley and Sons Inc., New York, London, Sydney.
- Lindgren, I., 1965. Alpha-, Beta- and Gamma-Ray Spectroscopy, Ed. K. Siegbahn, 2, Appendix 4. North Holland Publishing Company, Amsterdam.
- Løvholden, G. and Burke, D.G., 1973. Can. J. Phys. 51, 2354.
- Lu, M.T. and Alford, W.P., 1971. Phys. Rev. C, 3, 1243.
- Massmann, H., Rasmussen, J.O., Ward, T.E., Haustein, P.E. and Bernthal, F.M., 1974. Phys. Rev. C, 9, 2312.

- Mayer, M.G. and Jensen, J.H.D., 1955. Elementary Theory of Nuclear Shell Structure. John Wiley and Sons Inc., New York.
- Meredith, J.O. and Barber, R.C., 1972. Can. J. Phys. 50, 1195.
- Nathan, O. and Nilsson, S.G., 1965. Alpha-, Beta- and Gamma-Ray Spectroscopy, Ed. K. Siegbahn, 1, North Holland Publishing Company, Amsterdam.
- Nelson, D.E., Burke, D.G., Waddington, J.C. and Cook, W.B., 1973. Can. J. Phys. 51, 2000.
- Nilsson, S.G., 1955. Mat. Fys. Medd. Dan. Vid. Selsk. 29, #16.
- Nilsson, S.G., 1961. Mat. Fys. Medd. Dan. Vid. Selsk. 32, #16.
- Nilsson, S.G., Tsang, C.F., Sobiczewski, A., Szymanski, Z., Wycech, S., Gustafson, C., Lamm, I.-L., Møller, P. and Nilsson, B., 1969. Nucl. Phys. A, 131, 1.
- O'Neil, R.A., Burke, D.G. and Alford, W.P., 1971. Nucl. Phys. A, 167, 481.
- O'Neil, R.A. and Burke, D.G., 1972. Nucl. Phys. A, 182, 342.
- Panar, J.D. and Burke, D.G., 1975. Private Communication.
- Preston, M.A., 1962. Physics of the Nucleus. Addison-Wesley Publishing Co., Inc., Reading, Mass.
- Pyatov, N.I., 1963. Izv. Akad. Nauk. SSSR Ser. Fiz. 27, 1436.
- Rainwater, J., 1950. Phys. Rev. 79, 432.
- Reich, C.W., 1968. Private Communication to D.G. Burke.
- Reich, C.W. and Cline, J.E., 1970. Nucl. Phys. A, 159, 181.
- Rowe, D.J., 1970. Nuclear Collective Motion. Methuen and Co. Ltd., London

- Rytz, A., 1960. *Compt. Rend.* 250, 3156.
- Satchler, G.R., 1964. *Nucl. Phys.* 55, 1.
- Smith, K.F. and Unsworth, P.J., 1965. *Proc. Phys. Soc.*  
(London) 86, 1249.
- Soloviev, V.G., 1961. *Mat. Fys. Skr. Dan. Vid. Selsk.* 1, #11.
- Spencer, J.E. and Enge, H.A., 1967. *Nucl. Inst. and Meth.* 49,  
181.
- Stott, W.R., Waddington, J.C., Burke, D.G. and Løvholden, G.,  
1975. *Can. J. Phys.* 53, 922.
- Straume, O., Løvholden, G. and Burke, D.G., 1976. *Nucl. Phys.*  
A, 266, 390.
- Tjømm, P.O. and Elbek, B., 1967. *Mat. Fys. Medd., Dan. Vid.*  
*Selsk.* 36, #8.
- Tjømm, P.O. and Elbek, B., 1968. *Nucl. Phys. A*, 107, 385.
- Tjømm, P.O. and Elbek, B., 1969. *Mat. Fys. Medd. Dan. Vid.*  
*Selsk.* 37, #7.
- Valatin, J.G., 1958. *Nuovo Cimento* 7, 843.
- Vallièrès, M., 1976. Private Communication.
- Volkov, A.B., 1977. Private Communication.
- Wagner, L.K., Burke, D.G., Cheung, H.C., Kleinheinz, P.,  
and Sheline, R.K., 1975. *Nucl. Phys. A*, 246, 43.
- Zheleznova, K.M., Korneichuk, A.A., Soloviev, V.G., Vogel, P.  
and Jungklaussen, G., 1965. Dubna preprint D-2157.
- Zylicz, J., Jørgensen, M.H., Nielsen, O.B. and Skilbreid, O.,  
1966. *Nucl. Phys.* 81, 88.